

Numerical Simulation of Production from Tight-Gas Reservoirs by Advanced Stimulation Technologies

Von der

Fakultät für Geowissenschaften, Geotechnik und Bergbau
der Technischen Universität Bergakademie Freiberg

genehmigte

Dissertation

zur Erlangung des akademischen Grades

Doktor-Ingenieur
(Dr.-Ing.)

vorgelegt von

Dipl.-Ing. Torsten Friedel
geboren am 24.04.1976 in Freiberg

Gutachter
Prof.Dr.-Ing.habil. Frieder Häfner, Freiberg
Prof.Dr.ir. Cor van Kruijsdijk, Delft (NL)
Dr. Kurt M. Reinicke, Clausthal

Tag der Verleihung: 8. Juli 2004

Abstract

The present thesis focusses on two main issues: (i) the development of a multi-phase simulation tool for the characteristics of tight-gas reservoirs, and (ii) the investigation of advanced stimulation techniques. The latter mainly implies the analysis of certain damaging mechanisms, as well as the derivation of general modelling guidelines for fractured wells and underbalanced drilling.

A special simulation tool is developed, realised in a Fortran-MATLAB coupling. The numerical model is based on the control-volume method with finite differences. It accounts for inertial non-Darcy effects, non-Newtonian fluid rheology and stress dependency of permeability via a simplified approach. The discretisation framework is fully unstructured, using the connection list approach and the common two-point flow stencil. Wells and boundary conditions can be handled very flexible in the code. Contrary to conventional treatment in simulators, wells are discretely included in the simulator.

Inertial non-Darcy flow and stress dependency of reservoir permeability are shown to affect the accuracy of simulation models, despite low gas rates. Considering a realistic scenario, with non-Darcy flow and permeability (stress) dependent non-Darcy flow coefficients, stress dependency of reservoir permeability and fracture closure, a total reduction of 40 % is possible in a 10 year production period under realistic conditions. New type-curves are presented for non-Darcy flow in fracture and reservoir, allowing for the determination of non-Darcy flow related parameters. The stress sensitivity of tight-gas rocks is crucial when simulating such reservoirs. The stress dependency of the reservoir permeability impacts the productivity to a much higher degree than the fracture closure.

A two-phase model is presented for the simulation of cleanup processes in terms of load water recovery. The fracturing fluid is treated as the water phase. The load water, causing hydraulic damage, hardly curtails productivity. To get considerable reductions in productivity, permeability in the fracture vicinity needs to be severely impaired. Due to the flow pattern, fractured wells are generally less sensitive against near wellbore damage than radial wells. An enhanced three-phase cleanup model is presented for the investigations of the polymer gel cleanup, incorporating a yield power law rheology (the Herschel-Bulkley model). The combined occurrence of loadwater recovery including capillary forces and the gel cleanup, are investigated for the first time. First results indicate that both processes are only weakly coupled.

A new simulation methodology is presented to investigate underbalanced drilling, taking into account multi-phase reservoir flow with capillary forces. A sensitivity analysis points out that the degree of water encroachment is the key factor for a successful UBD operation. Countercurrent imbibition, causing water encroachment is also analysed. Hydraulic damage turns out to be far more pronounced in tight-gas formations.

Acknowledgement

My colleagues Dr. Aron Behr and Dr. Hans-Dieter Voigt have been a source of enthusiasm and support for this work during the last three years, and their untiring push and criticism were determining factors in shaping this dissertation. I owe both of them a lot.

I would like to thank my adviser, Prof. Frieder Häfner, for his support, encouragement and guidance during this work.

Thanks goes to David Hornidge and Prof. Steffen Wagner for reading the script. I also wish to thank the rest of the Institute of Drilling Engineering and Fluid Mining for their supports and contributions to my academic achievements.

I deeply appreciate the scholarship provided by the DFG (German Research Foundation) and the financial support provided by the DGMK (German Society for Petroleum and Coal Science and Technology).

Finally, I would like to thank my family for their continuous support, encouragement and love. This thesis is dedicated to my parents Heidrun and Michael.

Contents

1	Statement of the Problem	1
2	Physical and Mathematical Model of Multi-Phase Fluid-Flow in Porous Media	4
2.1	Derivation of a General Flow Equation	4
2.2	Grid Geometry	6
2.3	Discretisation of the Flow Equation	7
2.3.1	CVFD Formulation	9
2.4	Auxiliary Equations	10
2.5	Final Set of Equations	11
2.6	Discussion	11
3	Simulator Development	13
3.1	Computational Model	13
3.1.1	Newton's Method	14
3.1.2	Connection List Approach	15
3.1.3	Assembling the System of Equations	17
3.1.4	Solution of the Linear System of Equations	18
3.2	Consideration of Wells and Boundary Conditions	19
3.2.1	Treatment of Boundary Conditions	20
3.2.2	Implementation of Wells in the Simulation Model	20
3.3	Gridding Technology	23
3.3.1	Generation of Voronoi Grids	24
3.4	Software Design	26
3.5	Verification and Validation	27
3.6	Discussion	27
4	Simulation of Hydraulically Fractured Wells	29
4.1	Introduction to Fractured Well Simulation	29
4.2	Mechanisms Affecting the Accuracy of Hydraulic Fracture Simulation Models	31
4.2.1	Simulation Model Setup	31
4.2.2	Non-Darcy Flow in Fracture and Reservoir	32
4.2.3	Stress Dependent Reservoir Permeability and Fracture Closure	40
4.2.4	Combined Effect of Stress Dependency and Non-Darcy Flow	43
4.3	Load Water Cleanup and its Impact on Post-Fracture Production	45
4.3.1	Background	45
4.3.2	Cleanup Simulation Model	46
4.3.3	Hydraulic Damage	52
4.3.4	Combined Occurrence of Hydraulic and Mechanical Damage	55

4.4	Polymer Gel Cleanup and its Influence on Productivity	59
4.4.1	Introduction to Fracturing Fluids	59
4.4.2	Simulation of Non-Newtonian Fluid Flow	61
4.4.3	Simulation Results	63
4.5	Discussion	67
5	Simulation of Underbalanced Drilling Operations	68
5.1	Background	68
5.2	Simulation Methodology	70
5.3	Simulation Model Setup	71
5.4	Influence of UBD and Reservoir Parameters on the Productivity of the Well	73
5.5	Investigations on the Spontaneous Imbibition during UBD	76
5.6	UBD in Horizontal Wells	76
5.7	Discussion	78
6	Summary	79
	Bibliography	81
	Appendix	95
A	Validation of the Simulation Model	96
B	Algorithms for Determination of Fractured Well Grids	104
C	Non-Darcy Flow Type-Curves	105
C.1	Non-Darcy Flow Type-Curves for Fractured Wells with Constant Pressure Production	105
C.2	Non-Darcy Flow Type-Curves for Fractured Wells with Constant Rate Production	109
C.3	Type-Curves for Damaged Fractured Wells with Constant Pressure Production	111
D	Multi-Phase Flow Functions in Tight-Gas Reservoirs	113

Nomenclatura

Symbols

Symbol	Meaning	Unit
a	constant in the Forchheimer equation	
A	area,	m^2
	accumulation	kg/s
B	formation volume factor	
b_f	fracture width	m
c	compressibility	1/Pa
C	tortuosity constant	
d	diameter	m
dx, dy	grid block size	m
F	flux,	kg/s
	scaling factor	
F_{CD}	dimensionless fracture conductivity	
g	gravitational constant (=9.81 m/s ²)	
h	distance,	m
	thickness	m
i	index	
j	index	
J	productivity	m ³ /s
J	Jacobain matrix	
k	permeability,	m ² , Darcy
	index,	
	iteration counter	
K	fluid consistency index	Pa.s ^{n}
L	length	m
L_x, L_y	areal model extent	m
\vec{n}	normal vector	
n	fluid behaviour index,	
	index of time	
N	number	
p	pressure	Pa
(p_{DND})	dimensionless non-Darcy flow parameter	
q	mass source/sink	kg/(m ³ .s)
q_D	dimensionless rate	
(q_{DND})	dimensionless flow rate constant	
q_f	influx per unit length	m ³ /(s.m)

Q	(well) flow rate	m^3/s
Q_D	dimensionless cumulative production	
Q_{cum}	cumulative production	m^3
r	radius	m
R	residual	kg/s
RP	relaxation parameter	
S	saturation	
S_D	skin factor	
t	time	s
$t_{D_{x_f}}$	dimensionless fracture time	
T	geometrical transmissibility	m^3
u	velocity	m/s
V	volume	m^3
w	average velocity	m/s
x	coordinate, distance	m
\vec{X}	solution (pressure, saturation)	
x_f	fracture half length	m
y	coordinate	m
z	real gas compressibility factor, coordinate	m
Z	depth of grid block center	m

Greek Symbols

Symbol	Meaning	Unit
β	dimensionless factor in Carters formula	
β_t	non-Darcy flow coefficient	$1/m$
$\dot{\gamma}$	shear rate	$1/s$
δ	control parameter	
$(\delta \vec{X})$	solution variable change vector	
ϵ	perturbation variable	
$\epsilon_{acc}, \epsilon_{flow}$	truncation error	
Θ	angle	
λ	pore size distribution index	
Λ	mobility	$1/Pa.s$
μ	dynamic viscosity	$Pa.s, cp$
μ_{eff}	effective viscosity of a non-Newtonian fluid	$Pa.s^n . m^{1-n}$
Ω	domain	
ρ	density	kg/m^3
σ	stress	Pa
τ	shear stress, integration variable, error	Pa
τ_0	yield stress	Pa
$\tau_{s,p,R}$	variable and residual change criterion	
ϕ	porosity	
Φ	Potential	Pa

Indices

Index	Meaning
<i>a</i>	absolute
app	apparent
<i>b</i>	block
cap	capillary
const	constant
<i>d</i>	displacement
D	with Darcy flow
<i>D</i>	dimensionless
DND	with non-Darcy flow
DNN	with non-Newtonian fluid
Drill	drilling
<i>f</i>	fracture
fl	fluid
<i>g</i>	gas
<i>gc</i>	critical gas (saturation)
gel	gel
<i>h</i>	horizontal
HB	Herschel-Bulkley
<i>i</i>	initial
irr	irreducible (saturation)
inj	injection
<i>l</i>	liquid
<i>m</i>	average
<i>n</i>	neighbour
norm	normalised
out	outer
<i>p</i>	proppant, phase
prod	producing
<i>r</i>	radial, rock, relative
res	reservoir
<i>s</i>	segment
skin	skin zone (damaged)
<i>t</i>	total
true	true
UBD	underbalanced drilling
<i>V</i>	per unit volume
<i>w</i>	water, well
<i>wd</i>	dimensionless water (saturation)
<i>wf</i>	well flowing
<i>wi</i>	initial water (saturation)
<i>z</i>	vertical
0	reference condition

Functions and Operators

Function	Meaning
J	Leverett J-Function
Re	Reynolds Number
R'e	modified Reynolds Number
∇	divergence operator

List of Figures

1.1	Specific processes at hydraulically fractured wells in tight-gas reservoirs	2
2.1	Structure of a Voronoi grid system (from PALAGI /19/)	6
3.1	Illustration of the connection list approach	16
3.2	Schematic of the well flow modelling option and example of application	22
3.3	Generation of Voronoi grids	24
3.4	Voronoi grids	26
4.1	Type-curves for fractured wells with constant pressure production ($F_{CD} = 50$)	35
4.2	Type-curves for fractured wells with constant rate production ($F_{CD} = 50$)	37
4.3	Non-Darcy flow coefficients for reservoir and proppant pack as function of permeability (provided by VOIGT)	39
4.4	Influence of proppant type on the production with non-Darcy flow	40
4.5	Stress dependency of reservoir permeability and fracture conductivity	41
4.6	Impact of stress dependency on the productivity of a fractured well ($k_{res,i} = 0.01$ mD)	43
4.7	Combined effect of non-Darcy flow, stress dependent reservoir permeability and fracture closure on a fractured well ($k_{res} = 0.01$ mD)	44
4.8	Fracture propagation: field data and approximative functions	48
4.9	Initial saturation profile after fracturing via injecting the fluid	49
4.10	Pressure and saturation development during shut-in of the well using different shut-in realisations with and without considering the water volume in the well	50
4.11	Cleanup process with hydraulic damage	53
4.12	Schematic of fracture and well flow model	54
4.13	Cleanup process with hydraulic and mechanical damage	58
4.14	Non-Newtonian fluid characteristics	60
4.15	Cleanup process with unbroken fracturing fluid in the fracture (without yield stress)	63
4.16	Saturation distribution at the end of the cleanup process assuming constant viscosity fracturing fluids (Newtonian-type)	64
4.17	Gas rates (a-b), gel saturation within the fracture after one year of production (c-d) and development of gel saturation within fracture plan (e-f) for various yield stresses and $k_{res} = 0.05$ mD	65
4.18	Effect of capillary forces and leakoff invasion zone on gel phase cleanup	66
5.1	Multi-phase flow functions for UBD simulation runs	71
5.2	Drilling process with subsequent production: comparison of numerical results with analytical solutions	72

5.3	Effect of reservoir permeability (0.01-100 mD) on gas rate and saturation conditions	74
5.4	Effect of reservoir thickness on gas rate	74
5.5	Effect of UBD conditions on gas rate during drilling and production	75
5.6	Effect of penetration rate on gas rate and saturation conditions during drilling and production	75
5.7	Temporal development of the pressure, pressure gradient and water saturation at the sandface	77
5.8	Simulation of UBD of a 100 m horizontal well in a 0.1 mD reservoir	78
B.1	Example of fracture grid (with quarter symmetry)	104
D.1	Multiphase flow functions based on Brooks-Corey correlations ($k_{res} = 0.05$ mD)	114

List of Tables

4.1	Parameters for single-phase simulation	31
4.2	Non-Darcy flow coefficient of several proppant types (source: STIMLAB /114/)	40
4.3	Effect of stress dependent fracture conductivity (fracture closure) on gas production	42
4.4	Parameters for cleanup simulation	52
4.5	Results for cleanup simulation after 1 year of production	53
4.6	Effect of yield stress on recovery ratio (first column: $F_{CD} = 10$, second: $F_{CD} = 100$)	64
5.1	Range of reservoir parameters for sensitivity study	73

1 Statement of the Problem

Natural gas is a major energy resource with strategic importance on the energy supply. In 2003, German gas production reached 21.4 billion m³ - about 20% of the annual demand (PASTERNAK /1/). Contribution of the domestic production has been steadily decreasing over the last decades. At the same time, the total remaining proven German gas reserves of about 326 billion m³ will facilitate gas production only for the next 15 years. Most fields are in a mature stage of the development, where significant gains by exploration are unlikely.

To contribute to the supply guarantee, great endeavour has been made to facilitate new gas resources during the last decades. Besides the classical, conventional resources, a variety of fields have been discovered, characterised by very low permeabilities in very challenging environments. The current trend in the German E&P industry is to involve those reservoirs into the development and exploitation. Such reservoirs are, in the majority of cases, just marginally economical efficient and require considerable investment for exploration.

Fields with permeability less than 0.1 mD are termed tight-gas reservoirs. Sediments of the North German Rotliegendes as well as the Upper Carboniferous form the primary German tight-gas regions. Reservoir conditions in these regions are affected by the tremendous depth (\approx 4 km), corresponding temperatures ($>120^{\circ}\text{C}$) and the compaction due to the burial depth with its consequential low permeabilities. Frequently, diagenesis of clay minerals, in particular the Illite, further deteriorate the reservoir quality in the tight-gas environment.

Despite the difficulties, there is a strong need to develop the enormous reserves of tight-gas. Prospective German tight-gas reserves are assumed to be as large as 300 billion m³, with a potential recovery factor of 30-50%. This could extend the strategic range of the local gas reservoirs another 7-8 years, provided an economical exploitation (LIERMANN and JENTSCH /2/). The development of tight-gas reservoirs implies the application of advanced well stimulation techniques, mainly concerning hydraulic fracturing of vertical or horizontal wells. Some multiple fractured horizontal well, e.g., the Söhlingen Z 10, have already successfully demonstrated the capabilities of such development technologies since the mid-nineties.

Hydraulic fracturing as a stimulation technique was first performed in the second half of the 1940's, while the first fracturing experiments were conducted in the Houghton field (Kansas) in 1947 (ECONOMIDES and NOLTE /3/). Hydraulic fracturing is the process of pumping a fluid into a wellbore at an injection rate that is too high for the formation to accept in a radial flow pattern. As the resistance to flow in the formation increases, the pressure in the wellbore increases to a value that exceeds the breakdown pressure of the formation. Once the formation breaks-down, a fracture is formed, and the injected fluid begins moving down the fracture. Simultaneously, some of the fluid leaks off into the formation. In most reservoirs, a single, vertical fracture is created that propagates in two directions from the wellbore. The fracture wings are 180° apart, and are normally assumed to be identical in shape and size.

The benefits of a precise analysis of the transient flow in the fracture vicinity with the aim of improving well performance, have been well recognized. Furthermore, the enormous development costs of tight-gas reservoirs make accurate and reliable production forecasts a necessity. It is a peculiar problem of tight-gas reservoirs that productivity frequently remains

1 Statement of the Problem

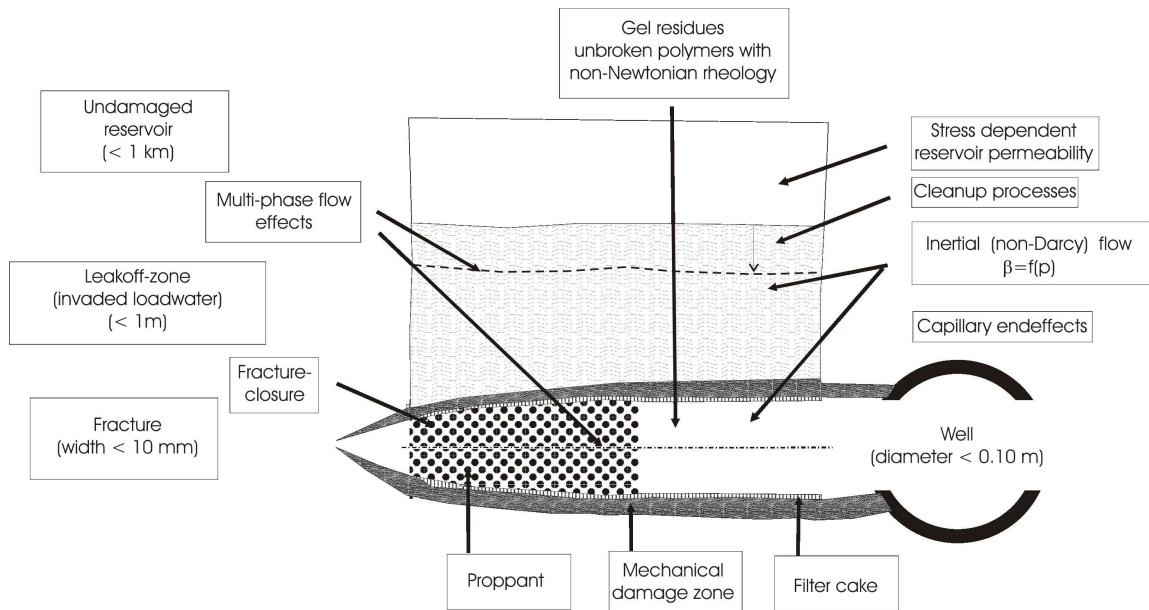


Figure 1.1: Specific processes at hydraulically fractured wells in tight-gas reservoirs

below the predictions. Inadequacies in the conventional simulation models and their applicability for tight formations can be considered as major reasons for that; highly nonlinear and complex mechanisms hamper the proper representation of fractured wells in reservoir simulation models.

Fig.1.1 presents the major specific physical processes at fractured wells. A wide variety of studies have been published in the literature dealing with these topics in detail; reference is given throughout the text in the corresponding sections. A realistic cleanup scenario may imply, among other things: (i) the simultaneous flow of three phases, (ii) the formation of a load water invasion zone accompanied by hydraulic and mechanical damage in the fracture vicinity, (iii) filtercake buildup and erosion, (iv) gel residue damaging the proppant pack, incorporating complex non-Newtonian rheology, (v) viscous fingering through the proppant pack, and (vi) unbroken fracturing fluids within the proppant pack. During the subsequent production, inertial non-Darcy flow and geomechanical effects, e.g., stress dependency of reservoir permeability and fracture closure, impact the behaviour of the fractured well. Furthermore, the fracture-reservoir system is characterised by highly discriminative magnitudes in space with fracture width in the range of millimeters and by distinct time scales of cleanup and post-fracture production period.

Traditionally, commercial simulators have been utilised for the simulation of hydraulically fractured wells. There are several simulation codes, diversely suited for the characteristics of such wells. A purpose built hydraulic fracture simulation tool (WellWhiz /4/) is recently available based on an established Black-Oil simulator (CMG IMEX), which is currently the only product on the market to model non-Darcy flow in fractures and the reservoir. However, it does not feature polymer (gel) cleanup, nor does it facilitate unstructured grids (/5/). The industry leading standard Black-Oil simulator, ECLIPSE, provides unstructured grids and basic polymer functionality, but is limited in its non-Darcian capabilities. Currently, there is development underway for a specific hydraulic fracture simulation tool inside ECLIPSE considering that handles, e.g., polymer (gel) cleanup and (multiple region) non-Darcy flow (/6/).

In this work, the advanced stimulation techniques, hydraulic fracturing and underbalanced

1 Statement of the Problem

drilling, are investigated numerically. Therefore, an appropriate reservoir simulation tool has been developed to improve the weak points of current commercial reservoir simulation tools regarding specific processes in the tight-gas environment. The tool is aimed at considering physical and technological aspects as accurately as possible. It is based on a special three-phase Black-Oil model, taking into account multi-domain inertial (non-Darcy) effects and complex non-Newtonian rheology with yield stress and shear thinning. Using state of the art numerical techniques, the tool features a fully unstructured discretisation framework, providing an accurate capture of the flow around fractures and wells and the opportunity for sophisticated wellbore flow modelling.

Primary objectives of the tool development and its application are: (i) a considerable increase in the quality of predictions from tight-gas reservoirs by taking into account the specific conditions with the corresponding petro-physical functions, (ii) improving the insight into complex and highly nonlinear multi-phase flow phenomena, and (iii) contribute to a more realistic simulation technology for such reservoirs.

Chapters 2 and 3 highlight the development of the physical, mathematical and the numerical model of the reservoir simulation tool. Chapter 4 presents a variety of topics on hydraulic fractured wells. These include mechanisms affecting the accuracy of hydraulic fracture models, investigations on the load water cleanup and finally an introduction to the fracturing fluid cleanup, i.e., gel cleanup. Chapter 5 introduces a further stimulation technique, known as underbalanced drilling, outlining the development of an appropriate simulation model for vertical and horizontal wells. Chapter 6 concludes this thesis.

2 Physical and Mathematical Model of Multi-Phase Fluid-Flow in Porous Media

The multi-phase flow of fluids in porous media is governed by physical laws and empirical relationships, which are valid in a broad variety of engineering disciplines. These laws are based on the conservation of mass and momentum. Additionally, several empirical relations, e.g., PVT-relations, rock and fluid properties and multi-phase flow behaviour, are necessary to formulate a flow equation such that the representation of the physical problem is as realistic as possible. The physical and mathematical models used to construct the flow simulator are briefly described in this chapter. For further reference, textbooks have been presented in the past discussing the subject in more detail, including AZIZ and SETTARI /7/, AZIZ and DURLOFSKY /8/, BEAR /9/, LAKE /10/ and HÄFNER et al. /11/.

2.1 Derivation of a General Flow Equation

The development of physical models always involves numerous assumptions in order to solve complex processes. However, some of them, which may be critical in particular situations, are:

- The flow is isothermal.
- There are no diffusion or dispersion processes or any chemical reactions.
- Thermodynamical equilibrium is established instantaneously.
- Three phases are considered: gas (g), water (w) and a third phase (gel). The third phase is primarily intended to represent drilling- and fracturing fluids with complex (non-Newtonian) rheology.
- There is no mass exchange between the phases; they are immiscible.
- Instantaneous phase distribution according to the capillary forces (equilibrium approach).

The starting point for the mathematical formulation of the flow equation is the application of the mass conservation law¹, which can be stated in vectorial notation:

$$-\nabla \cdot (\rho \vec{u}) = \frac{\partial}{\partial t}(\phi \rho) - q_V, \quad (2.1)$$

¹The critical reader may insist that the differential equation, eq.(2.1), is already derived from consideration of a finite, representative element volume by averaging the corresponding microscopic equation, eq.(2.5), and then, shrinking the volume ΔV to an infinitesimal value. Here, the method is used in reverse to illustrate the application of the control volume method by integration of any equation.

2 Physical and Mathematical Model of Multi-Phase Fluid-Flow in Porous Media

where q_V is a mass source/sink per unit volume. Since the pore space is occupied by several phases, eq.(2.1) is extended as follows:

$$-\nabla \cdot (\rho_p \vec{u}_p) = \frac{\partial}{\partial t} (\phi \rho_p S_p) - q_{p,V} . \quad (2.2)$$

The left hand side of eq.(2.2) denotes the mass flow rate of phase p by convection with a velocity u_p , whereas the right hand side describes the temporal accumulation of mass plus sources/sinks. Here, S represents the saturation, ρ is the density of the fluid and ϕ the porosity of the matrix.

Integration of the partial differential equation, eq.(2.2), over a finite control volume, ΔV , gives:

$$-\iiint_{\Delta V} \sum_{p=1}^{N_p} \nabla \cdot (\rho_p \vec{u}_p) dV = \sum_{p=1}^{N_p} \frac{\partial}{\partial t} \iiint_{\Delta V} (\phi \rho_p S_p) dV - \iiint_{\Delta V} \sum_{p=1}^{N_p} q_{p,V} dV , \quad (2.3)$$

for N_p phases. Applying the Gaussian divergence theorem /11, p.115/, the volume integral on the left hand side can be rewritten as:

$$\iiint_{\Delta V} \sum_{p=1}^{N_p} \nabla \cdot (\rho_p \vec{u}_p) dV = \iint_{\Delta A} \sum_{p=1}^{N_p} \rho_p \vec{u}_p \vec{n} dA , \quad (2.4)$$

where \vec{n} is the outward unit vector of the surface ΔA and $\iint_{\Delta A}$ denotes the integral over the total surface of the control volume.

Inserting eq.(2.4) into eq.(2.3), finally yields:

$$-\iint_{\Delta A} \sum_{p=1}^{N_p} \rho_p \vec{u}_p \vec{n} dA = \sum_{p=1}^{N_p} \int_{\Delta V} \frac{\partial}{\partial t} (\phi \rho_p S_p) dV - \sum_{p=1}^{N_p} q_p . \quad (2.5)$$

Here, the integral on the left hand side is a surface integral over all boundaries of the control volume ΔV . The source/sinks are uniformly distributed over the control volume ΔV :

$$q_p = \frac{1}{\Delta V} \iiint_{\Delta V} q_{p,V} dV . \quad (2.6)$$

Eq.(2.5) is the integral formulation of the flow equation². The method has been used by a variety of researchers, including HEINRICH /12/, NGHIEM /13/, FORSYTH /14/, FUNG et al. /15, 16/, AZIZ and his associates /7, 17, 18/, PALAGI /19/, HEINEMANN et al. /20/, HÄFNER et al. /11, p.114-128/ as well as others /21, 22, 23/. Consequently, the method have been termed a variety of names in the literature, e.g., integral method, integral finite difference method, control volume method, box method and balance method.

²Here, the term "flow equation" is taken generally. Some authors also quote that a flow equation is obtained after inserting a motion equation into the mass balance equation.

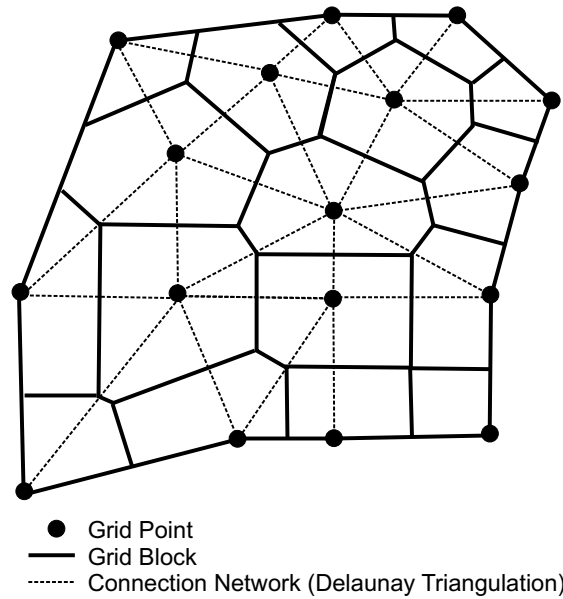


Figure 2.1: Structure of a Voronoi grid system (from PALAGI /19/)

2.2 Grid Geometry

The volume of interest, the domain Ω , is partitioned into imaginary control volumes and the conservation law is locally applied to each fluid phase in the system. To ensure a consistently conservative discretisation scheme, several constraints have to be maintained: (i) the sum over all control volumes must fill the entire solution domain Ω , $\sum_{i=1}^{N_n} V_i = V_\Omega$, (ii) every internal surface A_{ij} must be common to two adjacent control volumes i and j , and (iii) no mass may get lost or accumulated while flowing from cell i into cell j .

The grid system used in this work utilises a specific terminology. The main components are grid blocks, grid points and the network of connection. They are depicted in fig.2.1. The grid, which discretises the area of interest, is assembled by the set of all grid blocks. The mean properties of the grid block are assigned to the corresponding grid point which is representative for the entire grid block. The group of lines connecting neighbouring grid points form, finally, the connection network.

Due to the nature of common reservoir engineering problems, the reservoir geometry is partitioned into layers. The geometric characteristics of each layer (thickness and depth) may vary as functions of position (x-y coordinates); therefore, the major features of the geologic structure can be handled. The conventional stream-tube approach is used to map the areal refinement into the vertical direction, i.e., the horizontal projection of the grid system is the same for all layers.³

The current work facilitates the usage of Voronoi grids. A Voronoi block is defined as the region of space that is closer to its grid point than to any other, and a Voronoi grid is made of such blocks (PALAGI /19/).⁴ In the petroleum literature, the grid is mainly termed PeBi-grid⁵.

³Termed "2.5-dimensional" refinement in the literature, e.g. (GUNASEKERA /24/).

⁴Voronoi polyhedra, in honor of the mathematician (Voronoi, 1908) who first defined these polygonal regions.

⁵Originating from its method of construction by perpendicular bisection.

The connection network is formed by the Delaunay triangulation⁶ which is applied in the grid construction process to find the correct neighbours for all grid points. Mathematically, the major property of the Voronoi grid is its local orthogonality, i.e., the area open to flow between adjacent grid blocks is always orthogonal to the stream line between the corresponding grid points. Further details about the grid geometry as well as generation procedure are provided in section 3.3.

2.3 Discretisation of the Flow Equation

After flow equation and the grid geometry have been introduced, the flow equation, eq.(2.5), has to be discretised by finite-differences.⁷ The main advantages of the control volume method are: (i) applicability to grid blocks of any geometry, i.e., representation of the material balance of an arbitrary control volume, and (ii) exact treatment of known flow rates through external boundaries and boundary conditions in general. On the other hand, the method preserves the simple derivation and handling of finite-difference approximations, the local and illustrative modelling of flow in the neighbourhood of a grid point, and the universality of finite-differences with respect to various types of differential equations (HEINEMANN et al. /20/).

At first, the accumulation term on the right hand side is discretised. For a given grid block, the volume integral in eq.(2.5) can be approximated by means of a simple one-point quadrature formula⁸:

$$\frac{\partial}{\partial t} \int_V (\phi \rho_p S_p) dV = \frac{\partial}{\partial t} \{(\phi \rho_p S_p)_i V_i\} , \quad (2.7)$$

where $(\phi \rho_p S_p)_i$ denotes the average value over V_i . A first order finite-difference is used for the time derivative:

$$\frac{\partial}{\partial t} \{(\phi \rho_p S_p)_i V_i\} = \frac{V_i}{\Delta t} \{(\phi \rho_p S_p)^{n+1} - (\phi \rho_p S_p)^n\} + \epsilon_{acc} , \quad (2.8)$$

with time step level n , time step length Δt and the truncation error of the difference approximation ϵ_{acc} . Eq.(2.8) assumes a stationary grid block volume, i.e., a volume that is invariant in time.

To approximate the surface integral in eq.(2.5), surface A of a grid block i is divided into its subsurfaces A_{ij} for N_n neighbouring blocks:

$$A_i = \sum_{j=1}^{N_n} A_{ij} , \quad (2.9)$$

in order to represent the individual boundaries between the reference grid block i and its neighbours j . The flux F_{ij} of phase p through the boundary-interface A_{ij} can be written

⁶If formed by triangles only.

⁷Finite-Difference Methods are extensively discussed in numerical mathematics textbooks, e.g., THOMAS /25/ and LANGTANGEN /26/ or in reservoir simulation textbooks, e.g., AZIZ and SETTARI /7/, HÄFNER et al. /11/.

⁸Using a higher order quadrature formula, e.g., by means of the trapezoidal rule, leads to an "Extended Balance Method" (HÄFNER et al. /11, p.119/).

2 Physical and Mathematical Model of Multi-Phase Fluid-Flow in Porous Media

as:

$$F_{ij} = \iint_{A_{ij}} \rho_p \vec{u}_p \vec{n} \, dA . \quad (2.10)$$

Consequently, the surface integral in eq.(2.5) can be interpreted as the summation of the fluxes across each interface of the grid block i to its neighbours j :

$$\iint_{\Delta A} \rho_p \vec{u}_p \vec{n} \, dA = \sum_{j=1}^{N_n} F_{ij} = \sum_{j=1}^{N_n} \iint_{A_{ij}} \rho_p \vec{u}_p \vec{n} \, dA . \quad (2.11)$$

To derive a finite-difference expression, one has to approximate the surface A_{ij} and the value of the scalar product $\rho_p \vec{u}_p \vec{n}$ that represents the average component of the velocity vector orthogonal to area A_{ij} . The surface area A_{ij} is a purely geometric property of the grid block and can be computed exactly during the grid generation:

$$\iint_{\Delta A} \rho_p \vec{u}_p \vec{n} \, dA = \sum_{j=1}^{N_n} A_{ij} (\rho_p \vec{u}_p \vec{n})_{ij} . \quad (2.12)$$

The term in the bracket on the right side represents the flux of phase p over interface A_{ij} .

In order to obtain the vector of velocity for each phase in eq.(2.12), velocity \vec{u}_p needs to be related to the pressure gradient of the fluid phase. Traditionally, Darcy's law has been used in petroleum reservoir engineering, which describes velocity as a linear function of the pressure gradient. Its validity is restricted (WTI /27, p.16/). The "lower" limit of Darcy's law, i.e., the occurrence of slippage effects, is usually not of interest for high pressured tight-gas reservoirs and is hence neglected. Darcy's law takes only viscous forces into account, neglecting inertial forces (its "upper limit"). However, such inertial forces can be of interest in tight-gas formations. The present mathematical model therefore incorporates a relationship, which covers viscous, inertial and even turbulent effects. For simplicity, all deviations from Darcy's law are termed non-Darcy effects in the following.⁹

Inertial forces are captured by means of the Forchheimer-equation /29/, where large velocities cause deviations from the linear Darcy flow. This is primarily caused by the continuous de- and acceleration of fluid molecules travelling along a tortuous flow path through the interconnected pores and also in the proppant pack (GEERTSMA /30/).¹⁰ In vector form, it can be written as:¹¹

$$-\text{grad } p = \left(\frac{\mu}{k} + \beta_t \rho |\vec{u}| \right) \vec{u} . \quad (2.13)$$

Here, k is the permeability of the porous media, μ is the dynamic viscosity and β_t denotes the non-Darcy flow coefficient. A value $\beta_t = 0$ marks the transition to Darcy's law. In the simulator,

⁹The terminology "non-Darcy" flow does not imply a change in flow mechanism. Rather, KATZ and LEE /28/ suggested the terminology quadratic Darcy flow (quad-Darcy flow) instead of non-Darcy flow to mark the transition from viscous Darcy flow.

¹⁰It was shown in /28,31/ that friction pressure drops are a result of shear resistance in directions perpendicular to the flow direction, as the cross section of the pore changes its size. The transverse shear causes a separation of the fluid flowing adjacent to the wall which induces a secondary flow.

¹¹In the original work (1901), FORCHHEIMER formulated a general nonlinear constant a where $a = \beta_t \rho$.

2 Physical and Mathematical Model of Multi-Phase Fluid-Flow in Porous Media

permeability is assumed horizontally isotropic and vertically anisotropic. The permeability can be defined as function of the pressure, i.e., $k = f(p)$.

Darcy's law was derived for Newtonian fluids. Such fluids are characterised by: (i) the only stress generated in simple shear flow is the shear stress, (ii) the shear viscosity does not vary with shear rate, (iii) the viscosity is constant with respect to time of shearing and (iv) the stress in the liquid falls to zero immediately when the shearing is stopped. Contrary to this, a variety of important fluids exhibit non-Newtonian behaviour, i.e., the shear rate depends nonlinearly on the shear stress. Such fluids are primarily based on polymers and are often utilised for drilling or fracturing. In the current model, the resistance of those fluids to flow in porous media is captured with the Forchheimer equation, eq.(2.13), and an apparent viscosity¹², $\mu_{\text{app}} = \mu_p(\vec{u}_p)$, which is dependent on the flow velocity. The viscosity reflects the equivalent viscosity of a non-Newtonian fluid moving at the same velocity as its Newtonian fluid counterpart (/33/). The consideration of non-Newtonian fluids is extensively discussed in section 4.4.

Solving eq.(2.13) for the velocity u , while extending to multi-phase flow, yields:

$$\vec{u}_p = -\delta_p \frac{k k_{r,p}}{\mu_p} \text{grad } \Phi_p, \quad \delta_p = \frac{1}{1 + \frac{\beta_t \rho_p k k_{r,p}}{\mu_p} |\vec{u}_p|}, \quad (2.14)$$

with a control parameter δ_p accounting for the non-Darcy flow and the relative phase permeability $k_{r,p}$.

The classical model of simultaneous flow of immiscible fluids in porous media was constructed in the late thirties-early forties by MUSKAT and LEVERETT. The model was based on the assumption of local equilibrium, according to which the relative phase permeabilities $k_{r,p}$ and the capillary pressure p_{cap} can be expressed through the universal functions of the local saturation S_p (BARENBLATT et al. /34, 35/):

$$k_{r,p} = f(S_p), \quad p_{\text{cap}} = f(S_p). \quad (2.15)$$

A more thorough outline of the concepts of multi-phase flow theory can be found in reservoir engineering textbooks, such as DAKE /36/, LAKE /10/, CHIERICI /37/ or HELMIG /38/.

2.3.1 CVFD Formulation

Since the interface of two grid blocks i and j is orthogonal to the streamline between both grid points, the flux F_{ij} is a function of the potential only between the two grid blocks. Hence, the potential gradient is parallel to the streamline between i and j and can be approximated with a first order finite-difference:

$$|\text{grad } \Phi_p|_{ij} = \frac{\Phi_{p,j} - \Phi_{p,i}}{h_{ij}} + \epsilon_{\text{flow}}, \quad (2.16)$$

where h_{ij} is the distance between both grid points and ϵ_{flow} is the truncation error of the finite-difference formulation. Eq.(2.16) is typically termed a two-point flux stencil. Inserting eq.(2.16) into eq.(2.14) while neglecting ϵ_{flow} gives the velocity between grid points i and j :

$$u_p = -\delta_p \frac{k k_{r,p}}{\mu_p} \frac{\Phi_{p,j} - \Phi_{p,i}}{h_{ij}}. \quad (2.17)$$

¹²VALKO and ECONOMIDES /32, p.111/ called it "equivalent Newtonian viscosity".

2 Physical and Mathematical Model of Multi-Phase Fluid-Flow in Porous Media

Single point upstream weighting is used to calculate fluid properties and the mobility Λ , i.e.:

$$\Lambda_{ij} = \frac{k_{r,p}}{\mu_p} = \begin{cases} \Lambda_i, & (k\nabla\Phi_p)\cdot\vec{n} > 0 \\ \Lambda_j, & (k\nabla\Phi_p)\cdot\vec{n} < 0 \end{cases} \quad (2.18)$$

Upstream weighting is a first order scheme and presents just one possibility for evaluating the phase properties at the cell interface. Further methods have been introduced and extensively discussed in reservoir engineering, e.g., in HELMIG /38/. Additionally, the mobility can be evaluated by considering the direction of the flow process to incorporate hysteresis phenomena (i.e., separately for a drainage and imbibition processes).

After introducing the geometrical transmissibility T_{ij} :

$$T_{ij} = \frac{kA_{ij}}{h_{ij}}, \quad (2.19)$$

which is classically derived by means of harmonic averaging (AZIZ and SETTARI /7, p.83 foll./), the discretised form of the flow equation can finally be written as:

$$\sum_{j=1}^{N_n} (\delta_p \rho_p T_{ij} \Lambda_{ij} (\Phi_{p,j} - \Phi_{p,i}))^{n+1} = \frac{V_i}{\Delta t} \{ (\phi \rho_p S_p)^{n+1} - (\phi \rho_p S_p)^n \} - \rho_p q_{p,i,k}^{n+1}, \quad (2.20)$$

provided that truncation errors are small. In contrast to the accumulation term, the finite-difference approximation of the flux term strongly depends on the grid system. The use of curvilinear, cartesian or radial coordinates leads to different forms of the transmissibility coefficient.

2.4 Auxiliary Equations

Constitutional Relations. The mathematical model developed so far features mass conservation equations for three phases, each with two unknowns (phase saturation and phase pressure). Since there are only three continua equations, the set is undetermined and additional information is necessary. These equations define the intrinsic response of the physical system and depend on the internal constitution of the particular materials considered. They are termed constitutional equations (BEAR /9, p.82-83/).

The pore volume must always be filled by the fluids present; thus, a general volume balance for N_p phases can be stated:

$$\sum_{p=1}^{N_p} S_p = 1. \quad (2.21)$$

The pressures of the individual phases correlate with saturations by applying the concept of

2 Physical and Mathematical Model of Multi-Phase Fluid-Flow in Porous Media

capillarity:

$$p_w = p_{\text{gel}} - p_{\text{cap,gelw}}(S_w) \quad (2.22)$$

$$p_g = p_{\text{gel}} + p_{\text{cap,ggel}}(S_g) , \quad (2.23)$$

where p_{cap} represents the capillary pressure between the adjacent phases. The three constitutional equations complete the set of equations.

Fluid and Rock Properties. Eq.(2.20) contains variables which depend on the solution, such as the density $\rho_p(p)$ and the porosity $\phi(p)$. In case of slightly compressible fluids, constant compressibility c_{fl} is assumed for calculation of the density $\rho_p(p)$:

$$\rho_p = \rho_0^{c_{\text{fl}}(p-p_0)} . \quad (2.24)$$

For gas flow, it is not appropriate to assume a constant compressibility. The dependence of the pore volume on the fluid pressure is taken into account with:

$$\phi = \phi_0^{c_r(p-p_0)} , \quad (2.25)$$

where c_r denotes the compressibility of the rock.

2.5 Final Set of Equations

The density ρ_p is replaced by the formation volume factor $B_p = V_p/V_0 = B_0\rho_0/\rho_p$, since B_p is more common in the oil and gas industry. The index 0 specifies the reference conditions. Finally, the flow equation, eq.(2.20), can then be written as:

$$\sum_{j=1}^{N_n} \left(\delta_p T_{ij} \frac{\Lambda_{ij}}{B_p} (\Phi_{p,j} - \Phi_{p,i}) \right)^{n+1} = \frac{V_i}{\Delta t} \left\{ \left(\frac{\phi S_p}{B_p} \right)^{n+1} - \left(\frac{\phi S_p}{B_p} \right)^n \right\} - q_{p,i,k}^{n+1} , \quad (2.26)$$

with flow rate from any source/sink $q_{p,i,k}$, measured at reference conditions. The potentials are calculated as below:

$$\begin{aligned} (\Phi_{g,j} - \Phi_{g,i}) &= p_{g,j} - p_{g,i} - \bar{\rho}_g g(Z_j - Z_i) \\ &= p_{\text{gel},j} - p_{\text{gel},i} - \bar{\rho}_g g(Z_j - Z_i) + p_{\text{cap,ggel},j} - p_{\text{cap,ggel},i} , \end{aligned} \quad (2.27)$$

$$(\Phi_{\text{gel},j} - \Phi_{\text{gel},i}) = p_{\text{gel},j} - p_{\text{gel},i} - \bar{\rho}_{\text{gel}} g(Z_j - Z_i) , \quad (2.28)$$

$$\begin{aligned} (\Phi_{w,j} - \Phi_{w,i}) &= p_{w,j} - p_{w,i} - \bar{\rho}_w g(Z_j - Z_i) \\ &= p_{\text{gel},j} - p_{\text{gel},i} - \bar{\rho}_w g(Z_j - Z_i) - p_{\text{cap,gelw},j} + p_{\text{cap,gelw},i} , \end{aligned} \quad (2.29)$$

where the density $\bar{\rho}_g$ is evaluated with the arithmetic mean and Z is the depth of the grid block center.

2.6 Discussion

The physical and mathematical model developed in this chapter is based on the conceptual model of multi-phase flow in porous media, with respect to the objective of the thesis. Thus, the physical model is primarily affected by the processes actually occurring in tight-gas reservoirs.

2 Physical and Mathematical Model of Multi-Phase Fluid-Flow in Porous Media

According to the typical fluid system in tight reservoirs, the mathematical model facilitates the consideration of three immiscible phases, which is a special case of the common Black-Oil model. Solution of gas in water or the third phase is assumed negligible. With the current insight into the processes, this simplification can be considered sufficiently accurate for the treatment of engineering problems in such reservoirs. There is no need for a more sophisticated compositional model yet.

Special emphasis is placed on the flow regimes. Here, the flow is isothermal with either laminar or non-laminar characteristics. Inertial effects and non-Newtonian fluids are important with regard to the stimulation treatments, such as hydraulic fracturing, and are hence included in the formulation. The current approach utilises the third phase to represent technical fluids. Consideration of mixing or solution processes (with the water phase) is therefore excluded.

Reservoir rocks are considered to be stress-sensitive if their fluid-flow characteristics change substantially with changes in effective stresses. Stress-sensitivity increases in low-permeability reservoirs. That affects permeability, porosity and pore compressibility, causing changes in reservoir productivity. In the current physical model, provision is made to account for stress dependency of the permeability and of the porosity. However, a more rigorous or stronger coupling could be considered in the future, i.e., by the fully coupled solution of geomechanical and fluid-flow equations.

The integral form of the flow equation applies to any geometry, independent of the dimensionality of the problem. Hence, the spatial discretisation by means of a grid is not predefined *a priori*. Areal isotropic (but heterogeneous) permeability is a special requirement to facilitate Voronoi grids. Full tensorial permeability is generally not considered due to its extremely complex numerical treatment and the lack of data in common tight-gas reservoirs.

3 Simulator Development

The following chapter briefly describes the development of the three-phase reservoir simulation tool. In particular, the implementation of the physical model of multi-phase flow in porous media is illustrated by means of essential numerical techniques. Emphasis is placed on the open design, and hence, on the fundamental ideas of a flexible and adaptable code for application in tight-gas reservoirs.

3.1 Computational Model

Simulator development is a complex process. Furthermore, its development involves all the stages concerning conception, coding, validation and finally its application. Here, the tool is designed as research-code with the following ideas and requirements: (i) test of algorithms, (ii) integration of new concepts, (iii) flexibility, (iv) adaptability for a variety of problems (e.g., specifics of hydraulic fractures, underbalanced drilling, well test analysis), (v) robustness, and finally (vi) its performance.

The fundamental conceptual design of the reservoir simulation tool under development can be summarised:

- To ensure local mass conservation, a control-volume method based on finite-difference discretisation is chosen as the discretisation technique (see previous chapter).
- A general, unstructured grid approach is realised to facilitate arbitrary geometries (see previous chapter).
- Robustness and stability are achieved by using a fully implicit time discretisation.
- The highly nonlinear physical model of multi-phase flow is linearised by means of Newton's method and solved iteratively. Derivatives in the Jacobian matrix are derived numerically by finite-difference approximations.
- Both direct and iterative solvers are implemented for the solution of the system of linear algebraic equations.
- Derivation of underlying dependencies in the model (such as relative permeabilities, capillary pressure, gas properties, material parameters) is solely considered by either conventional table lookups or by correlations.
- The code is realised by means of a MATLAB-FORTRAN coupling. Formulation of the set of equations is accomplished within a highly efficient Fortran-environment and linked with MATLAB (/39/), where pre- and postprocessing as well as simulator control are performed.

3.1.1 Newton's Method

The residual form of the fluid-flow equation (as derived in the preceding chapter) at each grid block for phase p is:

$$R_{p,i} = \sum_{j=1}^{N_n} \delta_{ij}^{n+1} T_{ij} \left(\frac{\Lambda_{ij}}{B_p} \right)_{ij}^{n+1} (\Phi_{p,j} - \Phi_{p,i})^{n+1} - \frac{V_i}{\Delta t} \left[\left(\frac{\phi S_p}{B_p} \right)^{n+1} - \left(\frac{\phi S_p}{B_p} \right)^n \right] + q_{p,i,k}^{n+1} = 0 \quad p = g, w, \text{gel} . \quad (3.1)$$

The system of N discretised equations consists of three residual equations for the gas, water and gel phases. The set of residual equations (3.1) forms a system of highly nonlinear equations.

In order to solve the system of nonlinear equations in the current model, Newton's method is applied. A linear approximation is made to the nonlinear residual equations. The resulting linear equations are solved simultaneously for pressure and saturation changes. In order to obtain a sufficiently small value for the residuals, this process is repeated several times. Extensive discussions of the underlying theory can be found in textbooks of numerical mathematics, such as FAIRES and BURDEN /40/, SCHWETLICK and KRETZSCHMAR /41/, PRESS et al. /42/, LANGTANGEN /26/ or in reservoir simulation textbooks, e.g., AZIZ et al. /7,8/. For the sake of completeness, Newton's method is briefly summarised at first.

For the given system of residual equations in vectorial form:

$$\vec{R}(\vec{X}) = 0 , \quad (3.2)$$

the solution vector \vec{X} is obtained by the iterative procedure:

$$\vec{X}^{k+1} = \vec{X}^k - \frac{\vec{R}(\vec{X}^k)}{\vec{R}'(\vec{X}^k)} , \quad k > 1 , \quad (3.3)$$

starting from an initial estimate \vec{X}^k . Here, the iteration counter is denoted with k . The matrix of partial derivatives $\vec{R}'(\vec{X}^k)$ in eq.(3.3) is the Jacobian matrix \mathbf{J} :

$$\mathbf{J}(\vec{X}^k) = \vec{R}'(\vec{X}^k) = \left(\frac{\partial R_i(\vec{X}^k)}{\partial X_j} \right) . \quad (3.4)$$

Then, eq.(3.3) can be rewritten as:

$$\vec{X}^{k+1} = \vec{X}^k - \mathbf{J}(\vec{X}^k)^{-1} \vec{R}(\vec{X}^k) . \quad (3.5)$$

Since numerical effort of matrix inversion is high, a vector $(\delta \vec{X})^k$ is calculated instead, which satisfies the condition:

$$\mathbf{J}(\vec{X}^k)(\delta \vec{X})^k = -\vec{R}(\vec{X}^k) . \quad (3.6)$$

Then, the new approximation of the solution vector \vec{X}^{k+1} is the sum of the 'old' solution vector

3 Simulator Development

\vec{X}^k and $(\delta\vec{X})^k$:

$$\vec{X}^{k+1} = \vec{X}^k + (\delta\vec{X})^k . \quad (3.7)$$

The Newtonian iteration has second-order convergence characteristics. Given a proper choice of the initial estimate \vec{X}^0 , convergence normally occurs rapidly.

The derivative terms in the Jacobian are calculated numerically by substituting the partial derivatives by difference quotients, known as the discretised Newton's method. That is:

$$\frac{\partial R(X_i)}{\partial X_i} = \frac{R(X_i + \epsilon) - R(X_i)}{\epsilon} , \quad (3.8)$$

where ϵ is the perturbation variable (or discretisation step width). Examples of using numerical Jacobian have been presented, e.g., by AU and VINSOME /43/.

SCHWETLICK and KRETZSCHMAR /41/ stated that convergence behaviour is similar to Newton's method based on analytical derivatives.¹ To ensure proper convergence, Jacobian calculation in the simulator kernel utilises double precision with a relative accuracy of 10^{-15} . The ϵ -value in the simulator is fixed at 10^{-6} , resulting from a sensitivity analysis with respect to the number of nonlinear iterations.²

The numerical effort to calculate the numerical derivatives is analog to the analytical approach. Instead of N^2 derivatives, N^2 residual evaluations $R_i(X^k + \epsilon)$ evolve. However, complexity in the code is drastically reduced since the algorithms to derive the accumulation and flux terms are applicable for both the residual and the Jacobian calculation; there is no need for any subroutines computing the derivatives. Furthermore, the highly nonlinear residual equations regarding, e.g., non-Darcy flow and non-Newtonian fluids, imply complicated and lengthy derivatives. Thus, due to the complex physical system considered here and the aim of flexibility, the numerical derivation of Jacobian matrix drastically eases the simulator development while maintaining the convergence behaviour of Newton's method.

3.1.2 Connection List Approach

A major objective of the simulator development is the flexibility in spatial discretisation. There are two basic requirements: (i) the kind of geometry ought to be arbitrary (such as radial, Cartesian or entirely unstructured grid systems), and (ii) there exists no distinct dimensionality, i.e., the extension in one, two or three dimensions is not predefined.

Traditionally, discretisation in reservoir simulation is of a structured nature. For a 3D Cartesian grid there is a major x (i -index), y (j -index) and z (k -index) direction, provided that grid blocks are ordered in a regular scheme. By tracking the neighbouring connections on a grid block basis, the residual equations must include all possible connections.³ Furthermore, source/sink terms have to be included as well as non-neighbour connections, which can arise at sealing faults. Accordingly, the resulting residual form of the material balance equation can become lengthy.

¹The authors suggested to choose ϵ based on the solution vector: $\epsilon_j = \tau_r(\|X_j^k\| + \tau_a)$ with $\tau_a = 10^{-3}$ and $\tau_r \approx 10^{-3} \dots 10^{-5}$. However, to avoid cancellation errors, τ_r needs to be larger than the square root of the computation accuracy.

²Although the nonlinear iteration number turns out to be almost unaffected in the range $10^{-5} - 10^{-8}$.

³For a 2D Cartesian model there are four inter-block flux terms and for a 3D model there are six (as long as a two-point scheme is used).

3 Simulator Development

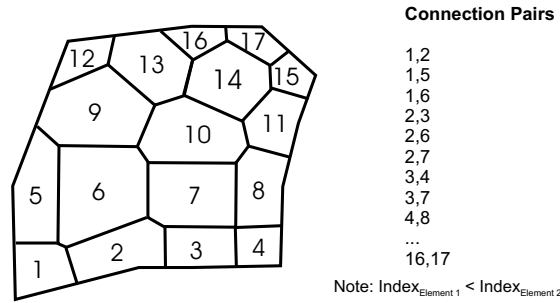


Figure 3.1: Illustration of the connection list approach

A main disadvantage of the block-based approach is the necessity in the algorithm to evaluate every term in the residual equation, and return a zero flux even if there is no physical connection. This is particularly the case if a 3D code is applied for a 1D geometry. Contrary to this, the calculation of inter-block fluxes is only necessary when pairs of grid blocks are connected. A further disadvantage of the approach is that different geometries are not readily implemented into such predefined structures. When irregular grids are used, these algorithms become complicated or even inapplicable because there are no distinct $i + 1$ or $i - 1$ directions.

Concentrating instead on the physics, the connection list approach is used, as presented by LIM et al. /44/ and applied by CAO /45/. Here, the focus is on the connections instead of grid blocks, when computing the flux terms. Each grid node may have a variable and arbitrary number of neighbouring or connected nodes, depending on the grid geometry. A connection pair can result from any linkage between nodes, such as arising between neighbouring grid blocks, source/sink nodes, well flow nodes or surface facility nodes. The simulator is devoid of any addressing or computational concepts founded upon the conventional " $i - j - k$ addressing". As BECKNER et al. /46/ stated, this fundamental departure influences code design as well as the construction of simulation models.

The simulator kernel, where Jacobian and residuals are computed, is free of any geometrical or gridding constraints. Rather, the preprocessor establishes an array map, where all possible pairs of connections are specified. Such a list is depicted in fig.3.1. In the connection list, (i) there are only two elements for each connection, (ii) the pairs of connected grid blocks are not repetitive, and (iii) no-flow boundaries imply the absence of connections and do, therefore, not appear (/44/).

Once the connection array has been established, the computation algorithm is exactly the same for 1D, 2D, or 3D models. The connection list contains, besides the node numbers, the geometric part of the transmissibility, which is a function of the grid geometry and block properties. The blocks are addressed by a unique number instead of spatial indices i, j, k . Necessary grid block data, such as volumes, depths and coordinates, are stored in a reference array.

The simulation domain, i.e., the reservoir under consideration, can be divided into arbitrary districts of certain properties. Thus, a further vector tracks the regional affiliation of each grid block with information regarding: (i) the saturation function type, (ii) PVT-properties region, (iii) non-Darcy flow region, and (iv) rock type region.

3.1.3 Assembling the System of Equations

After the connection list has been established, both the residuals as well as the Jacobian are computed in the simulator kernel. This is simply accomplished by processing the connection list from the first to the last entry and storing the result in a sparse matrix. Therefore, the system of residual eqs.(3.1) can be expressed as the sum of its components /44/, where:

$$\vec{R} = \vec{F}_b - \vec{A} + \vec{F}_w . \quad (3.9)$$

F_b , F_w and A represent the fluxes between connected grid blocks, between source/sinks and grid blocks, and the accumulation in the grid blocks, respectively. First, the accumulation term is evaluated for each grid block. The second step involves the computation of flux terms between connections by traversing the entries in the connection list. For each pair of connected nodes, the flux is computed. A positive flux or influx is assigned to the downstream block, and the upstream block is assigned a negative flux.

The Jacobian can be similarly treated:

$$\mathbf{J} = \frac{\partial \vec{R}}{\partial \vec{X}} = \frac{\partial \vec{F}_b}{\partial \vec{X}} - \frac{\partial \vec{A}}{\partial \vec{X}} + \frac{\partial \vec{F}_w}{\partial \vec{X}} . \quad (3.10)$$

The partial derivative of the accumulation term, $\partial \vec{A} / \partial \vec{X}$, is computed at first. It only contributes to the diagonal elements of the Jacobian because this term is not affected by the properties of neighbouring blocks. Subsequently, the connection list is processed by evaluating all derivatives resulting from the flux terms, and adding them to the Jacobian elements at locations where cross derivatives exist. To illustrate the methodology, the procedure is demonstrated for one connection between nodes i and j . There, the flux F_{ij} depends on the two primary variables X_i and X_j . The derivative terms $\partial F_{ij} / \partial X_i$ and $\partial F_{ij} / \partial X_j$ are calculated and assigned to the corresponding positions in the Jacobian. Again, since a positive flux into node i implies a negative flux for node j , each connection pair actually yields four derivative terms:

$$\frac{\partial F_{ij}}{\partial X_i} = \frac{F_{ij}(X_i + \epsilon) - F_{ij}(X_i)}{\epsilon} = -\frac{\partial F_{ji}}{\partial X_i} \quad (3.11)$$

and

$$\frac{\partial F_{ij}}{\partial X_j} = \frac{F_{ij}(X_j + \epsilon) - F_{ij}(X_j)}{\epsilon} = -\frac{\partial F_{ji}}{\partial X_j} . \quad (3.12)$$

The terms $F_{ij}(X_i)$ and $F_{ij}(X_j)$ have already been evaluated when computing the residual array.⁴ Hence, only two function evaluations, $F_{ij}(X_i + \epsilon)$ and $F_{ij}(X_j + \epsilon)$, are necessary to compute the derivatives.

The residual array \vec{R} for N_b grid blocks at time step $(n + 1)$ is organised as follows:

$$\vec{R}^{n+1} = \{ [R_{\text{gel},1}, R_{w,1}, R_{g,1}, \dots, R_{\text{gel},N_b}, R_{w,N_b}, R_{g,N_b}]^T \}^{n+1} . \quad (3.13)$$

The primary variables in the solution vector \vec{X} are the gel pressure p_{gel} and the saturations S_w

⁴Since i -index entries in the connection list always ascend, only the upper-triangular elements of the Jacobian are computed. The lower-triangular entries are derived by a simple sign change /44/.

3 Simulator Development

and S_g . Accordingly, the solution vector \vec{X} is stored:

$$\vec{X}^{n+1} = \{[p_{\text{gel},1}, S_{w,1}, S_{g,1}, \dots, p_{\text{gel},N_b}, S_{w,N_b}, S_{g,N_b}]^T\}^{n+1}. \quad (3.14)$$

In a two-phase case, the solution vector consists of the gas phase pressure p_g and the water saturation S_w .

The Jacobian \mathbf{J} takes the form:

$$\mathbf{J} = \begin{bmatrix} \begin{bmatrix} \frac{\partial R_{\text{gel},1}}{\partial p_{\text{gel},1}} & \frac{\partial R_{\text{gel},1}}{\partial S_{w,1}} & \frac{\partial R_{\text{gel},1}}{\partial S_{g,1}} \\ \frac{\partial p_{\text{gel},1}}{\partial R_{w,1}} & \frac{\partial S_{w,1}}{\partial R_{w,1}} & \frac{\partial S_{g,1}}{\partial R_{w,1}} \\ \frac{\partial p_{\text{gel},1}}{\partial R_{g,1}} & \frac{\partial S_{w,1}}{\partial R_{g,1}} & \frac{\partial S_{g,1}}{\partial R_{g,1}} \\ \frac{\partial p_{\text{gel},1}}{\partial p_{\text{gel},1}} & \frac{\partial S_{w,1}}{\partial S_{w,1}} & \frac{\partial S_{g,1}}{\partial S_{g,1}} \end{bmatrix} & \dots & \begin{bmatrix} \frac{\partial R_{\text{gel},1}}{\partial p_{\text{gel},N_b}} & \frac{\partial R_{\text{gel},1}}{\partial S_{w,N_b}} & \frac{\partial R_{\text{gel},1}}{\partial S_{g,N_b}} \\ \frac{\partial p_{\text{gel},1}}{\partial R_{w,1}} & \frac{\partial S_{w,1}}{\partial R_{w,1}} & \frac{\partial S_{g,1}}{\partial R_{w,1}} \\ \frac{\partial p_{\text{gel},1}}{\partial R_{g,1}} & \frac{\partial S_{w,1}}{\partial R_{g,1}} & \frac{\partial S_{g,1}}{\partial R_{g,1}} \\ \frac{\partial p_{\text{gel},1}}{\partial p_{\text{gel},N_b}} & \frac{\partial S_{w,1}}{\partial S_{w,N_b}} & \frac{\partial S_{g,1}}{\partial S_{g,N_b}} \end{bmatrix} \\ \vdots & & \vdots \\ \begin{bmatrix} \frac{\partial R_{\text{gel},N_b}}{\partial p_{\text{gel},1}} & \frac{\partial R_{\text{gel},N_b}}{\partial S_{w,1}} & \frac{\partial R_{\text{gel},N_b}}{\partial S_{g,1}} \\ \frac{\partial p_{\text{gel},1}}{\partial R_{w,N_b}} & \frac{\partial S_{w,1}}{\partial R_{w,N_b}} & \frac{\partial S_{g,1}}{\partial R_{w,N_b}} \\ \frac{\partial p_{\text{gel},1}}{\partial R_{g,N_b}} & \frac{\partial S_{w,1}}{\partial R_{g,N_b}} & \frac{\partial S_{g,1}}{\partial R_{g,N_b}} \\ \frac{\partial p_{\text{gel},1}}{\partial p_{\text{gel},1}} & \frac{\partial S_{w,1}}{\partial S_{w,1}} & \frac{\partial S_{g,1}}{\partial S_{g,1}} \end{bmatrix} & \dots & \begin{bmatrix} \frac{\partial R_{\text{gel},N_b}}{\partial p_{\text{gel},N_b}} & \frac{\partial R_{\text{gel},N_b}}{\partial S_{w,N_b}} & \frac{\partial R_{\text{gel},N_b}}{\partial S_{g,N_b}} \\ \frac{\partial p_{\text{gel},1}}{\partial R_{w,N_b}} & \frac{\partial S_{w,1}}{\partial R_{w,N_b}} & \frac{\partial S_{g,1}}{\partial R_{w,N_b}} \\ \frac{\partial p_{\text{gel},1}}{\partial R_{g,N_b}} & \frac{\partial S_{w,1}}{\partial R_{g,N_b}} & \frac{\partial S_{g,1}}{\partial R_{g,N_b}} \\ \frac{\partial p_{\text{gel},1}}{\partial p_{\text{gel},N_b}} & \frac{\partial S_{w,1}}{\partial S_{w,N_b}} & \frac{\partial S_{g,1}}{\partial S_{g,N_b}} \end{bmatrix} \end{bmatrix} \quad (3.15)$$

The variables in the solution vector are scaled, since the values range in several orders of magnitudes. Therefore, all derivatives with respect to saturations in eq.(3.15) and the entire residual array are divided by the maximum pressure $\|p_{\text{gel}}^k\|_{\text{max}}$. After the solution of the linear system, all entries in the solution vector are accordingly in a range 0...1. In order to obtain the correct pressures for the convergence checks and the new iteration, all pressure entries in the solution vector need finally to be multiplied with $\|p_{\text{gel}}^k\|_{\text{max}}$.

3.1.4 Solution of the Linear System of Equations

Computing the change of the solution vector $(\delta\vec{X})^k$ at iteration k (eq.(3.6)) and updating the solution vector \vec{X} (eq.(3.7)) is repeated until the variable change tolerances:

$$\|\delta p_{\text{gel}}^{k+1}\|_{\text{max}} < \tau_p \quad (3.16)$$

$$\|\delta S_{w,g}^{k+1}\|_{\text{max}} < \tau_S \quad (3.17)$$

$$\left\| \frac{R_p^{k+1} B_p \Delta t}{\phi S_p} \right\|_{\text{max}} < \tau_{R,\text{norm}} \quad (3.18)$$

are satisfied, where the norms are based on the maximum value (l_∞). The tolerance parameters τ_p and τ_S are problem dependent; for typical cases they are set to 10^3 Pa for the pressure (τ_p) and $5 \cdot 10^{-3}$ for the saturations (τ_S) /8, p.172/. According to eq.(3.2), $(\delta\vec{X})^k$ will be small if the residual \vec{R} diminishes (for a well conditioned problem). Conventional automatic time step control is applied, such as discussed by GRABOWSKI et al. /47/ or SAMMON and RUBIN /48/.

The solution of the linearised matrix system, eq.(3.6), is obtained with an iterative GMRES-solver, which determines the minimal residual solution of the linear system over a shifted Krylov space using the standard GMRES algorithm given in /49/. Preconditioning is performed by incomplete LU-factorisation as implemented in MATLAB /39/. However, MATLAB also provides

3 Simulator Development

a highly efficient sparse direct solver, which is conveniently utilised for small to medium scale simulation problems. The direct solver is a variant of Gaussian elimination. It uses either LU or Cholesky factorisation, depending on the computing costs. The required tests for triangularity and symmetry of the square Jacobian matrix are automatically performed in MATLAB /39/. The experiences of the author indicate that the direct solver is more reliable and robust than the iterative solver, in particular for structured systems (even for several ten thousand equations).⁵

The simulation tool utilises a natural ordering scheme (/7, p.247/), where grid blocks are enumerated according to their x and y coordinate. The natural ordering may not be the most efficient ordering scheme for these solvers (BEHIE and FORSYTH /50/). This scheme is selected here because it is very easily implemented. A scheme, which is based on the actual values of the matrix coefficients instead of its non-zero structure, was presented by D'AZEVEDO et al. /51/. Their scheme was developed especially for unstructured matrices with highly heterogeneous absolute permeability and preconditioners that use incomplete Gaussian elimination. Such a scheme might improve the performance of the iterative solvers.

Currently, an algebraic multigrid solver (SAMG /52/) is implemented to achieve a more powerful unstructured grid linear solver. That will be especially important if geometry is extended to true 3D unstructured grids (apart from the currently used 2.5D discretisation).

Linearisation of Non-Darcy Flow. Although fully implicit schemes have been introduced for solution of non-Darcy flow (ECLIPSE /53, p.567-577/), the current code uses an implicit realisation by iteration (LI and ENGLER /54/). In order to calculate the new solution, the new control parameter δ_p^{k+1*} is calculated at first, where δ_p^k is used to calculate the velocity u_p^* .

$$\delta_p^{k+1*} = \frac{1}{1 + \frac{\beta_t^k \rho_p^k k_{r,p}^k}{\mu_p^k} |u_p^*|}, \quad u_p^* = -\delta_p^k \frac{k_{r,p}^k}{\mu_p^k} \text{grad } \Phi_p^k. \quad (3.19)$$

Subsequently, the velocity for the new iteration $k + 1$ can be computed. To avoid oscillations, the control parameter for the next iteration needs to be damped:

$$\delta_p^{k+1} = \delta_p^k + (\delta_p^{k+1*} - \delta_p^k) * \text{RP}, \quad (3.20)$$

where RP denotes a relaxation parameter. Best results could be achieved with $\text{RP} = 0.4..0.6$. The total number of Newton's iterations required for non-Darcy flow are slightly increased compared with Darcy flow ($\delta_p = 1$). For common three-phase problems, 2-4 iterations are taken until solution convergence. Contrary to the fully implicit treatment, where non-Darcy effects are not supposed to be large (ECLIPSE /55, p.1634/), the present approach facilitates even the consideration of extremely "turbulent" flow with control parameters $0 < \delta_p \ll 1$.

3.2 Consideration of Wells and Boundary Conditions

Boundary conditions specify how the reservoir interacts with its surrounding area. A comprehensive outline of realisation of different boundary conditions in reservoir simulation can be found in AZIZ and SETTARI /7, p.184-191/.

⁵ The computational time spent to solve the matrix system is more affected by the band width of the Jacobian matrix for solvers that are based on complete Gaussian elimination than for solvers that are based on incomplete Gaussian elimination (PALAGI /19, p.77/).

3.2.1 Treatment of Boundary Conditions

By default, the connection based approach implies a no-flow condition at the outer boundary $\partial\Omega$, i.e.:

$$\left. \frac{\partial\Phi}{\partial n} \right|_{\partial\Omega} = 0, \quad (3.21)$$

because no connection exists between the boundary block and the external area. Due to the flexible gridding approach, no extra provision is made to specify a non-zero flux in terms of a general Neumann-condition.⁶ Due to its significance in tight-gas reservoirs, emphasis is placed on the realisation of constant pressure/constant saturation conditions. Therefore, the simulation tool utilises a special active/passive-block technique.

Each grid block is characterised by a status which corresponds to one of the following three situations:

1. The grid block is fully active. Pressure and saturations are unknown *a priori* (except for the initial conditions). (STATUS=1)
2. Pressures and, optionally, saturations of the grid block are explicitly specified, which are constant for the corresponding time step. This block can be either a boundary grid block, a inner boundary block or a well grid block (explained in the next section). (STATUS=2)
3. The grid block is passive and is excluded from the solution. Passive blocks do not affect other grid blocks. (STATUS=3)

By default, all grid blocks are assumed active (STATUS=1). Only the active grid blocks are considered for establishing the residual array and the Jacobian matrix by means of an internal re-numbering of all active grid blocks. This reduced system of equations is solved by the linear solver. The gaps in the 'full' solution vector (due to the blocks with status 2 or 3) are filled with zero entries. This procedure is repeated until the solution has converged within the time step.

The difference in treatment of blocks of (STATUS=2) and (STATUS=3) is in the way of calculating the fluxes. No mass exchange occurs between a passive block and its neighbours. On the contrary, if the boundary condition is fixed (STATUS=2) the block still communicates with the neighbouring blocks. This approach enables the flexible and time dependent specification of conditions prevailing in any grid block of the domain. Additionally, it is not restricted to blocks at the outer boundary of the reservoir.

3.2.2 Implementation of Wells in the Simulation Model

Traditionally, wells are non-discretely completed in large grid blocks. It has long been recognised that the pressure of the well block is not equivalent to the bottomhole flowing pressure at the well, because, in general, the grid block dimensions are substantially larger than the wellbore radius (VAN POOLEN et al. /56/, PEACEMAN /57/). Therefore, so called well models are traditionally used to relate these two pressures.

⁶Flow rates across borders or wells can be conveniently specified via the appropriate entry in the source/sink vector, which is a common simplification for multi-phase flow in full scale reservoir simulation models (/7/).

3 Simulator Development

In contrast to the conventional methodology, the well is represented by discrete grid blocks in the current model⁷ with a realistic diameter (according to the user specification). Although these blocks do not belong to the reservoir, they are fully incorporated in the block system and handled accordingly (i.e., solved fully implicitly). The porosity of the block is chosen arbitrarily large to avoid instabilities.

As HEINEMANN /59/ stated before, there are a variety of advantages against the usage of non-discrete well models: (i) no extra residual equations arise for the well, (ii) no supplementary equation is necessary to calculate the flowing bottomhole pressure of the well, since the computed block pressure of the wellbore block is already the well flowing pressure, (iii) no difficulties are encountered when calculating the production rate for multiple perforations, and (iv) crossflow is automatically integrated into the model. Of course, in the case of simulating field studies without special well grids, a well model needs to be implemented. However, since detailed investigations with corresponding grid systems are in the focus, this has not yet been accomplished.

The transmissibilities between the well blocks and the neighbouring blocks are derived by means of the common harmonic averaging. For a radial well in a single layer reservoir, transmissibility between well block i and block j is /53/:

$$T_{r,ij} = \frac{k_r \Theta_r h}{\frac{r_{j,\text{out}}^2}{r_{j,\text{out}}^2 - r_w^2} \ln \left(\frac{r_{j,\text{out}}}{r_w} \right) - 0.5}, \quad (3.22)$$

with the radial reservoir permeability k_r , segment angle Θ_r , thickness h , outer radius $r_{j,\text{out}}$ of grid block j and the well radius r_w . If the well is perforated in multiple layers, non-existing or shut perforation zones can be realised by setting the corresponding transmissibilities in the connection list to zero. The well grid blocks are treated as an independent "rock" region. There are no capillary forces ($p_{\text{cap}} = 0$) and relative phase permeabilities are set equal to the corresponding phase saturation ($k_{r,p} = S_p$).

Typical well constraints are rate and pressure conditions. In addition, situations may arise with a specified saturation in the well, which is important for simulation of underbalanced drilling (UBD). In such a case of predefined pressure and saturation, the well grid block is handled with STATUS=2. The net influx of each phase into the well grid blocks represents the well flow rate for the pressure boundary condition. Contrary to this, constant rate production is realised by setting the well flow rate into the source/sink vector, eq.(2.20). Here, the grid blocks are marked with STATUS=1. If the well is multiply perforated, the entire well flux is assigned to the uppermost grid block.

Advanced Well Flow Modelling Option. The discrete treatment of the well allows for further applications. The need to simulate advanced wells (horizontal and multilateral wells, or 'smart' wells containing flow control devices) requires a correspondingly sophisticated type of well model to be implemented in reservoir simulators, such as presented by HOLMES et al. /61/. The model must be able to determine the local flowing conditions (the flow rate and pressure of each fluid) throughout the well, and to allow for pressure losses along the wellbore and across any flow control devices.

⁷In 1993, DEIMBACHER and HEINEMANN /58, 59, 60/ introduced the so called Windowing technique to perform near wellbore studies. For detailed consideration of the flow near the well they implemented a discrete treatment of the well using Voronoi grids.

3 Simulator Development

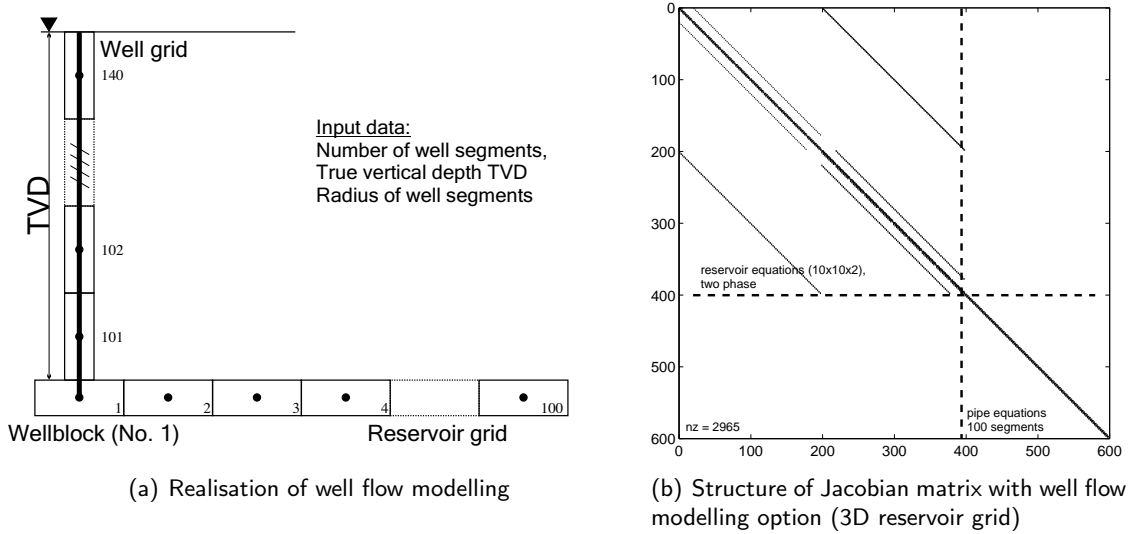


Figure 3.2: Schematic of the well flow modelling option and example of application

Here, the versatility of such well flow modelling is illustrated by the method whereby flow between the bottom hole and the tubing head is implemented in the research code. The schematic of this "well flow modelling option" is shown in fig.3.2.a. Starting from the face of the top reservoir layer, the well is divided into single segments each with a specific depth, radius and length.

The implementation of the well flow modelling facility can be realised by connecting the well block (e.g., block 1) with the first well segment (block 101), which is simple due to the connection list approach. Further on, the neighbour segments of the "vertical column" are continuously linked up to the tubing head (block 140). Each segment has an outlet junction which connects it to its neighbouring segment in the direction of the wellhead. Most segments will also have one inlet junction which connects it to its neighbour in the direction away from the wellhead. Branches or crossings are feasible by connecting corresponding grid blocks.

The flow in the well is assumed laminar in the present case.⁸ Accordingly, it can be calculated using the common Hagen-Poiseuille law for pipe flow⁹, where average velocity \bar{w} in the pipe with a segment radius r_s is given as $/62/$:

$$\bar{w} = -\frac{r_s^2}{8\mu} \nabla \Phi . \quad (3.23)$$

Due to the analogy between Darcy's law and the Hagen-Poiseuille equation, the Darcy's law is applicable for laminar pipe flow if permeability is substituted with $k = r_s^2/8$, where r_s is the segment radius. The storage term is considered using a porosity of one and the density according to the fluid inside the pipe.

All equations derived for the well flow are added to the system of equations of the reservoir model and solved simultaneously fully implicit to ensure stability and sound convergence. The

⁸Re < 2320

⁹Representing laminar flow in void porous media ($\phi = 1$).

3 Simulator Development

structure of the Jacobian matrix for a 3D structured grid is depicted in fig.3.2.b. Boundary conditions, such as pressure or flow rates, can be arbitrarily specified at the bottom hole or at the tubing head.

In principal, the well flow modelling option can be extended to consider non-laminar flow, sophisticated (countercurrent) multi-phase flow and complex wells. The unstructured framework also provides an architecture for directly coupling a surface facility model with the reservoir model increasing the computational stability of the entire system. In terms of the general unstructured conception, the integrated facility network is treated as a set of nodes and connections which is simply a natural extension of the reservoir model. Of course, this can be further enhanced to facilitate reservoir coupling based on boundary conditions provided from a shared surface facility network.

3.3 Gridding Technology

Gridding and fluid-flow simulation are separate parts of the workflow in the current reservoir simulation tool. The gridding preprocessing is performed in so called toolboxes, where standard modules are provided for common tasks, e.g., Cartesian, radial or unstructured (irregular) grids. Additionally, the external gridding approach enables the usage of third party gridding software, subject to the condition that the output is appropriate or at least adoptable for the simulator. In order to make the gridding software and the simulator work together, a list of grid block connection properties (i.e., the connection network) is required.

A key element of the simulation tool is the use of unstructured grids (or at least the unstructured framework). Away from the traditional rectangular or regular grid systems, they enable more accurate and detailed representation of complex geologic and engineering features such as faults, pinchouts, fluid contacts, and horizontal or multi-lateral wells, fractured vertical and also multiple horizontally fractured wells (/46/).

In general, unstructured gridding is a spatial discretisation that (i) consists of polygons (in 2D) or polyhedrons (in 3D), which (ii) locally vary in shape and size (VERMA and AZIZ /18/). The regular point distributed Cartesian grid is a special case of a Voronoi grid with the additional advantage that it is also block-centered (HEINEMANN /59/). Furthermore, cylindrical (or radial), curvilinear, hexagonal, as well as locally refined Cartesian and hybrid-Cartesian grids can be considered special cases of Voronoi grids.¹⁰ The methodology of unstructured grid facilitates the usage of different geometries. It should be selected according to the objective of the simulation study, the requested level of accuracy and the availability of computational resources.

A main aspect from the users point of view, is the introduction of so called "fit for purpose grids". Such grids correspond to the actual physical process of flow and transport in porous media according, e.g., to the resulting flow pattern resp. potential distribution. This guarantees, on the one hand, accuracy of discretisation scheme (e.g., by minimising grid orientation effects) and, at on the other hand, the automatisation of the gridding process by applying proper grid generations algorithms.¹¹ Using a finer grid only where needed employs computational resources most effectively. For detailed understanding of behaviour in a particular region, localised grid

¹⁰There may be some slight differences between a Voronoi block and a curved-boundary block like curvilinear or cylindrical geometries, because a Voronoi block is a polygon made of straight lines.

¹¹The methodology has even been termed "gridless simulation" (ref.16 in /24/). However, this is misleading since control volume techniques generally imply physical presence of a grid by its definition.

3 Simulator Development

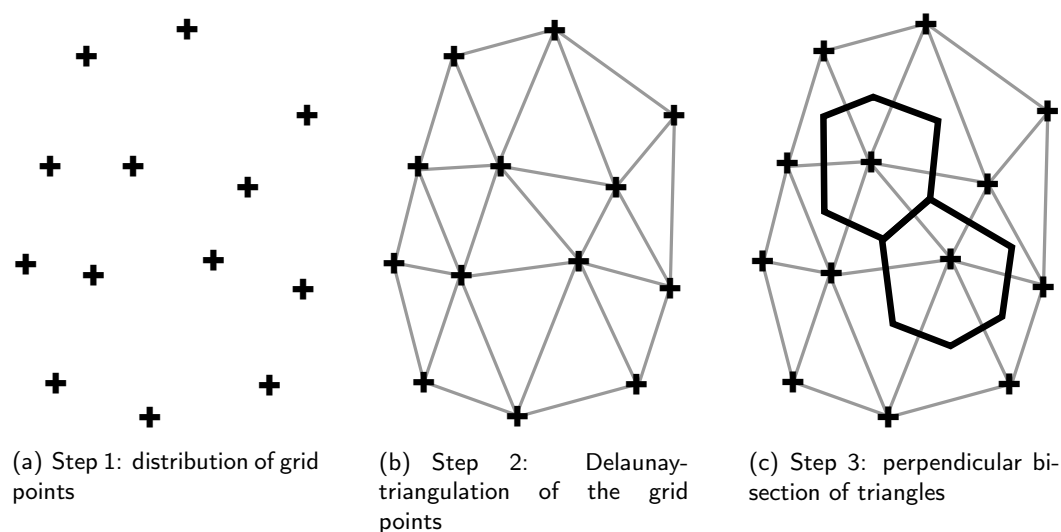


Figure 3.3: Generation of Voronoi grids

refinement provides flow details without affecting the model in other connected regions. Grids in areas of lesser interest are easily coarsened.

From a discretisation point of view, the main advantage of the Voronoi grids are the orthogonality (like the common Cartesian grids) and the flexibility of curvilinear grid systems (such as corner point grids). The code design, adopted to accommodate unstructured grids, also provides a natural framework for the integration of well facilities and reservoir calculations for increased computational stability as shown in the previous section.

The theory, implementation and application of unstructured grids has been extensively discussed in literature since the late 1980's. A major theoretical contribution, including, e.g., error analyses, was given by HEINRICH /12/ (1987). HEINEMANN and BRAND /63/ were the first to introduce Voronoi grids to petroleum engineering naming them PeBi-grids (1988). Later, several researchers contributed to the development of unstructured grids, e.g., HEINEMANN et al. /63, 59, 58/, FORSYTH /14/, PALAGI et al. /19, 64, 65/, FUNG et al. /15, 16/, VERMA /18/ and GUNASEKERA et al. /24/. Based on their developments, unstructured grids have been implemented into commercial simulators since the mid-1990's. Examples are SURE /66/ (developed by HEINEMANN), ECLIPSE (described in GUNASEKERA et al. /24/) and recently, EM^{power} (the Exxon-Mobil in-house simulator (/46/)). However, industry has generally been reluctant to apply this capability to practical reservoir simulation, due in part to concerns about potential loss in computational efficiency /46/. Simulators providing unstructured grid technology are commonly termed next generation reservoir simulators and represent, from the opinion of the author, the standard discretisation technology for reservoir simulation in the future.

3.3.1 Generation of Voronoi Grids

The generation of a Voronoi grid is composed of three steps. The process is depicted in fig.3.3 and briefly summarised in the following. A more thorough treatise can be found in PALAGI /19/, GUNASEKERA et al. /24/, HEINEMANN et al. /59/ or KOEBERBER /67/.

Distribution of Grid Points. Probably the most important stage of constructing Voronoi

3 Simulator Development

grids is the proper definition and placement of the grid points (fig.3.3.a). The distribution depends on the global grid style, the features to discretise and the refinement parameters. Features implemented at present are: radial wells, horizontal wells, fractured vertical wells, fractured horizontal wells, 2D faults and boundary points (see fig.3.4). Points are distributed according to the characteristic flow pattern of the feature (e.g., radial for a vertical well with logarithmical spacing in radial direction). The bulk of the domain is discretised using a regular spaced rectangular or, preferably, a hexagonal grid. The spatial reservoir boundaries can run (almost) arbitrarily.

Delaunay Triangulation. The neighbours of each grid point are determined which form the connection network of the grid points (fig.3.3.b). The domain is consequently partitioned into triangles. The grid points are simultaneously the vertices of the triangles. The triangulation is of Delaunay type if no vertex falls inside the circumcircle (the circle that passes through all three vertices) of any triangle in the triangulation (SHEWCHUK /68/). Then, the triangular elements cover the whole reservoir domain but do not intersect or overlap.¹² The freeware 2D mesh generator and Delaunay triangulator, TRIANGLE /68/, is used to generate the connection network in the preprocessor.

Perpendicular Bisection of Triangles and Block Generation. The perpendicular bisection is the geometric dual of the Delaunay triangulation (fig.3.3.c). The grid block is defined as the region enclosed by all perpendicular bisectors of the edges joining the grid point with its neighbours. Thus, the Voronoi grid block is always a convex polygon (in 2D). To construct the grid blocks, all perpendicular bisectors of a vertex are tracked and assembled to form a closed area. The vertex represents the grid point and the perpendicular bisector is the shared interface between two neighbouring vertices. The perpendicular bisection is also provided from the TRIANGLE code; although the cells still have to be assembled. Cell properties, such as grid block volume or transmissibility to the neighbours, are calculated subsequently.

The procedure can be applied in three dimensions as well. Instead of triangles, tetrahedrons have to be considered. Fully three-dimensional Voronoi grids are rarely used today because of several difficulties, such as visualisation of the grid geometry, assignment of physical properties, treatment of well terms, interpretation of the results, the vertical dimension of the reservoir is usually much less than the horizontal dimension and the geologic interpretation of the reservoir is usually based on its division into layers (PALAGI /19/). However, usage of complex (undulating) horizontal wells may require extremely complex grid systems. Expected further improvements in the quality and quantity of reservoir data will make fully 3D unstructured gridding a must to ensure accurate representation of reservoir details in simulation models.

Voronoi grids are not able to regard anisotropy, i.e., areal anisotropy if the stream tube approach (2.5D refinement) is utilised. The common two-point flow stencil is not applicable in an anisotropic case since non-orthogonalities arise, i.e., the vector of flow between two grid points is not normal to the shared interface. In the literature, several approaches have been presented to overcome that limitation, e.g., the usage of k-orthogonal Voronoi grids /20,24,67/ or multi point flux (MPF) schemes /69/ which are beyond the scope of this thesis.

¹²In order to construct Voronoi grids in the next step, the following conditions need to be satisfied to produce a valid Delaunay triangulation: (i) for any two adjacent triangles, the sum of the two angles at the vertices opposite the common edge (of the two triangles) must not exceed 180°, and (ii) for a triangle at the boundary, the angle at the vertex opposite the boundary must not exceed 90° (/20/).

3 Simulator Development

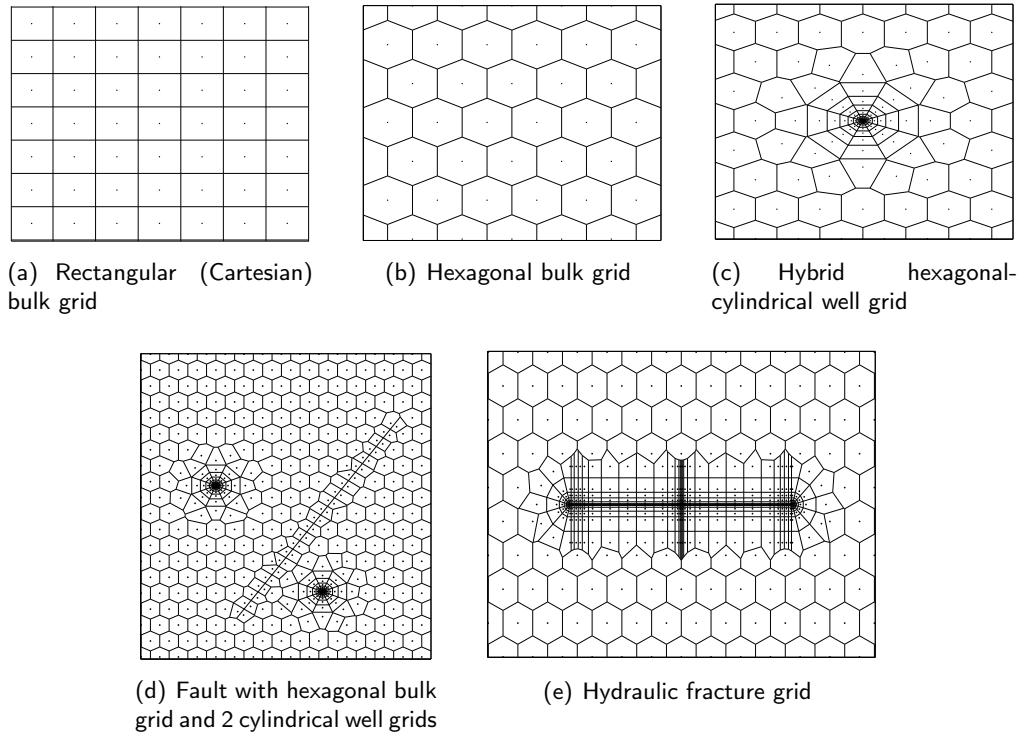


Figure 3.4: Voronoi grids

Results from various authors (/19,20/) suggest that the use of hybrid Voronoi grids, especially the hybrid-hexagonal grid, fig.3.4.c, is at least as effective as the nine-point difference scheme for typical problems in terms of reducing the grid orientation effect. The radial distribution of grid points around wells is potentially more accurate than conventional square grid geometries. This is especially important for processes that require high resolution around wells such as coning problems.

The use of Voronoi grids with a single point, upstream weighting scheme for mobilities does not improve the numerical resolution around sharp fronts /19/. Higher order methods have been implemented successfully for Cartesian grids and need to be extended to the flexible Voronoi grid discussed in this thesis. Until now, there has been little research in making higher order schemes applicable to unstructured grids.

3.4 Software Design

The simulation tool is realised within by combining MATLAB with Fortran 77. MATLAB is a high-performance language for technical computing. It integrates computation, visualisation, and programming in an easy-to-use environment where problems and solutions are expressed in familiar mathematical notation (MATLAB /39/). The variety of implemented routines accelerates the development cycle of the reservoir simulation tool significantly.

All stages from preprocessing, solution of the problem and, finally, the postprocessing are performed in one unified MATLAB M-file which is essentially a scripting language similar to C. However, the most important part, the simulator kernel is compiled as a Fortran F77 dy-

3 Simulator Development

dynamic link library and can be accessed by the MATLAB M-file (e.g., during every iteration) to assemble the system of equations. The simulator kernel hosts the physics of the system under consideration, i.e., the formulated set of residuals and the subroutines to calculate subsidiary data such as fluid parameters. The implementation of additional residual equations (such as energy conservation for non-isothermal flow) or extending the tool to full Black-Oil capabilities (see AZIZ and SETTARI /8, p.60 foll./) is, thus, readily feasible.

Traditionally, reservoir simulators are controlled by an input file. Grid and data processing, Newton's method and calculating the residuals and the Jacobian matrix is performed within one (non-accessible) layer of the software. Using instead a scripting language such as MATLAB to provide the input data, carry out grid processing and performing Newton's method, grants the user access to all stages of the simulation process.

The methodology encompasses a wide range of features such as repeating simulations, e.g., for parameter studies, applying macros, incorporating decision making facilities by if-then-else branching, do-loops or case-selection, and the common scalar, vector and matrix operations. Accessing the Newton's method on an iteration or time step level implies a very simple treatment of time dependent boundary conditions. The discretisation can be transiently altered since gridding is part of the M-file and can be called during the time loop of the simulator. Dynamic, adaptive gridding is a possible application. Such methods are rarely used in today's reservoir simulators.

Realtime monitoring of results is intrinsically supported by MATLAB; the output can be arbitrarily manipulated. Furthermore, the coupling is the foundation for sophisticated features such as process optimisation or history matching in the framework of inverse modelling. The main drawback of the coupling is the lack of a stand-alone application and the need for some proficiency in M-file programming. Furthermore, the numerical efficiency can be considered lower compared to conventional Fortran applications because of some overhead in handling data between MATLAB and FORTRAN.

3.5 Verification and Validation

To ensure the reliability of the code, it has been tested against analytical solutions as well as results from a commercial simulator for a variety of cases (see appendix A). Validation included single-, two- and three-phase cases utilising both structured and unstructured grids. Non-Darcy flow and non-Newtonian fluids have also been verified. The simulation tool generally gave very accurate results.

3.6 Discussion

The current chapter presented the main features of the simulation tool and techniques for its development. The tool is characterised by high flexibility and follows the concept of a research tool rather than a commercial type of simulator. Thus, the focus is placed on the physics behind the multi-phase flow.

Critical remarks and recommendations have already been given throughout the text. The four main suggestions, which can be considered a guideline for future work, are briefly summarised as follows:

- Improving numerical efficiency and robustness

3 Simulator Development

- Implementation of more efficient iterative solvers and preconditioners for unstructured grid in order to solve large scale problems.
 - Realisation of parallel computing by domain decomposition. Implementation is feasible by means of the connection list approach (LIM et al. /44/) to provide the corresponding boundary conditions.
 - Enhancing convergence of nonlinear equations with Newton's method (e.g., implementation of Cascade method (APPLEYARD et al. /70/) or the Appleyard Chop (in NACCACHE /71/)).
- **Improving the discretisation capabilities**
 - Coupling external mesh generators such as LaGriT (/72/) or PetraGrid (/53/) with the simulator. LaGriT provides extremely sophisticated 3D well and tunnel modelling capabilities (CHERRY et al. /73/) and can enable fully 3D unstructured gridding.
 - Expanding of the current toolbox library.
 - **Improving the current workflow**
 - Converting the code to a stand-alone application.
 - **Extending the physics of the simulator** (such as non-isothermal flow or multi-component modelling.)

4 Simulation of Hydraulically Fractured Wells

The following chapter presents an extensive numerical study on the performance of hydraulically fractured wells with an emphasis on tight-gas reservoirs. The main objective is the investigation of major physical processes occurring in context of the stimulation treatment and the subsequent depletion of the reservoir. The processes can be distinguished into intrinsic (or natural) mechanisms and artificially induced mechanisms due to the technological execution of the treatment as explained in chapter 1.

In the first section, mechanisms are investigated which affect the accuracy of a hydraulic fracture model, in particular its production forecasts. Such effects are non-Darcy flow and stress dependency of the tight reservoir rocks. Load water recovery is analysed in the second part by means of a two-phase cleanup model. There, hydraulic damage and the combined occurrence of hydraulic and mechanical damage are considered, especially how they affect the post-fracture performance of the well. Finally, polymer cleanup is simulated using an enhanced three-phase cleanup model taking complex rheology into account.

All investigations are performed by means of the reservoir simulation tool as presented in the two previous chapters, illustrating its versatility. The analyses refer to conditions commonly prevailing in North German tight-gas reservoirs. Where available, data is adapted from case studies and the literature to perform the investigations as realistically as possible.

A variety of textbooks dealing with hydraulic fracturing have been published in the past, e.g., GIDLEY /74/, ECONOMIDES and NOLTE /3/ or VALKO and ECONOMIDES /32/. These contain excellent and comprehensive reviews of the basics of hydraulic fracturing. The introduction here is restricted to a brief outline of past activities in the numerical simulation of hydraulic fractures. A more thorough introduction of hydraulic fracture simulation is given in HÄFNER et al. /75, p.47 foll./.

4.1 Introduction to Fractured Well Simulation

The first papers concerning reservoir engineering aspects of hydraulic fractures appeared in 1958. In 1960, MCGUIRE and SIKORA /76/ presented pseudo-steady state curves accounting for boundary and conductivity effects in finite-conductivity fractures. These were used until the late 1970's (/3/). The first analytical solution was presented by PRATS /77/ for finite (1961) and infinite-conductivity fractures (1962).

Reservoir simulation followed a similar evolution. CRAFT et al. investigated the combined effect of fracturing and damage bypass by means of an analog computer with electric circuits in 1962. A further early work was presented by RUSSEL and TRUITT /78/ (1964), analysing a vertical fracture located at the boundary of a quadratic quarter spot reservoir. Both infinite-conductivity and constant rate boundary conditions were taken into consideration. Their numerical model was later utilised for comparisons with analytical solutions.

4 Simulation of Hydraulically Fractured Wells

DOWDLE and HYDE /79/ introduced a finite-difference model of a fractured vertical well with cylindrical coordinates in 1970. The fracture was presented with a small row of grid blocks, where porosity and permeability were adjusted corresponding to a constant fracture width. The single-phase model incorporated effects such as wellbore storage, stress dependent porosity and permeability as well as a damage zone in the fracture vicinity.

BASTIAN et al. /80/ presented a three-dimensional two-phase model using a radial geometry for the early radial flow period and a Cartesian grid for the subsequent flow periods. The radial model included the consideration of cleanup and gas breakthrough processes. The production period, i.e., the post-fracture period, was simulated using structured Cartesian grids.

Local grid refinement has been commonly utilised for simulation of fractured vertical or horizontal wells, regarding multi-phase flow conditions, e.g., by HOLDITCH /81/, SOLIMAN and HUNT /82/ and EHRL and SCHUELER /83/. However, within the framework of a rectangular (structured) grid, the refinement necessary for an accurate and stable solution can result in excessive CPU and computer memory requirements, especially in large scale, multi-phase full-field simulations. A further problem is how to represent the actual relation between the fracture width and the well radius in the model, so as to correctly reproduce the flow in the immediate vicinity of the well (FRIEDEL et al. /84/).

BANERJEE et al. /85/ were the first to report the usage of unstructured grids for hydraulic fracture simulation based on k-orthogonal PeBi-grids, implemented in a commercial reservoir simulator (GUNASEKERA et al. /24/). The fractured vertical well domain consisted of a radial well refinement, linear fracture refinement and a semi-cylindrical tip refinement. Their grids accurately honoured the fracture and well geometry. Furthermore, such grids can be adapted to the structure of flow. The authors demonstrated the usage of their concept by means of a well test application, where well test accuracy could be achieved. Additionally, unstructured grids for multiple fractured horizontal wells were introduced and validated.

In reservoir engineering, the fracture is traditionally presented by a two-dimensional row of grid blocks with equal width. The areal refinement is mapped from layer to layer by means of the stream tube approach. Elliptical and true 3D grids for fractures have not been presented yet. However, hydraulic fracture reservoir simulation tools such as WellWhiz /4/ use pore volume maintenance to consider elliptical shaped fractures. First attempts, presented by BEHR et al. /86/, of coupling hydraulic fracturing software with the reservoir simulator, aimed at more realistic description of the fractures in a reservoir simulation model.

Besides modelling in the framework of conventional reservoir models, there are further approaches to represent the post-fracture production. One is based on the usage of source/sink terms. Flow equations in the fracture and the reservoir are discretised by separate grids and coupled through a mass exchange term, determined by the corresponding pressures in the fracture model and in the adjacent reservoir grid blocks. Flow into the fracture can be assumed linear (SETTARI /87/) or elliptical, as in Muskat's solution for the steady-state single-phase flow into the infinite-conductivity fracture (NGHIEM /88/, NGHIEM et al. /89/). The analytical solution for the case of finite-conductivity elliptical fracture has also been employed in similar numerical algorithms (SETTARI et al. /90/).

The second approach considers the fracture non-discretely within a conventional reservoir model by means of increased transmissibilities. A reservoir model can communicate with a fracture model via an interface module, which performs the transformation of the time-dependent characteristics of the fracture and its vicinity into the values of modified transmissibilities in the reservoir grid. In the context of this approach, there are no differences between the fracture block pressure and fracture pressure. Modified transmissibilities in the reservoir model present

4 Simulation of Hydraulically Fractured Wells

Table 4.1: Parameters for single-phase simulation

Reservoir parameters		Production scenario	
Initial pressure (bars)	600	<i>Constant Rate</i>	
Net thickness (m)	10	Gas rate, $k_{res} = 0.01$ mD (m^3/h)	667
Porosity	0.1	Gas rate, $k_{res} = 0.1$ mD (m^3/h)	3750
Permeability (mD)	0.01-0.1	Well flowing pressure limit (bars)	100
Temperature (°C)	150	<i>Constant-Pressure</i>	
Rock compressibility (1/bars)	7.5e-5	Well pressure (bars)	100
Youngs-Modulus (bars)	0.345e-6	Production time (years)	10
Model size (m)	1000x1000		
Fracture parameters			
Half length (m)	75		
Dimensionless conductivity	1-100		
Width (m)	0.005		
Closure Pressure (bars)	720		

the combined effect of the conductivity of the reservoir and fracture. A comparison study of the different approaches is included in FRIEDEL et al. /84/.

4.2 Mechanisms Affecting the Accuracy of Hydraulic Fracture Simulation Models

There are several effects which may influence predictions from tight-gas reservoirs. Hence, the objective is to outline the required accuracy to ensure reliable forecasts or valid parameter estimations from well tests.

Mechanisms such as non-Darcy flow and stress dependency of reservoir and fracture parameters are frequently neglected in analytical or numerical studies for the sake of simplicity. These effects are, in contradiction to mechanical formation damage (will be treated later), not a kind of "artificially" induced damage, rather a natural process. The processes are separately discussed first. The realistic case, where both are acting simultaneously, is subject of the investigations in the last part of this section.

Due to the nature of the effects, the analysis is by means of a single-phase model. The single-phase simplification is applicable if there is neither free water or gas condensate in the reservoir nor damage occurred due to infiltrated fracturing fluid. After the back production of the fracturing fluid, the representation of the longtime productivity can be simplified using single-phase models in a majority of cases.

4.2.1 Simulation Model Setup

The input data for the simulation is summarised in table 4.1. The calculation of the PVT behaviour of the real gas is based on the gas composition: 92 % methane, 2 % ethane, 5 %

4 Simulation of Hydraulically Fractured Wells

nitrogen and 1% carbon dioxide. An external program /91/ generates the PVT input tables for the reservoir simulation tool.

The fractured well and the reservoir are discretised using structured grids. Because of the common character of the investigations, a single layer reservoir with homogeneous and isotropic properties is considered. The hydraulic fracture spans the complete thickness of the reservoir. Due to symmetry of the flow pattern (and to reduce the the number of required grid blocks), discretisation is restricted to a quarter of the domain. Grid construction is based on the algorithms of BENNETT et al. /92/. The authors investigated an optimum grid in the framework of a numerical sensitivity analysis to ensure accuracy when simulating finite and infinite-conductivity fractures.¹ A complete summary of the algorithm is given in appendix B (p.104).

4.2.2 Non-Darcy Flow in Fracture and Reservoir

The significance of non-Darcy flow has been emphasised in the literature in the context of highly productive fractured wells. In contradiction to this, typical tight-gas wells exhibit low gas rates. At the same time, non-Darcy flow effects in the reservoir have been almost completely neglected yet - particularly the coincidental occurrence in both the reservoir and fracture.

An early study of non-Darcy flow in fractured wells was presented by MILLHEIM and CICHOWICZ /93/ in 1968. Using a radial model, they investigated non-Darcy flow in the reservoir. In 1969, WATTENBARGER and RAMEY /94/ considered non-Darcy reservoir flow in an infinite-conductivity fracture by means of a finite-difference model. They concluded that non-Darcy flow in the reservoir particularly affects short fractures. It turned out that non-Darcy flow in the fracture is significantly more important. HOLDITCH and MORSE /95/ restricted their investigations on non-Darcy flow in the fracture and proved the significance for large flow velocities. To determine the non-Darcy flow factors β_t , they referred to COOKE's /96/ correlations for different proppant types.

GUPPY et al. /97,98,99/ introduced type-curves for finite and infinite-conductivity fractures considering non-Darcy flow in the fracture. The authors addressed the constant rate boundary condition /97,98/ as well as the constant pressure condition /99/ using a semi-analytical model. In the case of constant rate production the authors pointed out that non-Darcy flow reduces the true fracture conductivity to a steady state apparent conductivity. On the other hand, constant pressure production is characterised by a transient apparent conductivity where the correlation methodology of constant rate production is not applicable.

Later, semi-analytical models were also used to study the effects of non-Darcy flow, e.g., by UMNUAYPONWIWAT et al. /100/. Others investigated the significance of non-Darcy flow effects on the productivity of fractured wells, frequently referring to experimentally determined non-Darcy flow coefficients, e.g., VINCENT et al. /101/ and SETTARI et al. /102/. JIN and PENNY /103/ presented an empirical model that uses the liquid to gas ratio to predict the effective permeability or conductivity of a proppant pack under two-phase non-Darcy flow conditions. Based on an extensive experimental study they found that Forchheimer correlation is not valid at high liquid saturations. A further paper investigating inertial effects in two-phase flow through fractures was published by FOURAR and LENORMAND /104/.

ROBERTS et al. /105/ analysed the productivity of multiple fractured horizontal wells in tight-gas reservoirs with choked transverse fractures. The limited communication between the fractures and the wellbore created a choking effect near the fracture offset, reducing the apparent

¹Following the authors, grid block sizes dx and dy are chosen according to the fracture half length x_f , fracture width b_f and the model extent L_x, L_y .

4 Simulation of Hydraulically Fractured Wells

fracture conductivity in light of significant inertial pressure drops. Cumulative production was shown to be severely curtailed by that effect.

GIL et al. /106/, ALVAREZ et al. /107/ and also UMNAYPONWIWAT et al. /100/ analysed the impact of non-Darcy flow on the evaluation of well tests. They demonstrated that neglecting non-Darcy flow will result in incorrect reservoir parameters, fracture conductivities and fracture half lengths. ALVAREZ et al. /107/ stated that disregarding of non-Darcy flow will lead to an overestimation of production potential of the fractured well. The authors conducted their investigations at a reservoir permeability of 0.1 mD for different production scenarios and reported losses up to 25 % after 10 years of production.

Recently, BELHAJ et al. /108/ presented a numerical model taking viscous, inertial and frictional effects into account for matching of experimental data. The frictional effects were considered in terms of the Brinkman equation.² At high velocity flow, the frictional term counteracted the inertial effect and held the pressure gradient closer to the Darcian trend.

Constant Pressure Production. The main production period in tight-gas reservoirs attributes to the constant pressure flow regime. For the sake of generality, the analysis here is by means of dimensionless parameters. In doing so, it is possible to apply graphical methods of interpretation (such as type-curve analysis), and to provide a general solution for a broad range of parameters. The dimensionless rate q_D for real gas is calculated as:

$$q_D = \frac{CTQ}{kh|m(p_i) - m(p_{wf})|} ; \quad (4.1)$$

the dimensionless time with:

$$t_{Dxf} = \frac{kt}{\phi c_t \mu x_f^2} , \quad (4.2)$$

where total compressibility c_t and the dynamic viscosity μ of the gas are considered at initial conditions.³ C is a constant and T the temperature. The real gas pseudopressure $m(p)$ accounts for the variation of viscosity and density with pressure.

To account for the non-Darcy flow, GUPPY et al. /99/ introduced a dimensionless parameter $(p_{DND})_f$ as a kind of additional pressure drop:

$$(p_{DND})_f = \frac{2\pi\rho\beta_f k_f k_{res}(p_i - p_{wf})}{b_f \mu^2} \frac{T_0 p_m}{T z_m p_0} . \quad (4.4)$$

where β_f is the non-Darcy Flow coefficient⁴. All fluid parameters are inserted in eq.(4.4) at

²A second order velocity term $\mu' \nabla^2 u$ with the effective viscosity of fluid, μ' , flowing with velocity v .

³In case of a slightly compressible fluid, the dimensionless rate is calculated with:

$$q_D = \frac{QB\mu}{2\pi kh(p_i - p_{wf})} . \quad (4.3)$$

Given a real gas pressure above 140 bars, gas essentially behaves like a slightly compressible fluid since $p/(\mu z)$ is *de facto* constant. Provided that further conditions for its applicability, given from KATZ and LEE /28, p.334-336/, are fulfilled, eq.(4.3) can be used for the calculation of dimensionless gas rate in tight-gas reservoirs under typical pressure conditions.

⁴Previously, the coefficient was termed "turbulence coefficient for non-Darcy flow" (DAKE /36/), "high velocity factor" (KATZ and LEE. /28/) or "coefficient of inertial resistance" (GEERTSMA /30/).

4 Simulation of Hydraulically Fractured Wells

initial conditions. The latter quotient on the right hand side is a modification of GUPPYS original parameter $(p_{\text{DND}})_f$ in order to apply the methodology to real gas.⁵ Index 0 represents the reference state (e.g., standard conditions) and index m the average conditions, i.e., at an average pressure $((p_i + p_{wf})/2)$. According to this, eq.(4.4) is multiplied with the median formation volume factor.⁶

The parameter $(p_{\text{DND}})_f$ can be illustrated by means of the Reynolds-Number $Re = d\rho v/\mu$, which describes the ratio of inertial to viscous forces. That is worth noting, since to the fact that transition from viscous Darcy flow to inertial flow is characterised by that similarity criterion.⁷ The analogy between both is clear after introduction of flow velocity v in eq.(4.4):

$$(p_{\text{DND}})_f \sim \frac{\rho v}{\mu} (\beta_f k_f) . \quad (4.5)$$

$(p_{\text{DND}})_f$ is therefore an equivalent Reynolds-Number, where the product $\beta_f k_f$ reflects the characteristic length of the system (MARTINS et al. /109/). The product can be considered constant despite the dependency $\beta_f k_f$ on the proppant type, pressure, temperature or any kind of damages. Beginning from the limiting case⁸ $(p_{\text{DND}})_f = 0$, where solely viscous Darcy flow prevails within the fracture, the portion of the inertial pressure losses increases with ascending Reynolds-Numbers.

In the literature, type-curve analysis⁹ is restricted to non-Darcy flow in the fracture. To take account of non-Darcy flow in the reservoir, a dimensionless parameter $(p_{\text{DND}})_r$ is introduced, similar to GUPPYS dimensionless parameter for the fracture:

$$(p_{\text{DND}})_r = \frac{2\pi\rho\beta_r k_{\text{res}}^2 (p_i - p_{wf})}{x_f \mu^2} \frac{T_0 p_m}{T z_m p_0} . \quad (4.6)$$

Here, the maintenance of fracture conductivity (k_f/b_f) is substituted with the reservoir conductivity (k_{res}/x_f). The characteristic length of the reservoir in eq.(4.6) is $\beta_r k_{\text{res}}$. In contradiction to the fracture system, this product is nonlinear due to the relationship $\beta_r = f(k_{\text{res}})$.

GUPPY et al. /99/ presented their type-curves for values $(p_{\text{DND}})_f = 0 \dots 1$, which can be considered sufficient for slightly compressible fluids. However, for real gas, the range is too small. According to typical conditions, the range is extended to $(p_{\text{DND}})_f = 0 \dots 100$. The ratio of non-Darcy flow in fracture to non-Darcy flow in the reservoir $(p_{\text{DND}})_f / (p_{\text{DND}})_r$ is:

$$\frac{(p_{\text{DND}})_f}{(p_{\text{DND}})_r} = \frac{x_f^2 \beta_f}{b_f^2 \beta_r} F_{\text{CD}} . \quad (4.7)$$

Evaluation of eq.(4.7) using typical tight-gas parameters supports the established fact that non-Darcy flow in the fracture affects the productivity of the well to a distinctly higher degree than

⁵In the original paper /99/, the parameter is defined without the latter part although real gas potential was used. Without the modification, their type-curves could not be reproduced for gas flow. It is unclear so far, which reference state needs to be considered if eq.(4.4) is used without modification.

⁶Accuracy varies with the degree of pressure difference. For large Δp the real gas behaviour of the gas may lead to (small) deviations, despite the modification.

⁷GEERTSMA /30/ introduced in 1974 an identical parameter $R'e$ to investigate the upper validity limit of Darcy's law: $R'e = \frac{\rho v}{\mu} (\beta_t k)$. This proved correct for values $R'e \leq 0.01 \dots 0.1$.

⁸The case $(p_{\text{DND}})_f = 0$ is theoretically impossible since the quadratic term in eq.(2.13) does not diminish until $v = 0$.

⁹A comprehensive outline of type-curve analysis is presented by HORNE /110/.

4 Simulation of Hydraulically Fractured Wells

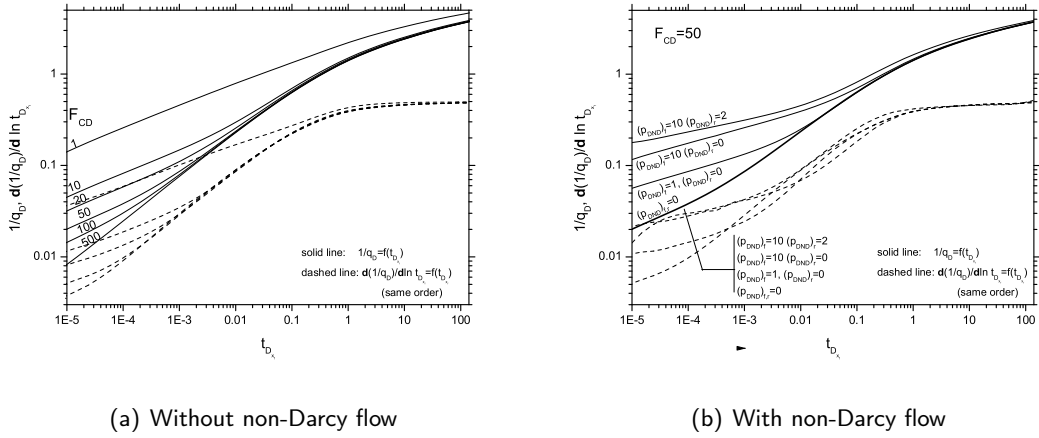


Figure 4.1: Type-curves for fractured wells with constant pressure production ($F_{CD} = 50$)

inertial effects in the reservoir. The ratio depends quadratically on the fracture half length and linearly on the dimensionless fracture conductivity.¹⁰ Short fractures are therefore more affected by inertial effects in the reservoir than longer ones, as already proposed from WATTENBARGER et al. /94/. At the same time, the relation between eq.(4.7) and the reservoir permeability is comprised via the term β_f/β_r . As will be explained later (p.37 foll.), this term is a function of the corresponding permeabilities in fracture and reservoir. The non-Darcy flow coefficient of the reservoir increases by more than the coefficient of the fracture. Hence, the rate of the reservoir on the overall inertial pressure drop will ascend.

Fig.4.1.a shows the relation of dimensionless time and rate for a wide range of fracture conductivities F_{CD} , neglecting non-Darcy flow effects. As typical for type-curve analysis, the derivative function of the rate is included. The type-curves $\log(1/q_d) = f(\log t_{Dxf})$ for fractured wells, considering non-Darcy flow in the fracture and reservoir, are presented in appendix C.1 (p.105). A second graph contains the reduction of the productivity $J_{(DND)}/J_D$ due to non-Darcy flow against a well assuming solely Darcy flow as function of dimensionless time.

The bilinear flow period is of special interest when analysing fractured wells. The period is characterised by a quarter slope for viscous Darcy flow if dimensionless fracture conductivity is low. In the course of well test analysis, this period is mainly used for the evaluation of dimensionless fracture conductivity F_{CD} . During this period, linear flow occurs both within the fracture and, dominating, from the reservoir into the fracture. In a tight-gas environment, it typically lasts up to several days.¹¹

At first, only non-Darcy flow in the fracture is considered, i.e., $(p_{DND})_r = 0$. Large values $(p_{DND})_f$ affect the fractured well dramatically (see fig.C.1 on p.105). The bilinear flow period is completely masked due to the increase of the inertial effects and the resulting additional pressure drops. Hence, the real fracture conductivity is lowered. That apparent conductivity varies as a function of time. Pertaining to fig.4.1.b, the typical slope of 0.25 does not occur.

¹⁰Normally, finite-conductivity fractures have large fracture half lengths, i.e., both parameters have a counter-current effect.

¹¹According to BENNETT et al. /92/, this is the case after a dimensionless time of: $t_{Dxf} \approx \frac{0.0694}{F_{CD}^2}$ for fracture conductivities larger than 5.

4 Simulation of Hydraulically Fractured Wells

While increasing $(p_{\text{DND}})_f$, the slope decreases further. The reduction of productivity is most distinct for small values of t_{Dx_f} which is primarily caused by the large pressure gradients and the corresponding flow velocities within the fracture. Due to the higher productivity, non-Darcy flow effects are more pronounced in highly conductive fractures.

The impact of reservoir non-Darcy flow is also illustrated in appendix C.1 (p.105). As previously mentioned, its influence is less severe than inertial effects within the fracture: see the cases $(p_{\text{DND}})_f = 0$ with $(p_{\text{DND}})_r > 0$. Nonetheless, the productivity may be further decreased as a consequence of the reservoir inertial effects. Unlike the fracture flow, the bilinear of flow period is practically unaffected. After the end of the bilinear flow period and the beginning linear reservoir flow, the influence of the reservoir non-Darcy flow on the well becomes more pronounced. Simultaneously, the impact of non-Darcy fracture flow declines. This continues in the subsequent pseudo radial flow period. The reason for this behaviour is the increase of reservoir domination due to the increasing drainage area, while the fracture reduces to a point source.

The graphs $J_{(\text{DND})}/J_D$ clearly indicate that non-Darcy flow in the fracture is of secondary importance on the longtime behaviour of the well. In contrast, neglecting the non-Darcy reservoir flow may result in an overestimation of fractured well potential. In summation, to ensure the quality of the simulation model it appears essential to include both components of non-Darcy flow into the simulation model.

Type-curves are also suitable in determining the non-Darcy flow coefficients. This is particularly an advantage if non-Darcy flow coefficients are not available despite the plurality of available correlations. First, the real dimensionless fracture conductivity needs to be evaluated, by applying very small pressure differences in the course of a well test. For this case, $(p_{\text{DND}})_f = 0$ and $(p_{\text{DND}})_r = 0$ are almost valid. Once F_{CD} is known, the true well test data can be graphically analysed by determining the values $(p_{\text{DND}})_f$ and $(p_{\text{DND}})_r$. Following this, the non-Darcy flow coefficients can be simply calculated from eq.(4.4) and eq.(4.6).¹²

Constant Rate Production. Constant rate production is typically restricted to a short period in tight-gas reservoirs. Again, results are presented using the traditional $\log p_D = f(\log t_{Dx_f})$ graphs.¹³ The dimensionless pressure p_D is calculated as follows:

$$p_D = \frac{2\pi kh(p_i - p_{wf})}{Q\mu B} . \quad (4.8)$$

Dimensionless time is based on eq.(4.2). To account for non-Darcy flow within the fracture, GUPPY et al. /97/ introduced a dimensionless parameter called the *Dimensionless Flow Rate Constant*, $(q_{\text{DND}})_f$, where¹⁴:

$$(q_{\text{DND}})_f = \frac{k_f \rho \beta_f Q}{b_f h \mu} . \quad (4.9)$$

¹²It should be mentioned, however, that the reservoir non-Darcy flow can only be distinguished once the bilinear flow period has ended. During the bilinear flow period, reservoir non-Darcy flow affects the response of the well almost linearly; a unequivocal identification is then impossible. If data is unavailable, it is recommended to use correlations for β_r .

¹³The methodology in the following is adopted and extended from the original work by GUPPY et al. /97/, for this boundary condition and for non-Darcy flow in the fracture.

¹⁴GUPPY et al. /97/ replaced the density with the molecular weight when considering real gas. This, however, turned out to be unnecessary for tight-gas conditions.

4 Simulation of Hydraulically Fractured Wells

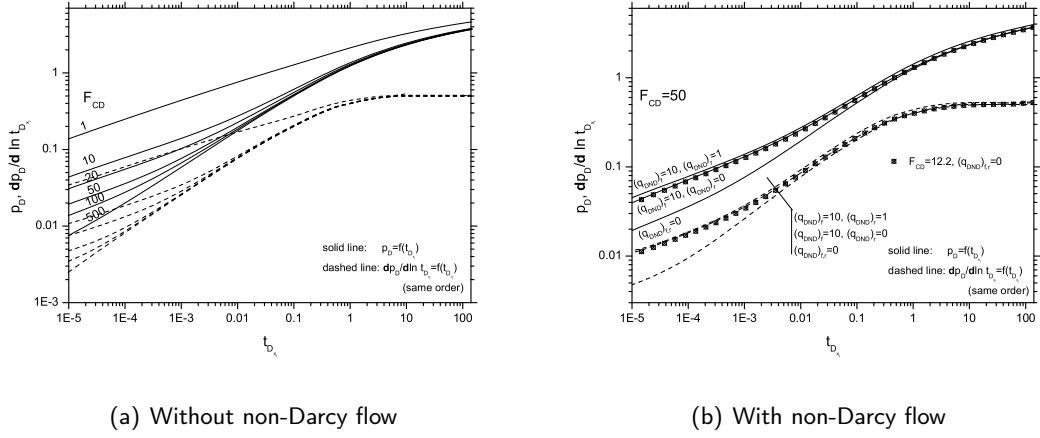


Figure 4.2: Type-curves for fractured wells with constant rate production ($F_{CD} = 50$)

The constant $(q_{DND})_f$ characterises the transition from laminar Darcy flow ($(q_{DND})_f \rightarrow 0$) to the inertial non-Darcy flow. Therefore, $(q_{DND})_f$ is equivalent to the constant $(p_{DND})_f$, eq.(4.4).¹⁵ GUPPY et al. restricted the investigations to non-Darcy flow in the fracture. To account for reservoir non-Darcy flow, a parameter $(q_{DND})_r$ is introduced:

$$(q_{DND})_r = \frac{k_{res} \rho \beta_r Q}{x_f h \mu} . \quad (4.10)$$

All fluid parameters in eqs.(4.8), (4.9) and eq.(4.10) are taken at initial conditions.

Neglecting any non-Darcy effects, type-curves are presented for a typical range of F_{CD} in fig.4.2.a. Appendix C.2 (p.109) contains the corresponding non-Darcy flow type-curves. The general trend is identical for different values of $(q_{DND})_{f,r}$, according to the shape of the dimensionless pressure and its derivative in fig.4.2.b. Consequentially, the degree of non-Darcy flow does not affect the principal slope of the curve during all relevant flow periods (/97/). However, inertial pressure losses increase with $(q_{DND})_f$ and $(q_{DND})_r$.

Non-Darcy flow lowers the true fracture conductivity. Contrary to the constant pressure case, the apparent fracture conductivity is not a function of time. As stated by GUPPY et al. /97/, it is instead a function of $(q_{DND})_f$ and F_{CD} :¹⁶

$$\frac{(F_{CD})_{true}}{(F_{CD})_{app}} = 1 + 0.31(q_{DND})_f . \quad (4.11)$$

Fig.4.2.b shows the reduction of real fracture conductivity ($F_{CD} = 50$) to an apparent conductivity ($F_{CD} = 12.2$) for $(q_{DND})_f = 10$. The authors specified the maximum degree of reduction in fracture conductivity as 85%. If non-Darcy flow in the reservoir is also considered, eq.(4.11) is still applicable with certain restrictions.

¹⁵By analysing $(q_{DND})_f$, the relation to the familiar Reynolds-Number becomes clear: $(q_{DND})_f \sim \frac{\rho v}{\mu} (\beta_f k_f)$.

¹⁶GIDLEY /111/ presented a simple correlation $(F_{CD})_{app} = f(Re)$ considering non-Darcy flow.

4 Simulation of Hydraulically Fractured Wells

Non-Darcy Flow Coefficients. Besides the flow velocity, the magnitude of the non-Darcy flow coefficient β_t is the crucial factor for the actual productivity restriction owing to inertial forces. The coefficient is a characteristic of the morphology of the porous media; hence, its magnitude differs in matrix and fracture. The fluid itself does not affect the coefficient.

In most cases, β_t is experimentally determined. If such data is not available, non-Darcy flow coefficients can be derived from the evaluation of well tests, e.g., from the type-curve analysis as previously presented or, classically, from multi rate tests. If neither of these are available, one can still revert to a broad variety of existing correlations. There are single-phase as well as multi-phase correlations; both based on the evaluation of experiments. Furthermore, several theoretical models are available in the literature to determine the coefficient. A comprehensive review of correlations and theoretical models were presented by LI and ENGLER /112/.

Fig.4.3.a shows the non-Darcy flow coefficient of the reservoir as function of absolute permeability. The correlation of the data from different sources and authors is:

$$\beta_r = 1.3 \cdot 10^5 k_{\text{res}}^{-1.5} , \quad (4.12)$$

where k is in μm^2 and β_t in $1/\text{cm}$. Nonetheless, the data scatters within a magnitude of order.¹⁷ The relationship $\beta_f = f(k_f)$, used to determine the fracture non-Darcy flow coefficients, is illustrated in fig.4.3.b for a variety of proppants. The data correlates with:

$$\beta_f = 1 \cdot 10^9 k_f^{-1.11} , \quad (4.13)$$

where k_f is in mD and β_f in $1/\text{cm}$. It is very common in reservoir simulation to use a fictitious fracture width (/84/). Applying eq.(4.13) will tend to forge the results, e.g., non-Darcy flow effects are likely to be underestimated. Thus, the original β_f of the true fracture permeability has to be corrected to the artificial width using eq.(4.4) and eq.(4.9). For both cases the quotient β_f/b_f^2 must be constant. Apart from those general correlations, several research institutions, such as the STIMLAB-Consortium /114/, and proppant manufacturers provide data under specific conditions. The data supplied accounts for particular pressure and temperature environments or damaged proppant packs.

The proppant type turns out to be a controlling factor for the magnitude of potential inertial effects. Ceramic or coated proppants are characterised by distinctly lower coefficients than sand based proppants. Apart from the type and the material, the non-Darcy flow coefficient of the proppant depends particularly on its geometry and surface structure. Low mesh sizes imply small particles coinciding typically with low fracture conductivities. Consequently, they promote an increase of the non-Darcy effects which is indicated by large β_f factors. On the other hand, the concentration of the proppant pack is less important if a limiting value is once reached. For ceramic materials, this is the case for concentrations of 2 lb/ft^2 or more.

If there is a residual water saturation, or even a real multi-phase flow, the non-Darcy flow coefficients increase dramatically. This coincides with raising inertial pressure drops.¹⁸ The theoretical models of WONG /115/ and GEERTSMA /30/ suggest an increase of up to a factor

¹⁷Rock permeability is the input in the correlation. In tight formations, this permeability is not essentially equal to the permeability of the gas phase. The in-situ permeability for the gas phase as a function of the residual water saturation may be significantly lower than the rock permeability (BYRNES and CASTLE /113/, REITENBACH et al. /75/). To calculate the non-Darcy flow coefficients with eq.(4.12), the corresponding permeability needs to be corrected accordingly to avoid an overestimation of β_t .

¹⁸There are additional collisions between the gas molecules and the residual fluid molecules which slow the gas molecule down. This causes an increase of energy required to accelerate the molecule again.

4 Simulation of Hydraulically Fractured Wells

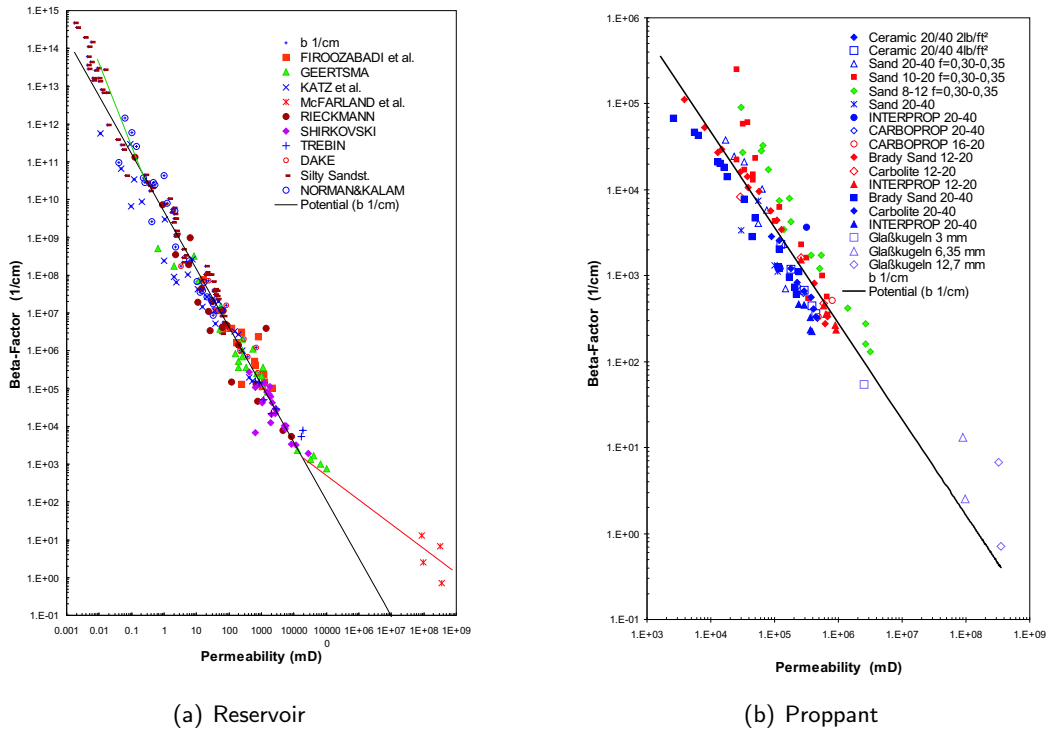


Figure 4.3: Non-Darcy flow coefficients for reservoir and proppant pack as function of permeability (provided by VOIGT)

of 10 against single-phase predictions. PENNY and JIN /116/ provided an empirical correlation for the non-Darcy flow coefficients with a gel damaged proppant pack:

$$F = 10^{\frac{\%Damage}{100}}, \quad (4.14)$$

where F is a scaling factor for the undamaged non-Darcy flow coefficients.

Example. The impact of non-Darcy flow on the productivity is investigated by means of a typical production scenario of a fractured tight-gas well. Initially, the well produces at a constant rate until the lower well pressure limit is reached. The entire production lasts 10 years. Several simulation runs are conducted using two proppant types. Properties of the simulation model are summarised in table 4.1. Reservoir permeability is assumed 0.01 mD with a dimensionless fracture conductivity $F_{CD} = 50$ and fracture width $b_f = 5$ mm. The latter is adapted from the STIMLAB-Consortium. Hence, the experimental data of β -values coincide with their representation in the simulation model. Two proppant types are considered: (i) 16/20 C-Lite: concentration 2 lb/ft² and (ii) 18/30 Carbo-HSP: concentration 2 lb/ft².

According to STIMLAB-data, the permeabilities of the undamaged proppant pack under in-situ conditions are 976 D for 16/20 C-Lite and 691 D for 18/30 Carbo-HSP. Such permeabilities are rarely achieved in tight-gas conditions. Hence, the β -factor needs to be corrected. A *Frac Fluid Damage Factor* accounts for the lower "true" permeability or damage by fracturing fluid residuals. The factor specifies the ratio of ideal to real permeability of the proppant pack.

4 Simulation of Hydraulically Fractured Wells

Table 4.2: Non-Darcy flow coefficient of several proppant types (source: STIMLAB /114/)

	16/20 C-Lite	18/30 Carbo-HSP	20/40 Carbo-HSP	16/30 PRB
β_t , undam. (1/m)	3.3e5	9.1e4	7.4e4	3.9e6
β_t , damaged (1/m)	3.2e6	8.9e5	7.2e4	3.8e7

Assuming a dimensionless fracture conductivity of 50, the real fracture permeability is about 7.5D - just 1% of the theoretical predicted permeability.

Based on the experimental data of the STIMLAB-Consortium, the non-Darcy flow coefficients for such conditions are summarised in table 4.2. Resin coated sand proppants exhibit distinctly higher non-Darcy flow coefficients (see proppant type 16/30 PRB). When considering non-Darcy flow effects, such proppant types are less appropriate. Resin coated ceramics, meanwhile have similar properties to the uncoated ceramics in the table.

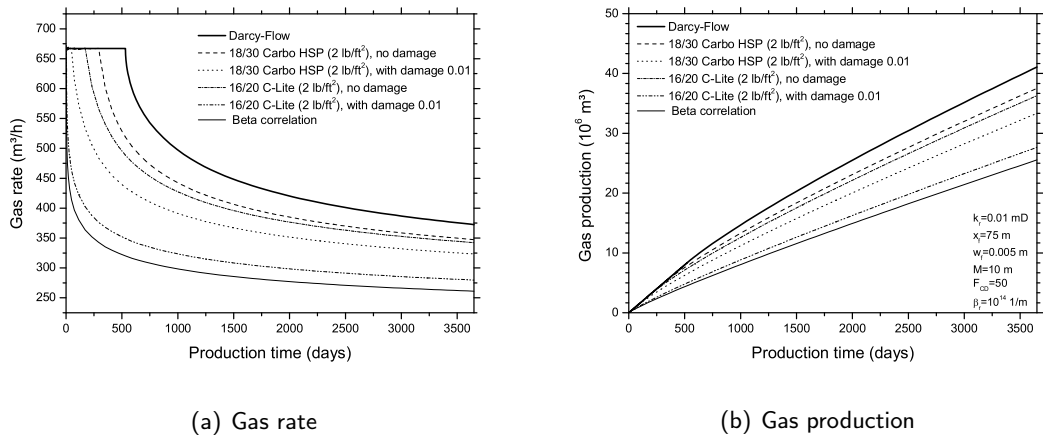


Figure 4.4: Influence of proppant type on the production with non-Darcy flow

The simulation results are illustrated in figures 4.4.a and b. If non-Darcy flow effects are neglected, the well produces for about 600 days at a gas rate of 670 m³/h, until a well flowing pressure of $p_{wf} = 100$ bars is reached. Subsequently, the rate drops to 380 m³/h after 10 years of production. If undamaged 18/30 Carbo-HSP proppant is considered, productivity loss is low, even though the plateau phase already ends after 300 days. The final rate drops to 347 m³/h. If proppant damage is taken into account, the initial rate can be sustained just 50 days, with a final rate of 323 m³/h at the end of the production term. Using 16/20 Carbo-Lite proppant will cause an increase of inertial effects. There is almost no plateau phase, the terminal rate is about 280 m³/h. Using a β_f value from the correlation eq.(4.13) will provoke similar results.

4.2.3 Stress Dependent Reservoir Permeability and Fracture Closure

Consideration of stress dependent parameters was introduced in reservoir engineering in the early 1950's. Some of the first important publications were from FATT and DAVIES /117/ (1952) and DOBRYNIN /118/ (1962). In their papers, the authors investigated the relation

4 Simulation of Hydraulically Fractured Wells

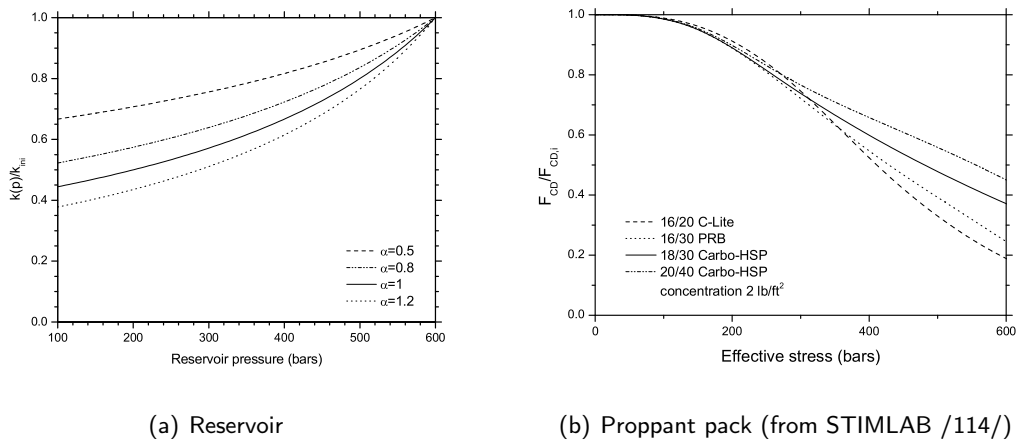


Figure 4.5: Stress dependency of reservoir permeability and fracture conductivity

between effective stress and reservoir permeability. They concluded that permeability declines with increasing effective stress.¹⁹

There are strong indications that tight-gas reservoirs are stress sensitive. First investigations were conducted by VAIROGS /120/ in 1971. FRIEDEL et al. /121/ analysed the production of a German Rotliegend reservoir by means of history-matching of a fractured vertical case study well. It was impossible to reproduce the actual history of the well using constant properties, giving ample indications for the time dependency of certain parameters. Stress dependency could be supportingly observed during the evaluation of well tests. Finally, usage of pressure dependent permeabilities enabled a good history match.

SETTARI et al. /122/ showed the significance of pressure dependent permeability using case studies in North American tight-gas reservoirs and hypothetical examples. Moreover, the authors investigated the relation between cleanup and geomechanical factors by applying history-matching of microseismic²⁰ data. Based on the results, they concluded a distinct increase of permeabilities at low effective stresses (such as during the fracturing process), promoting the leakoff of the fracturing fluid. The authors furthermore presented, by means of well test analysis, that pressure dependent permeability is an identifiable coefficient.

Pressure dependency is affected by a variety of rock parameters, e.g., clay contents, rock heterogeneity, natural fissures and fractures, initial permeability, compressibility, authigenic cementation as well as pore structure (DAVIES et al. /123/). It can be assumed that the significance of pressure dependency increases with decreasing permeability (LORENZ /124/), which makes it particularly important in tight-gas reservoirs. The influence of the compaction on the pore space, i.e., the pore volume, is negligible in gas reservoirs. The gas compressibility exceeds the rock compressibility in magnitudes of orders. It must be only considered in the scope of early reserves estimations (VOIGT /125/).

To quantify the dependency of permeability and stress conditions, DOBRYNIN introduced in

¹⁹A comprehensive outline concerning stress dependency of permeability, porosity or compressibility can be found in TIAB and DONALDSON /119, p.440-461/.

²⁰The fracturing process is observed from a neighbouring well to gather data concerning propagation, propagation velocity, extent and fluid leakoff distribution.

4 Simulation of Hydraulically Fractured Wells

Table 4.3: Effect of stress dependent fracture conductivity (fracture closure) on gas production

	Conc. (lb/ft ²)	$Q_{cum}/Q_{cum,0}$			
		0.01 mD		0.1 mD	
		$F_{CD}=10$	100	10	100
$k_f=constant$	2	1	1	1	1
16/20 C-Lite	2	0.89	0.97	0.92	0.99
16/30 PRB	2	0.91	0.98	0.94	0.99
18/30 Carbo-HSP	2	0.94	0.99	0.96	0.99
20/40 Carbo-HSP	2	0.95	0.99	0.97	1

1970 the following relation derived by means of a capillary model:

$$\frac{k}{k_{const}} = \left[\frac{(\sigma - p)_{const}}{(\sigma - p)} \right]^\alpha \quad (4.15)$$

Focusing on clayey Rotliegendes sandstone, VOIGT et al. /27, p.9 foll./ (1979) determined the material coefficient α for a permeability range 0.01-0.1 mD, based on experimental data from IFFLAND. The correlation of all data indicated a mean value of approx. 1 with increasing tendency for lower permeabilities.²¹ Fig.4.5.a illustrates the relation $k_{res} = f(\sigma - p)$ for stress conditions typically existing in a 4500 m deep tight-gas reservoir. In the simulation tool, the dependency is considered using a transmissibility multiplier $k(p)/k_i$ in tabular form, analog to the *Rock-Compaction* Option in ECLIPSE /53/.

Apart from the reservoir parameters, the increase of the effective stress affects the fracture parameters as well. That means primarily the reduction of fracture conductivity. Analogously, that can be interpreted as a successive closure of the fracture during depletion. The first experimental investigations were conducted by COOKE, who analysed the relation between effective stress and fracture conductivity for certain sand based proppant types. Such proppants fail at high effective stresses if compressive strength is at anytime exceeded. High strength proppants, utilised in tight-gas reservoirs, resist such conditions. Although, the embedment of the proppant into the fracture wall results in a gradual closure of the fracture.²²

Fig.4.5.b shows the dependency of fracture conductivity on effective stress for representative proppant types, based on experimentally determined data from the STIMLAB-Consortium /114/. The values are valid for conditions listed in table 4.1. In the simulator, the decrease of fracture conductivity is solely realised by adjusting the permeability k_f . The width of the corresponding grid blocks remains constant.

In a first set of simulations, only the fracture closure is considered. The parameters for the simulations are adapted from the previous non-Darcy flow example (table 4.1), with a permeability of 0.01 mD and F_{CD} equal to 50. Assuming constant properties, a plateau rate of 670 m³/h can be maintained during the first 600 days before a well flowing pressure of 100 bars is reached. Regarding high strength ceramic proppants, very moderate reductions of productivity emerge. Table 4.3 summarises the results as the ratio $Q_{kum}/Q_{kum,0}$, where $Q_{kum,0}$ is the

²¹The measured values scattered between $\alpha = 0.4...1.1$.

²²The fracture close can be interpreted analogously as steadily decreasing fracture half length, as shown in /126/ by means of history matching field data.

4 Simulation of Hydraulically Fractured Wells

cumulative gas production after 3 years without fracture closure. Assuming realistic fracture conductivities $F_{CD} = 10 \dots 100$, the impact of fracture closure can be neglected. Due to the fact that fracture pressure distribution is steady state after a relatively short flowing time, the level of productivity reduction can be considered almost independent of time. Its influence increases for lower conductivities and reservoir permeabilities.

The reservoir stress dependency impacts the productivity to a much higher degree. The effect of reservoir stress dependency is less pronounced and commonly disregarded in the literature. However, neglecting stress dependency of reservoir parameters seems prohibitive when simulating tight-gas reservoirs according to the results in fig.4.6. The duration of constant rate production declines if stress dependency is taken into account. Terminal rates are considerably lowered. The degree of reduction increases with larger material coefficients α . To isolate the effect of α , only proppant type 18/30 Carbo-HSP (2 lb/ft²) is used.

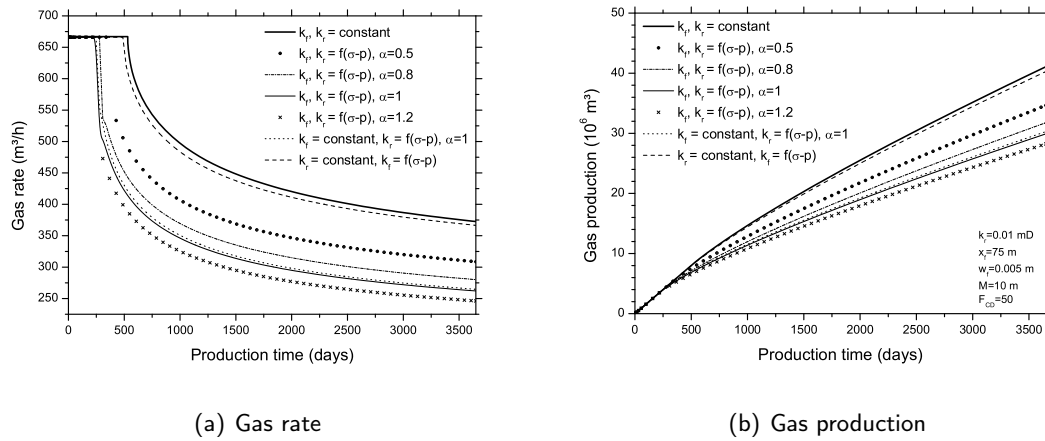


Figure 4.6: Impact of stress dependency on the productivity of a fractured well ($k_{res,i} = 0.01 \text{ mD}$)

In the case where $\alpha = 1$ and considering fracture closure, a total production reduction of 29% has to be expected after 10 years. For a larger reservoir permeability of 0.1 mD and a constant rate production of 3750 m³/h lasting 600 days, similar production constraints arise if $\alpha = 0.8$. Obviously, similar productivity impairments need to be expected for fractured wells below a reservoir permeability of 0.1 mD. To figure out the minimum significance of stress dependency on the productivity, the lower limit of the measured material coefficient ($\alpha = 0.5$) is also considered. Applying the same conditions as in previously, the simulation results still indicate a reduction of 15% gas recovery after 10 years of production.

4.2.4 Combined Effect of Stress Dependency and Non-Darcy Flow

For fractured tight-gas reservoirs with typical properties according to table 4.1 (i.e., F_{CD} of 50 and $x_f = 75 \text{ m}$), an overestimation of gas recovery should be expected in the course of a 10 year production period, if the following factors are neglected:

- Non-Darcy flow in fracture and reservoir: approx. 20-30 %,
- Stress dependency of reservoir permeability and fracture closure: approx. 15-25 %.

4 Simulation of Hydraulically Fractured Wells

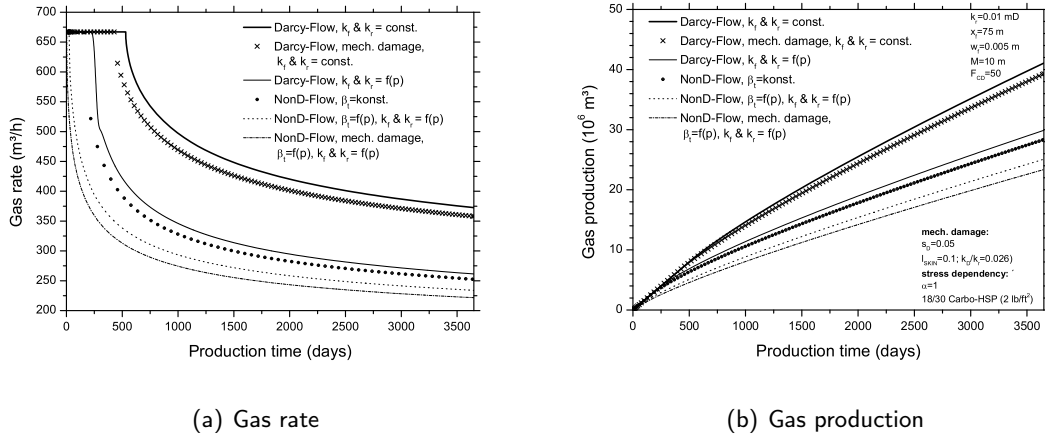


Figure 4.7: Combined effect of non-Darcy flow, stress dependent reservoir permeability and fracture closure on a fractured well ($k_{res} = 0.01$ mD)

All factors were considered separately until now. In reality, the mechanisms will not occur in isolation. In fact, they tend to mutually affect each other. A decrease of reservoir permeability during production (a consequence of lowering the pore pressure) is accompanied by a cutback of flow velocities. Hence, the non-Darcy flow effects will be lowered (which depend quadratically on the velocity). On the contrary, non-Darcy flow coefficients increase with reduced permeabilities.²³

To determine the realistic production from a fractured well, all effects are simultaneously taken into account in another set of simulations. The input data is summarised in table 4.1. The stress dependency of reservoir permeability is considered using eq.(4.15) with a material coefficient α equal to 1. The fracture with $F_{CD} = 50$ is propped using 18/30 Carbo-HSP. Both dependencies of reservoir permeability and fracture closure on the effective stress are depicted in fig.4.5. Non-Darcy flow coefficients for the reservoir are calculated using eq.(4.12). The initial value is $\beta_r = 1 \cdot 10^{14}$ 1/m. To capture the permeability and therefore the pressure dependency of the β -coefficients, stress dependent non-Darcy flow coefficients were implemented into the simulation model using the correlation eq.(4.12) and eq.(4.13). Fracture non-Darcy flow is considered with both damaged and undamaged proppant packs according to table 4.2.

The results are summarised in fig.4.7. As expected, there is no linear superposition if all three effects are considered simultaneously. Instead, the overall reduction is distinctly lower than the sum of the single effects due to their mutual interaction. Assuming a scenario with non-Darcy flow in the fracture and reservoir, stress dependency of permeability as well as fracture closure, a total reduction of 40% is possible in a 10 year production period (instead of 55% when considered separately).

²³ZENG et al. /127/ presented a corresponding experimental study of overburden and stress influence on non-Darcy effects at Dakota sandstones.

4.3 Load Water Cleanup and its Impact on Post-Fracture Production

Productivity impairment is considered a typical phenomena in tight-gas formations. Experiences from the field show that rates are frequently lower than the predictions. Some potential reasons for that discrepancy were discussed in the previous section. However, fracturing tight formation involves a risk of damaging the reservoir. In this section, hydraulically and mechanically induced damage is investigated by analysis of the load water cleanup process.

4.3.1 Background

During the fracturing process, a large volume of technical fluid is injected into the reservoir utilising high pressure and high flow rates. As soon as the fluid is in contact with the rock, some of it leaks off along the fracture face into the formation. After pumping is stopped, the remaining low viscous fracturing fluid still imbibes into the formation due to capillary forces and overpressure in the fracture. Eventually, after the treatment is finished, an invaded zone around the fracture will be formed. The extent of that zone depends, e.g., on the exposure time of the fluid to the formation, as well as fluid and reservoir parameters.

The saturation conditions in the invasion zone are responsible for the occurrence of hydraulically induced damage, either by capillary forces or relative permeability effects, or a combination of both. Those functions may have considerable impact on the cleanup behaviour of a fractured well. In contradiction to conventional gas reservoirs, they are distinctly different in tight formations. This may affect the characteristics of the well significantly (BENNION et al. /128/, REITENBACH et al. in /126/). The capillary pressure is inversely proportional to the pore radius. Hence, capillary forces are acting stronger in tight formations, where effective pore radii are small (PENNY et al. /129/). It is characteristic of low permeability gas reservoirs to have a poor single-phase water permeability, 3 to 10 times smaller than the of the rock permeability. In the presence of a gas phase, the waters relative permeability is further decreased. That is a reason for a strong decline of the water phase mobility during cleanup, combined with low water production in the subsequent production period (/126/).

The limited water mobility and the capillary forces imply that: (i) the load water of the fracturing fluid can not be drained completely from the gas phase, and (ii) the gas relative permeability is permanently lowered due to the water retained in the invasion zone. HOLDITCH /81/ investigated factors affecting water blocking and the gas flow from fractured wells using numerical simulation. He stated that the gas flow can even be blocked totally if the drawdown pressure does not exceed the capillary pressure in the invaded zone. This is particularly the case if permeability in the invaded zone is impaired as a consequence of so called mechanical damage. In the course of the fracturing treatment, the permeability within the immediate fracture vicinity may be severely reduced. That usually implies tremendous capillary forces and, thereby, an accumulation of water in the mechanical damage zone causing additional flow resistance for the gas phase (/81, 126/).

A variety of numerical cleanup studies have been published in the past, such as those by TANNICH /130/, HOLDITCH /81/, SOLIMAN and HUNT /82/ as well as others /80, 131, 132, 133/. Recently, further case studies have been presented from SETTARI et al. /122/, FRIEDEL et al. /121, 134, 135/ and BEHR et al. /136/. Besides the numerical studies, experimental studies have been conducted to improve the load water recovery, e.g., by PENNY et al. /129/.

4.3.2 Cleanup Simulation Model

Leakoff Modelling. To perform cleanup simulations, it is essential to consider the saturation conditions within the leakoff zone. There are several approaches how to take account of the leakoff in the simulation model, which are briefly introduced here.

The initialisation of the reservoir post-fracture simulation model with respect to the fluid saturation can be obtained via the numerical modelling of the fracture treatment. In the special fracture simulators developed by SETTARI /90,102/ and NGHIEM et al. /89/, a fracture mechanics model was coupled with the fracture and reservoir two-phase flow equations.²⁴ These implied the mass exchange between the fracture and formation on the basis of Darcy's law. Thus, the formation of the invaded zone during the fracture propagation was described by the general theory of fluid flow in porous media.

The peculiar conditions on the fracture surface (e.g., deposition of the filter cake) and the features of the fluid properties cause a need for a special model describing the flow of fracturing fluid into the reservoir. In the classical leakoff theory, the flow rate varies inversely with the square-root of time. The factor of proportionality, the leakoff coefficient, is a characteristic of the formation and the fracturing fluid. On this basis, other fracturing modelling algorithms (HOWARD and FAST /137/) were developed where the fracture propagation model was solved independently of the reservoir equations. However, such approaches are not aimed at providing the solution for the saturation profile in the invaded zone.

On the basis of a generalised leakoff model²⁵, SETTARI /90/ suggested a partially decoupled modelling of the fracturing whereby processes in the formation were taken into account, but in a manner that did not require numerical solving of the reservoir model. The flow through the invaded zone was considered as piston-like displacement (with some corrections for two-phase flow effects). This led to the build up of an idealised uniform saturation profile, in a normal direction to the fracture surface.

When the modelling is focused upon the post-fracture well performance only, the problem of estimating the fluid distribution in the damage zone is handled in radically different manner. In this case, it is assumed that monitored data (fluid and proppant injection during the fracture treatment) and geometry parameters of the stationary fracture are available. In a typical - and simplest - approach, the whole amount of invaded fluid, calculated from the material balance, is placed in the fracture surrounding region (TANNICH /130/ and BASTIAN et al. /80/). In doing so, the depth of invasion can depend on the porosity, net thickness value and reservoir water saturation, and may even be correlated in a way to take varying exposure times into account.²⁶

Furthermore, the flow of fracturing fluid into the reservoir can be represented by solution of common multi-phase flow equations in porous media. Hence, usage of reservoir simulation is capable of an improved treatment of fluid loss with appropriate boundary conditions, e.g., properties and pressure at the wall (behind the filter cake). Nonetheless, the multi-phase simulation approach also suffers from limitations. The process of fracture fluid filtration is more complicated than the reservoir multi-phase flow (/138/). Simplifying the fracturing fluid phase as a reservoir fluid phase (water) may be mistaken, since properties can greatly deviate and vary with time because of breakers, temperature changes, and mixing processes. The fracturing fluid can be miscible with one of the resident fluids. A proper formulation then

²⁴The filtrate assumed the properties of the reservoir water.

²⁵A detailed introduction to leakoff in porous media is given by VALKO et al. /32, p.183 foll./.

²⁶Exposure time at the tip is much less than at the fracture center.

4 Simulation of Hydraulically Fractured Wells

requires solution of three-phase flow (one phase being the fracture fluid) with time dependent relative permeabilities, capillary pressure and viscosities. In spite of the feasibility of such a formulation and its solution, the multi-phase data is almost impossible to obtain because of the nonlinearity and instability of the gels. Consequently, one must make simplifying assumptions (SETTARI /138/), e.g., the filtrate assumes the properties of the reservoir water.

An advantage of the multi-phase approach is that the immediate transition to further simulation of the post-fracture production is provided. At the same time, replacing the fracturing process with a fictive water injection can be mistaken in many points. For example, the time which the water front takes to arrive at a specified location of the fracture depends heavily on the fracture conductivity.

Other approaches are suitable to consider the history of the fracturing process more accurately if detailed information about the fracturing process is available. BEHR et al. /86/ presented an external coupling based on a simplified fracture propagation model. The fracturing treatment scenario was translated into the spatial distribution of the exposure time of the fracturing fluid to the formation.²⁷ The reconstructed exposures times and leakoff coefficients were used to calculate the saturation profiles by means of Buckley-Leverett displacement equations, performing a similarity transformation of the dimensionless semi-analytical solution.

In the current cleanup model, the leakoff is represented by injecting an appropriate volume of fluid into the formation. Fluid efficiency factors at closure can be taken into account to ensure proper saturation distributions, if the leakoff volume is unknown *a priori*.²⁸ In addition to the leakoff volume, a volume equal to the fracture grid block pore volume should be injected to displace the entire leakoff volume into the formation. Furthermore, the pumping schedule can be discretely considered if available.

The gas and the water phase present the relevant fluids during the load water recovery and in the subsequent post-fracture period. To permit this simplification, there are several assumptions. The most critical are:

- The fracturing fluid is represented by the water phase. This implies that the infiltrated fluid is purely the load water with identical properties like those of connate water within the reservoir. No polymers or any other highly viscous fracturing additives are supposed to exist in the formation.
- There are no solid residues within the fracture. The polymers break up completely and the fracturing fluid is solely degraded to a fluid with corresponding water properties.

This approach is in accordance with a variety of cleanup studies in the literature (/81, 82, 130, 132/). However, realistic treatment of leakoff requires the solution of the physics of the complex fracturing process, e.g., formation and erosion of a filtercake²⁹. This is beyond the scope of common reservoir simulation issues. Rather, the simplified approach of injecting fluid is combined with a fracture propagation imitation to gather saturation profiles as realistically as possible.

²⁷Therefore, the leakoff coefficient had to be iteratively adjusted in the course of solving this model.

²⁸Real leakoff volume can be derived by comparing the injected fluid and the volume back produced.

²⁹Fluid loss additives and polymers in the fracturing fluid are intended to form a filter cake to minimise the leakoff. Filter cake is an essential part of the general leakoff theory, see SETTARI /138/. A theoretical and experimental outline of filter cake was given by MAYERHOFER et al. /139/.

4 Simulation of Hydraulically Fractured Wells

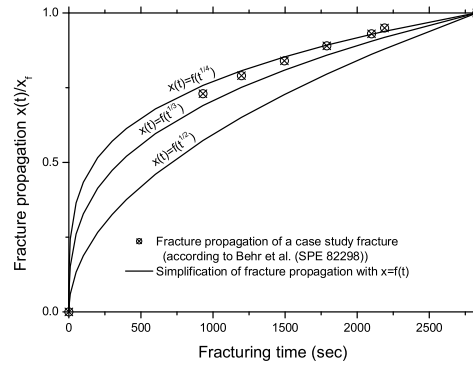


Figure 4.8: Fracture propagation: field data and approximative functions

Fracture Propagation. To account for the propagation of the fracture and the corresponding saturation distributions, time dependent transmissibility multipliers can be utilised. The fracture grid blocks are determined in every time step such that:

$$x_f = f(t) , \quad (4.16)$$

with the boundary conditions $x_f(t_0) = 0$ and $x_f(t_{\text{end}}) = x_f$. Fracturing is completed at t_{end} . In principal, every user defined function can be applied to describe the propagation of the fracture with time. Initially, all fracture grid blocks are treated as belonging to the reservoir domain. If a grid block shifts from reservoir domain to the fracture domain, its properties and regional affiliation, e.g., describing the multi-phase flow behaviour, are adjusted correspondingly.

Sophisticated fracture propagation simulation involves the coupled solution of elasticity, flow and material balance equations. Nonetheless, the implementation of a fracture propagation model based, e.g., on the common PKN³⁰ or KGD³¹ fracture geometry models, is not intended in the framework of this simplified approach. Those models are capable of predicting the evolution of fracture dimensions and wellbore pressure, given a particular fluid injection history (VALKO and ECONOMIDES /32/).³²

An example for a fracture propagation is given in fig.4.8. The propagation process of a case study fracture (opened dots) in a North German Rotliegend reservoir was presented by BEHR et al. /86/ using a simplified propagation model. The additional graphs show distinct root functions which are suitable to represent the fracture propagation at least approximately. Fig.4.9 illustrates the distinct saturation conditions for two approaches: (a) with explicit consideration of the fracture propagation and (b) with imitation of leakoff history by injecting into a stationary fracture instead. By accounting for the propagation, the saturation profile is more realistic and

³⁰PERKINS, KERN and NORDGREN model /32/.

³¹KHRISTIANOVITCH, ZHELTOV, GEERTSMA and DE KLERK model /32/.

³²A simpler model was presented by Carter (/140/):

$$x_f(t) = \frac{Q_{\text{inj}} b_f}{\pi h_f C_l^2} \left[\frac{2\beta}{\sqrt{\pi}} - 1 + e^{\beta^2} * \text{erfc} \beta \right] , \quad (4.17)$$

with injection rate, fracture height h_f , fluid loss coefficient $C_l = \Delta p \sqrt{\phi c_t k_{\text{res}} / (\pi \mu)}$ and $\beta = C_l \sqrt{\pi t} / b_f$. For large times, eq.(4.17) implies the proportionality $x_f = f(\sqrt{t})$.

4 Simulation of Hydraulically Fractured Wells

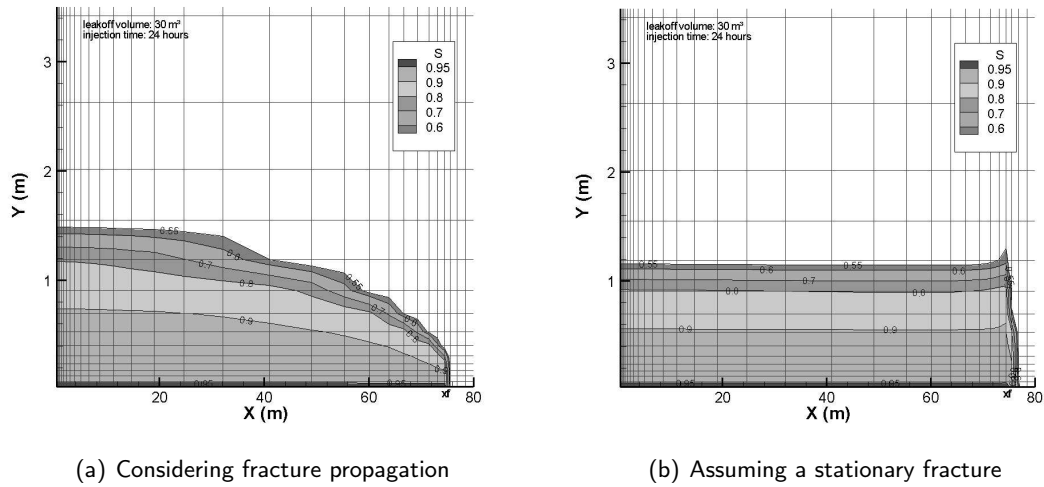


Figure 4.9: Initial saturation profile after fracturing via injecting the fluid

of the expected elliptical shape. In contrast, injecting into a stationary fracture, i.e., considering the leakoff implicitly via the propagating water front, results in a water block of rectangular shape with an essentially higher water saturation at the fracture tips.³³ This is even the case if fracture conductivity F_{CD} is as low as 2.

The two different types of saturation profiles can be related to the kind of fluid loss. If the mechanisms are mainly controlled by the leakoff coefficient, then the corresponding saturation profile is of elliptical shape. Contrary to this, a spurt loss³⁴ dominated leakoff, is typically characterised by a more rectangular shape of the invasion zone (/3, p.9-46/). Hence, if there is no spurt loss during fracturing, it is a better alternative to consider the propagation. For spurt dominated treatments, injection into an open fracture yields good results.

The methodology chosen can affect the gas breakthrough time as well as gas rate level. In particular, if those parameters are considered in the framework of history matching, their sensitivity inheres potential errors. It should be noted that numerical effort is increasing if propagation is considered.

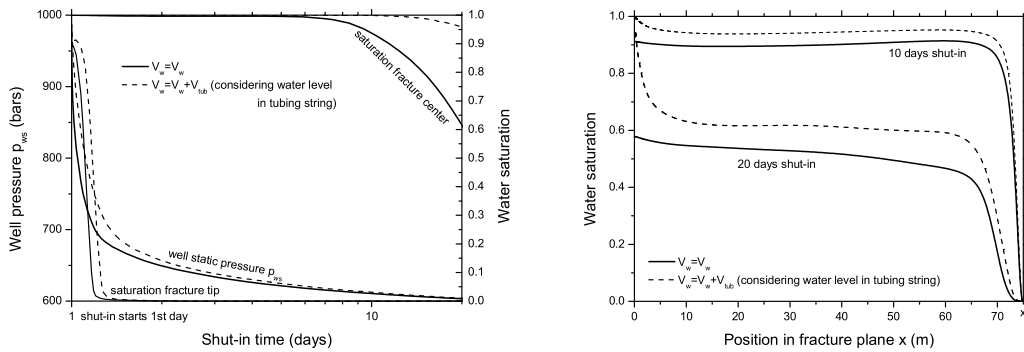
Shut-In Consideration. In the field, the stimulation treatment is followed by a shut-in of the well to initiate fracture closure and proppant embedment. To simulate the "dissipation" of the pressure perturbation, the well can be closed for a specified period of time. A duration of one to several days is usually sufficient to nearly restore the initial pressure conditions. The development of the well pressure with a final fracturing pressure of 960 bars and a reservoir permeability of 0.05 mD is shown in fig.4.10.a. The bottom hole pressure drops quickly to 650 bars within one day, and asymptotically approaches the initial field pressure of 600 bar during 20 days of shut-in.

Strong capillary forces may lower the water saturation within the fracture by the imbibition

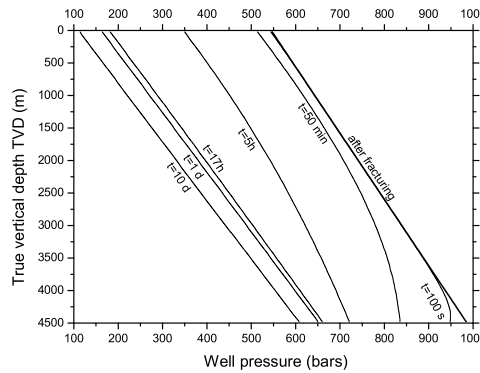
³³The lower the reservoir permeability, the more rectangular becomes the shape of the invaded region with nearly equal filtrate penetration depths at the wellbore and at the propped fracture tips (/141/).

³⁴The instantaneous volume (spurt) of liquid that passes through a filter medium, prior to deposition of a competent and controlling filter cake (/142/).

4 Simulation of Hydraulically Fractured Wells



(a) Well pressure at the bottom hole and saturation distribution at fracture center and fracture tip (b) Saturation distribution in the fracture plane



(c) Development of pressure inside the well during shut-in ($\rho_{fl} = 1146 \text{ kg/m}^3$)

Figure 4.10: Pressure and saturation development during shut-in of the well using different shut-in realisations with and without considering the water volume in the well

process during the shut-in period. The lower water saturations away from the fracture imply larger capillary pressures and, hence, a pressure gradient in the water phase from the fracture into the reservoir. This is even more pronounced due to the pressure gradient as a consequence of the fracturing treatment. Therefore, water will flow from the fracture and its vicinity deeper into the matrix. The process occurs rather slowly due to the low reservoir permeability and restricted water mobility. However, if water flows from the fracture into the matrix, the pressure in the fracture is lowered due to the low compressibility of the water phase. The fracture gas saturation successively increases. This process occurs in the field as well as in the simulation model if capillary forces are taken into account. A premature gas breakthrough is likely though if the saturation and pressure conditions in the cleanup model deviate from reality.

In a typical simulation model, the well is shut either within the perforation or on the top of the perforation. On the contrary, a well in the field is water filled up to a certain level in advance of the cleanup process. The fictitious well in the simulation model does, therefore, not

4 Simulation of Hydraulically Fractured Wells

consider the real level of the fracturing fluid in the tubing string. The water in the well acts as a pressure storage "reserve". Consequently, the pressure in the simulation sinks faster than would be expected in the field if the additional water volume is neglected. As explained, this may also affect the saturation conditions in the fracture.

To take the true water volume into account, there are two different options implemented in the current cleanup model. The first simply adds the volume of the wellbore to the volume of the well block during the shut-in period. This operation can also be applied in commercial codes utilising pore volume multipliers. Although considering the proper water volume, the pressure of the water volume is intrinsically equal to the well block pressure. After the injection, this pressure can easily amount up to 1000 bars. Hence, the energy of the water is much higher than that which the water would have in a vertical pipe, where pressure is distributed hydrostatically, causing a delay in the pressure drawdown. The second option discretely considers the well track in the simulation model as explained previously.

Fig.4.10.c shows the development of the transient pressure distribution of a slightly compressible fluid in a vertical well, after the well was shut at the tubing head. The initial pressure distribution is hydrostatic. A comparison of all three options for shut-in treatment is presented in fig.4.10.a and b. The well is shut immediately after the fracturing. Shut at the bottom hole (thick solid line), the pressure sinks relatively fast, causing gas accumulation at the fracture center from the 6th day of shut-in. The saturation at the fracture tip, however, declines to zero during several hours.

Considering the entire tubing volume in the well block (dashed line), the water pressure decline is significantly decelerated. Thus, the lowering of water saturation occurs more slowly. The usage of the discrete well flow modelling option (chain dotted line), also decelerates the pressure decline at the bottom hole, although to a lesser extent than the previous option. The saturation profiles inside the fracture plane in fig.4.10.b present both the initial conditions as well as those prevailing after 10 and 20 days of shut-in, and pronounce the differences of all three approaches.

If detailed investigations, e.g., in the framework of a history matching process, are not in the scope of the analyses, there is another simple method that ignores the shut-in period and starts the cleanup simulation immediately after the injection. The simulation then needs to be restarted, with the saturation distribution from the end of the fracturing process and a pressure distribution according to the initial (undisturbed) conditions. For most cases this is not supposed to curtail accuracy.

Multi-Phase Flow Functions. Linear functions are used in order to describe the simultaneous flow of water and gas within the fracture, $k_{r,w} = S_w$ and $k_{r,g} = 1 - S_w$. Capillary forces are not supposed to affect the flow, $p_{cap} = 0$. These simplifications are in accordance to studies reported in the literature (/81, 130, 141/).³⁵

The multi-phase flow in the reservoir domain is regarded by means of a Brooks-Corey model. Instead of using the common tabular form of saturation versus relative permeability or capillary pressure, the entire model, based on normalised saturations, is implemented in the simulator. The entire method is briefly summarised in appendix D (p.113); the input functions for a permeability of 0.05 mD are presented in fig.D.1.³⁶

³⁵ALVAREZ et al. /107/ used slightly concave functions for the relative permeabilities.

³⁶The critical gas saturation was determined to be just 0.05, which can be considered extremely low. This parameter can easily range up to 0.25 or more; however, "real" comparative values were not available.

4 Simulation of Hydraulically Fractured Wells

Table 4.4: Parameters for cleanup simulation

Reservoir parameters		Scenario	
Reservoir permeability (mD)	0.05	<i>Fracturing process</i>	
Reservoir porosity	0.1	Leakoff volume (m ³)	15-60
Residual water saturation S_{wr}	0.5	Duration of injection (h)	12-48
Material parameter λ	1	<i>Well shut-in</i>	
Initial Pressure (bar)	600	<i>Cleanup process</i>	
Fracture parameters		Well pressure (bar)	600-150
Half length (m)	75	<i>Production period</i>	
Dimensionless conductivity	20	Well pressure (bar)	150
Porosity ³⁸	0.05	Duration (days)	365
Width (m)	0.1		

4.3.3 Hydraulic Damage

To analyse the impact of the hydraulic damage³⁷, first a simple numerical experiment is conducted. Using the cleanup model, the treatment volume, i.e., the injected volume, is varied from 15 to 60 m³ in order to investigate the relation between leakoff volume and productivity impairment of the fractured well.

Fracture and reservoir parameters are summarised in table 4.4. In order to realise the different scenarios, the injection time is changed, while injection rate (into the open fracture) is held constant at 30 m³/d. Fracture propagation is not considered to be important in this general type of analysis. The maximum injection pressure in the simulation may exceed the "real" fracturing pressures (up to 1000 bars).³⁹ The initial saturation profiles, orthogonal to the fracture face at the wellbore $x/x_f = 0$, are illustrated in fig.4.11.b. The invasion zone extends from a few decimeters to about 1.5 m into the formations.

Following the leakoff, pressures are reset to the initial pressure after the injection to ensure identical starting conditions for all scenarios. During the subsequent cleanup period, the bottom hole pressure is linearly interpolated over the time axis, between initial reservoir pressure and final bottom hole pressure. This is done since the fluid column within the well, after the fracturing in the field, can not be removed immediately. Here, the length of this period is assumed equal to the injection time.

The simulation results are shown in fig.4.11.a and summarised in table 4.5. Gas breakthrough time, gas rate and load water recovery are the characteristic variables for cleanup processes (/126/). The thick line presents the undamaged gas rate. The gas rate hyperbolically declines during the first year of production. If cleanup effects are considered, it takes some time until gas breakthrough occurs at the wellbore, depending on the leakoff volume. In case of 60 m³ leakoff volume, the breakthrough occurs after approx. 1 day at the bottom hole.

³⁷Hydraulic damage, considered here, is caused by increased water saturation in the nearer fracture vicinity. Accordingly, gas relative permeability is lowered in the invaded zone, causing additional flow resistance for the gas.

³⁸Reduced according to pore volume maintenance due to enlarged, fictitious fracture width.

³⁹MONTGOMERY et al. /132/ injected at constant rate until the maximum treatment pressure was reached to continue with this pressure until the entire treatment volume was injected.

4 Simulation of Hydraulically Fractured Wells

Table 4.5: Results for cleanup simulation after 1 year of production

Injected volume (m ³)	Gas recovery (10 ⁶ m ³)	Water recovery ⁴⁰ (m ³)	Water production time (days)
0	1.04	0	0
15	1.02	11.7	15
22.5	1.01	15.0	33
30	1.0	20.5	66
45	0.98	27.2	159
60	0.96	36.1	316

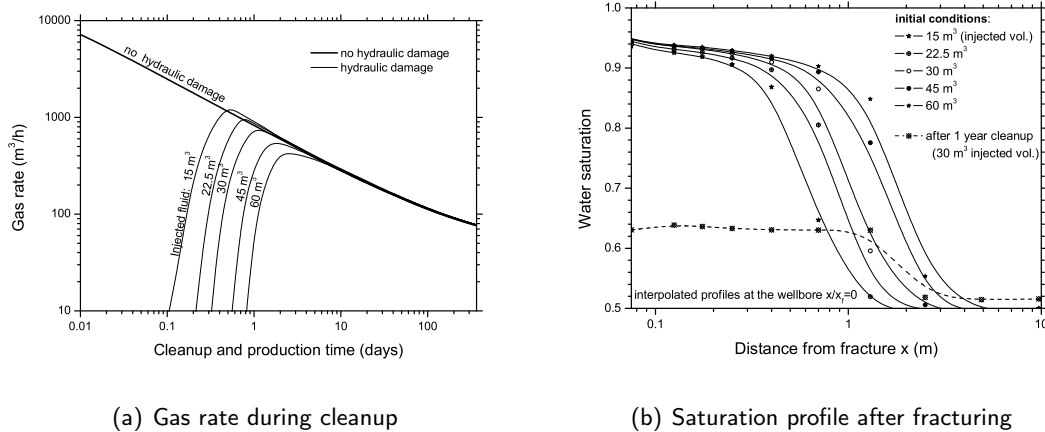


Figure 4.11: Cleanup process with hydraulic damage

Following the gas breakthrough, the gas rate steeply increases to its maximum typically during several hours. After the production peak is reached, the rate declines *de facto* identical to the undamaged case. As obvious from the results in fig.4.11.a, gas rates are practically equal after some days. Furthermore, the gas rate turns out to be independent on the injected volume and, hence, on the depths of the invaded zone (if solely relative permeability and capillary pressure effects are considered in the simulation model). The maximum loss in cumulative gas recovery is about 7 % for the case of greatest damage. The saturation profile after one year of production is illustrated in fig.4.11.b for 30 m³ leakoff volume. The dependence of duration of load water recovery on the leakoff volume is presented in table 4.5.

The level of ultimate load water recovery is roughly constant for all cases at 60 %. In contrast, load water recovery in the field is frequently lower, commonly 25-55 % (/143, 144/). The water remaining in the formation is essentially immobile.⁴¹ The mobility of the water phase depends on its relative permeability as well as on the viscosity. Using the the Brookes-Corey model (fig.D.1, p.114), the water phase relative permeability is *de facto* less than 1e-4 for $S_w < 0.63$. Due to the gas-water mobility ratio, it is, hence, almost impossible to reduce the

⁴⁰Including the fracture volume of 3.75 m³.

⁴¹Eventually, some of that formation water becomes mobil in the course of the production due to the water compressibility. The amount is typically 2-5 % for common tight-gas conditions.

4 Simulation of Hydraulically Fractured Wells

water saturation within the invasion zone below that value. This manifests in the stationary saturation profile with a constant value $S_w = 0.63$ (despite $S_{w,irr} = 0.5$). The reason here is the flat slope of the water relative permeability in the Brookes-Corey model.

The results indicate that capillary pressure and the resulting end effect do not have significant impact on the gas production. Water recovery may be affected but as shown in the case under consideration, the water remaining in the fracture vicinity does not impact on the gas flow. Typical drawdown pressures are supposed to exceed the capillary forces in common (undamaged) tight-gas reservoirs. In summary, the simulation results indicate that only hydraulic damage itself is not likely to curtail productivity of tight-gas wells.⁴² The conclusion is of course restricted to the validity of the underlying assumptions, i.e., no hysteresis in capillary pressure or relative permeability and applicability of conventional multi-phase flow correlations in tight formations.

Comparison of Damage for Fractured and Radial Wells

Hydraulic fractured wells are less affected by hydraulic damage than common unfractured wells, where productivity may be severely lowered. This is mainly caused by the difference in the flow patterns. The geometry of both is illustrated in fig.4.12.

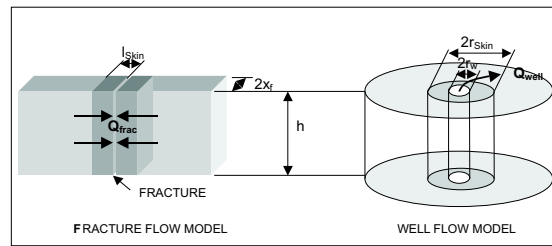


Figure 4.12: Schematic of fracture and well flow model

Flow is considered approximatively stationary with identical damage zone dimensions, see fig.4.12. The skin zone can be either an area of reduced absolute permeability or of reduced relative permeability (i.e., in the invasion zone), or a combination of both. Having equal flow rates, the relation of the pressure drop between the fractured well, Δp_f , and the unfractured well, Δp_w , in the skin zone can be derived as:

$$\frac{\Delta p_w}{\Delta p_f} = \frac{2x_f \ln(r_{skin}/r_w)}{l_{skin} \pi}, \quad (4.18)$$

where $r_{skin} = r_w + l_{skin}$. Assume an identical permeability reduction in both cases with an invaded zone $l_{skin} = r_{skin} - r_w = 1$ m, a fracture half length $x_f = 75$ m and a well radius $r_w = 0.1$ m. The resulting pressure drop in the radial well skin zone is then about one hundred times higher than in the fracture skin zone, i.e., $\Delta p_w = \Delta p_f * 114$. The strongly differing pressure reductions in the damaged zones will therefore affect the unfractured well to a distinctly higher degree. The gas rate will be much more reduced.

⁴²The controlling factor is the shape of the gas relative permeability function. With $S_w = 0.63$, the gas relative permeability $k_{r,g}$ is reduced to 40% of the end point permeability. Using the skin equation eq.(4.22) and an invasion zone extension of 1 m (fig.4.11.b), the corresponding damage is comparable to a skin factor of 0.02 in a single-phase system.

4.3.4 Combined Occurrence of Hydraulic and Mechanical Damage

Previously, other authors (HOLDITCH /81/, SETTARI et al. /122/) stated that hydraulic damage is not likely to occur, as long as invasion of the fluid is not accompanied by mechanical damage. Following the methodology of HOLDITCH /81/, the effect of mechanical damage is regarded as isolated by means of a single-phase model first. There are two basic kinds of mechanical damage: (i) the fluid-flow impairment at the fracture surface, and (ii) the flow impairment as a consequence of reduced conductivity in the fracture near the wellbore. The latter case is termed choked fracture and is not in the scope of the investigations.

Mechanical Damage in Single-Phase Systems

Mechanical damage results in a reduction of permeability and porosity close to the fracture vicinity. Its primary origin is the fracturing process. Injecting large volumes of technical fluid into the formation is frequently accompanied by a deposition of solids near the fracture wall or the formation of a filter cake. Additionally, dilatancy effects, caused by alternating stress load during the fracturing process, may further lower the permeability in the nearer fracture vicinity (REITENBACH et al. /145/). Clay minerals, interacting with the invading fluid, can swell and blockade the conductible pores. During the cleanup, an incomplete breaking of the gel plugs the pore space next to the fracture wall. Eventually, migration of fines, as well as diverse physical resp. chemical processes⁴³, are conducive to the occurrence of mechanical damage even in the course of subsequent production.

First investigations on the impact of mechanical damage trace back to VAN POLLEN /146/ (1957). He studied the subject by means of a single-phase model. HOLDITCH /81/ conducted a sensitivity analysis using characteristic tight-gas parameters and a single-phase model. For the present analysis, the type-curve analysis is again utilised. Both main parameters, dimension and degree of permeability reduction, are unknown *a priori*. Preferentially, both should be determined by history matching of field data or, if at all possible, by experiments. Core analyses, performed at tight samples, demonstrated a potential fracture face damages caused by gel filter cake. The corresponding permeability reductions ranged from one tenth to one hundredth of the formation permeability (VONEIFF et al. /141/).

A dimensionless skin factor is introduced to incorporate the mechanical damage in the type-curve analysis. It can be derived assuming a fracture surrounded by a damaged zone of width l_{skin} and permeability k_{skin} which is less than the formation permeability k_{res} . Since gas flows from the reservoir into the fracture, it has to pass the damage zone. If stationary and linear flow is considered, the additional pressure drop in that region, Δp_{skin} , can be computed by subtracting the pressure drop occurring in a damaged case ($k_{\text{skin}} = k_{\text{res}}$) and the pressure drop in the undamaged case:

$$\Delta p_{\text{skin}} = \frac{q_f \mu l_{\text{skin}}}{h k_{\text{skin}}} - \frac{q_f \mu l_{\text{skin}}}{h k_{\text{res}}} = \frac{q_f \mu l_{\text{skin}}}{h k_{\text{res}}} \left(\frac{k_{\text{res}}}{k_{\text{skin}}} - 1 \right). \quad (4.19)$$

Here, q_f is the influx into the fracture per unit length. Substituting q_f with the total well flow rate $Q = 4q_f x_f$, the pressure drop in the skin zone can be computed:

$$\Delta p_{\text{skin}} = \frac{Q \mu}{4h k_{\text{res}}} \frac{l_{\text{skin}}}{x_f} \left(\frac{k_{\text{res}}}{k_{\text{skin}}} - 1 \right). \quad (4.20)$$

⁴³Such as the precipitation of solids or salt minerals.

4 Simulation of Hydraulically Fractured Wells

For a radial well, the pressure drop caused by the skin is defined as /36, p.117/:

$$\Delta p_{\text{skin}w} = \frac{Q\mu}{2\pi kh} S_{Dw} . \quad (4.21)$$

After equating eq.(4.20) with eq.(4.21) and rearranging, the skin factor for the fractured well can be derived as follows:

$$S_D = \frac{l_{\text{skin}}}{x_f} \left(\frac{k_{\text{res}}}{k_{\text{skin}}} - 1 \right) , \quad \text{where} \quad \Delta p_{\text{skin}} = \frac{\pi}{2} \frac{Q\mu}{hk_{\text{res}}} S_D . \quad (4.22)$$

This skin factor S_D is similar to the parameters of PRATS /77/ (1961) as well as CINCO-LEY and SAMANIEGO /147/ (1977). The type-curves $\log 1/q_D = f(\log t_{Dx_f})$ are presented in appendix C.3 (p.111) for constant pressure production and $F_{CD} = 10$ and 50.

The range of the skin factor S_D from 0 to 1 is based on conceivable and common conditions. However, the proportion of fracture skin factors (eq.(4.22)) and the skin factors for radial wells are not readily comparable, since both quantities are referenced to different characteristic lengths and flow patterns (/3, p.12-22/). According to the same source, typical values of fracture face skins, solely induced by the usage of clean-breaking fracturing fluids, are generally low (in a magnitude of 0.015 or less). To appraise the impact of mechanical damage on the total gas production, a dimensionless cumulative gas production is introduced in fig.C.3 (p.111) which is the integral of the dimensionless production rate. This chart is useful to predict a potential loss of recovery at any arbitrary point of time, provided that the skin effect does not decrease with enduring production or completely diminish. The methodology is applied to two examples in the following.

Consider again the example with $F_{CD} = 50$, $x_f = 75$ m and $k_{\text{res}} = 0.1$ mD. Due to the fracturing process, the permeability is reduced to a tenth of the initial value within a skin zone of $l_{\text{skin}} = 0.1$ m. Inserting into eq.(4.22) yields a skin factor S_D of 0.012. To estimate the resulting productivity loss after 2 years of constant pressure production, the dimensionless time needs to be calculated then. With $c_t = 9.3 \cdot 10^{-9}$ 1/Pa and $\mu = 0.029 \cdot 10^{-5}$ Pa s for the reservoir under initial conditions, the dimensionless time t_{Dx_f} is 41.3. The resulting impairment of productivity can be graphically determined at roughly 1% by means of the dimensionless cumulative gas production graph in C.3. Decreasing the permeability further to 0.25% of the initial permeability, will result in an impairment of 24%. The corresponding skin factor S_D is then about 0.5.

Cleanup in Mechanically Damaged Reservoirs

In the previous single-phase model, mechanical damage was considered by reducing the permeability within the fracture vicinity. On the contrary, the change of the pore structure resp. of the morphology of the matrix will affect porosity and, most notably, the multi-phase flow behaviour as well (see FRIEDEL et al. /135/). In the scope of the following analysis, the reduction of absolute permeability is assumed to influence solely the capillary pressure instead of relative permeabilities. Additionally, porosity is kept constant during the runs.

When capillary pressure increases in the damaged zone, water starts to flow from the adjacent domain into the zone of lower permeability. This is due to the water pressure gradient. Therefore, water accumulates there and, possibly, a total water blockage occurs. Gas production can be even permanently impaired (/81/). To account for the impact of the mechanical damage

4 Simulation of Hydraulically Fractured Wells

on the multi-phase flow, the methodology of the Leverett J-function is used. Capillary pressure can be correlated as a function of permeability and porosity (/37, p.71/):

$$p_c(S_w) = \sigma \cos \theta J(S_w) \sqrt{\frac{\phi}{k}} . \quad (4.23)$$

The function $J(S_w)$ is assumed the same for a particular type of rock. The Leverett function is implemented in the simulator by calculating a scaling factor $F = \sqrt{\phi/k}$ for every grid block. Subsequently, the constant product $\sigma \cos \theta J(S_w)$ is multiplied with the value of F to get the capillary pressure in the damaged region.

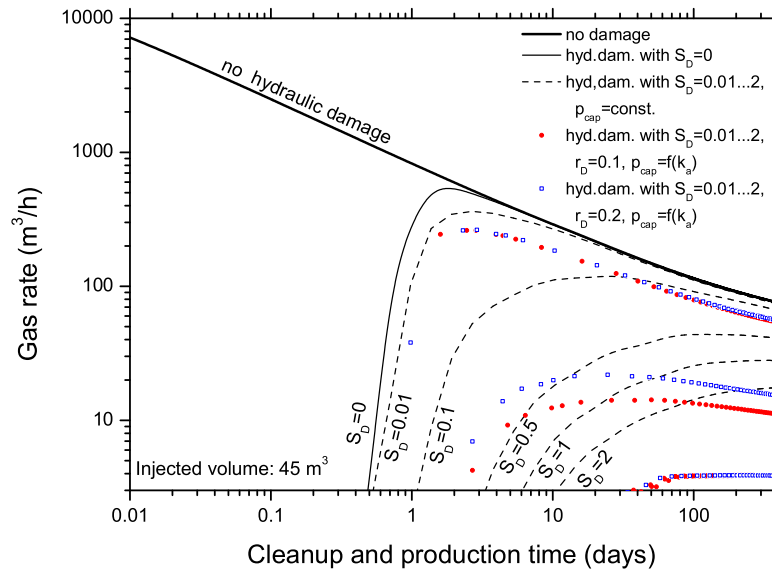
In the course of the investigations, two damaged regions are considered: $l_{\text{skin}} = 0.1$ m and $l_{\text{skin}} = 0.2$ m. The permeability reduction in the zone is calculated by means of the skin equation eq.(4.22). Starting from the undamaged case $S_D = 0$, the values range up to 2 which can be considered an extreme damage. Simulation of multi-phase flow is based on the parameters from table 4.4. At first, a treatment volume of 45 m³ is injected into the formation. The resulting saturation profile is shown in fig.4.9. The mechanical damage zone is introduced next, entirely spanning the length of the fracture. This is done since no information concerning the real shape of that zone is available.

Fig.4.13 shows the the gas rate (a) and the cumulative gas production (b) for the first year. Having $S_D = 0$, the gas rate is affected solely by hydraulic damage. As stated before, a real productivity reduction is not likely to occur in this case. Maximum gas rate is achieved after one day of production. If fracturing treatment caused a mechanical damage, the rate levels are lowered. Simultaneously gas breakthrough times increase.

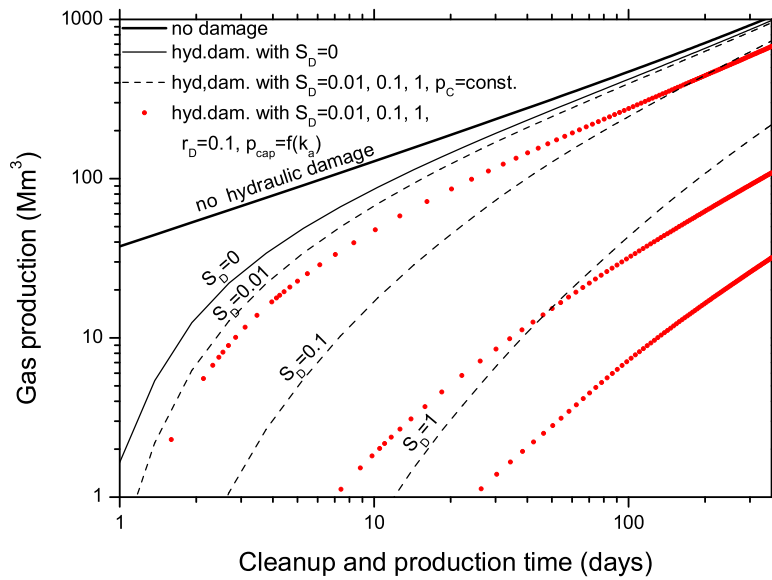
At first, mechanical damage is not considered to affect the multi-phase flow behaviour, given that the response of the model can be approximated by neglecting the water phase. The dashed lines in fig.4.13 indicate the varying degree of damage. If permeability reduction coincides with an increase of capillary pressure, primarily the rates further decrease (coloured dots). Even if there is just a slight damage of $S_D = 0.01$, the gas recovery decreases another 20%. On the contrary, gas breakthrough time is not affected. Skin factors S_D larger than 0.1 will dramatically impair the productivity.⁴⁴ Gas rate level and recovery are reduced by between five and ten times.

⁴⁴Here, a skin of 0.1 is equivalent to a permeability reduction of a hundredth of the initial permeability and a skin of 0.01 implies a permeability reduction of 90%.

4 Simulation of Hydraulically Fractured Wells



(a) Gas rate during cleanup



(b) Cumulative gas production

Figure 4.13: Cleanup process with hydraulic and mechanical damage

4.4 Polymer Gel Cleanup and its Influence on Productivity

Hydraulic damage, caused by the usage of water based fracturing fluid, is not solely responsible for potential productivity impairment in tight-gas reservoirs. Furthermore, many tight-gas wells do not respond to hydraulic fracturing as expected to. Following the fracturing treatment, a typical tight-gas well achieves its maximum gas rate within a few days after stimulation and then experiences a rapid production decline. Some tight-gas wells, however, do not show such obvious production peaks but instead sustain a flat production profile or exhibit a slowly increasing production rate for several weeks or months (VONEIFF et al. /141/).

Commonly, crosslinked polymers facilitate hydraulic fracturing treatments, the intent being that the polymer will be recovered when production initiates. In the field, only some portion of the injected polymer can be recovered during the cleanup process, typically up to 50 % (/144, 148/). Slugs of unbroken residuals were reported during the post-fracture production and indicate the existence of gel residues inside the fracture. The incomplete degradation of the polymers in the fracturing fluid may result in productivity impairments due to formation and proppant pack permeability damage.⁴⁵ Fracturing fluid issues are suspected to be related to the discrepancy of effective and propped fracture half lengths; fracture conductivities are commonly much less than anticipated. According to VONEIFF et al. /141/, unbroken fracturing fluids are considered relevant in 25 % of the cases where crosslinked gels are used.

The following section focuses, therefore, on the cleanup of fracturing fluid exhibiting a yield stress. The issue has been rarely discussed in literature; there is just one previous numerical study to the knowledge of the author (MAY et al. /33/).⁴⁶ Consequently, the first objective is to develop an advanced three-phase cleanup model taking complex rheology of fracturing fluids into account. Subsequently, a sensitivity analysis will be conducted where influence of unbroken polymers on well performance is investigated. However, since real field data is not available, the analysis is more of a qualitative nature, providing insight into the processes rather than quantifying its real damage.

4.4.1 Introduction to Fracturing Fluids

Fracturing fluids are essential to facilitate fracture initiation (breakdown), propagation of the fracture and the transport of the proppant. Furthermore, the fluid is intended to support minimisation of leakoff and any longtime residual damage to the proppant pack permeability (VALKO and ECONOMIDES /151, p.11/). To meet these requirements, fracturing fluids are chemically complicated fluids with several additives. A comprehensive overview of fracturing fluids can be found in /3, p.7-1 to 8-26/ or /152/. A discussion of the effect of fracturing fluid on fracture conductivity was presented by COOKE /153/.

Viscosity can be considered its most important property. When the fluid enters the fracture, a high viscosity is necessary to create large fracture widths and ensure an effective proppant transportation. In order to thicken the fracturing fluid, polymers are added to the base fluid, e.g., natural gums (guar), starches and cellulose derivatives. Such additives are simultaneously utilised for the filter cake formation. In contradiction to the water based components of the

⁴⁵Although, formation damage is more pronounced in higher permeability reservoirs (DEVINE et al. /149/).

⁴⁶In contrast, several authors investigated the polymer recovery as a function of flowback rate (without reverting to numerical techniques), such as WILLBERG et al. /148/ and POPE et al. /150/. Using field data from tight-gas case study wells (0.01 mD), the authors concluded that flowback procedure can be optimised to maximise polymer recovery, fracture fluid cleanup and well productivity. Significant polymer concentrations were recorded in produced water samples up to five month after the cleanup (/148/).

4 Simulation of Hydraulically Fractured Wells

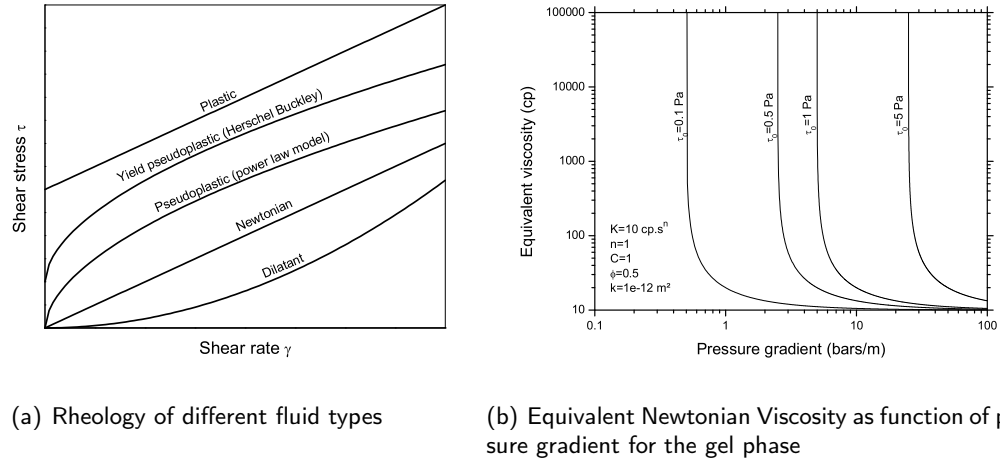


Figure 4.14: Non-Newtonian fluid characteristics

fracturing fluids, polymer molecules are supposed to be too large to invade the formation, where pore sizes are small. Hence, the polymer concentration increases dramatically in consequence of the leakoff process during the fracture closure - up to the 20 times the initial pump-in concentration (ECONOMIDES and NOLTE /3/).

After the proppant has been placed in the fracture, the crosslinked fracturing fluid must be degraded, i.e., the highly viscous polymers must be broken. Otherwise, the gel inside the fracture can detrimentally impede the flow of gas (VALKO et al. /151/) and inhibit a rapid loadwater cleanup. Although thermal degradation is an important breaking mechanism under prevailing temperature conditions (/154/), breaking the polymers is typically accelerated by so called breakers. Those chemicals cleave the crosslinked polymer molecules into smaller pieces of lower molecular weight (RAE and DI LULLO /152/).

Recent studies suggest that rheology of the fluid in the fracture at the end of the treatment is significantly different than that of the originally pumped fluid (MAY et al. /33/). Furthermore, its characteristics deviate from fluids of the common Newtonian type. Such non-Newtonian fluids do not exhibit the linear relationship of shear rate $\dot{\gamma}$ with shear stress τ of Newtonian fluids, where viscosity is constant at all shear rates. The non-Newtonian flow behaviour implies an apparent viscosity which is dependent on the shear stress that the fluid is exposed to (/3, p.8-7/). There are several simple models to describe the non-Newtonian rheology of a fracturing fluid, as depicted in fig.4.14.a. The most widely used is the power law model:

$$\tau = K\dot{\gamma}^n, \quad (4.24)$$

where K is the fluid consistency index and n the fluid behaviour index. Both parameters are usually determined under laminar flow conditions in a rotational cylinder viscosimeter. The power law model incorporates typical shear thinning effects. Occurrence of a yield stress, however, is not taken into account.

Yield stress has been suspected to affect fracture fluid cleanup by several authors, such as SHAH et al. /155/, MAY et al. /33/, BALHOFF and MILLER /156/ and AL-FARISS and PINDER /157/. If the gel within the fracture exhibits a yield stress, flow will not occur across

4 Simulation of Hydraulically Fractured Wells

the entire fracture. This is because at some specific distance from the wellbore, the shear stress will not exceed the yield value. A model which honours both the power law behaviour and a yield stress is the so called Herschel-Bulkley model:

$$\tau = \tau_0 + K\dot{\gamma}^n, \quad (4.25)$$

where τ_0 is the yield stress. This most general yield-power law model can be used to explain the behaviour of the pump-in fluid, where no yield stress exists. It can also explain the behaviour of the highly concentrated gels, which appear to indicate a certain threshold pressure gradient to initiate the flow (/33/). The yield stress is the shear stress where the fluid begins to flow (see fig.4.14.a). Beyond the yield stress, the fluid behaves essentially like a power law fluid. The apparent viscosity is identical for both fluid types, except in the range of very low shear rates. There, the apparent viscosity tends asymptotically to infinity.

Besides such fluid models, more sophisticated kinetic rheology models for fracturing fluids were published recently, taking into account nonlinear kinetics of crosslinker chemistry with the in-situ changes in fluid rheology, e.g., by WALTERS et al. /158/. Those models accurately predict the effects of shear rate, shear history, temperature, temperature-time history, pH, gel loading, crosslinker concentration and breaker concentration on the apparent viscosity function.

4.4.2 Simulation of Non-Newtonian Fluid Flow

First studies concerning simulation of non-Newtonian fluid behaviour were reported in the late seventies, e.g., by McDONALD /159/, IKOKU and RAMEY /160/, MURTHA and ERTEKIN /161/ or AZOUZ et al. /162/. *De facto* all of them considered power-law fluids, using special solution techniques rather than the framework of a multi-phase numerical simulation.

Simulation of enhanced oil recovery frequently implies non-Newtonian fluids, e.g., for polymer flooding. Decreasing the mobility of the injected water is a major objective there. Furthermore, pore throats plugging, polymer adsorption and relative permeability effects are of interest. Most commercial simulation packages feature a polymer flood option, where polymer are usually treated as component of the aqueous phase. However, fluids exhibiting a yield stress are not typical for those applications.

MAY et al. /33/ investigated the fracturing fluid cleanup process by means of numerical simulation. They implemented a yield power-law model (based on an explicit realisation) and investigated the impact of a potential yield stress on the productivity of a fractured well. The authors used their model for history matching of field data and, finally, for evaluation of realistic fracture parameters. One result was that yield stress contributes to the shorter effective fracture half lengths in comparison to the propped distances.

BALHOFF and MILLER /156/ developed a model to investigate fracture fluid cleanup by means of three dimensionless variables: (i) reservoir to fracture mobility ratio, (ii) clean to fouled fracture permeability ratio, and (iii) yield stress. They stated that yield stress is expected to have the greatest effect on the cleanup.

VONEIFF et al. /141/ presented a sensitivity analysis concluding that unbroken fracture fluids can decrease gas reserves by 30% in a tight gas well and reduce the initial gas rate by up to 80%, flattening the production profile. They found that the ultimate gas recovery reaches a maximum when the fracture gel breaks back to 50 cp or less. However, fracturing fluid was simplified as Newtonian fluid without a yield point.

The present approach facilitates a special gel phase to represent the fracturing fluid. The

4 Simulation of Hydraulically Fractured Wells

equation used to calculate the viscosity of the gel phase is derived from the Herschel-Bulkley fluid model. The velocity of a Herschel-Bulkley fluid can be written analogue to the Darcy velocity in a generalised form:

$$\vec{u}_{\text{HB}} = \begin{cases} - \left[\frac{k k_{r,\text{gel}}}{\mu_{\text{eff}}} \left(1 - \sqrt{\frac{\phi C}{2k}} \tau_0 \frac{1}{|\text{grad } p|} \right) \text{grad } p \right]^{1/n}, & |\text{grad } p| \geq \sqrt{\frac{\phi C}{2k}} \tau_0 ; \\ 0, & |\text{grad } p| < \sqrt{\frac{\phi C}{2k}} \tau_0 . \end{cases} \quad (4.26)$$

where C is a tortuosity constant. Gravity effects are neglected. The derivation of eq.(4.26) for a one dimensional flow of a Herschel-Bulkley fluid through a single capillary, using the Blake-Konzeny equation for laminar flow of Newtonian fluids in packed beds, can be found in MAY et al. /33/. An effective viscosity coefficient μ_{eff} for multi-phase flow of such fluids is defined as follows (/33, 157, 163/):

$$\mu_{\text{eff}} = \frac{K}{12} \left(9 + \frac{3}{n} \right)^n (150C\phi(S_{\text{gel}} - S_{\text{gel,irr}})k k_{r,\text{gel}})^{\frac{1-n}{2}} . \quad (4.27)$$

In order to adapt the numerical framework with the Darcy velocity to accommodate the non-Newtonian fluid behaviour, a gel viscosity μ_{gel} is introduced. This viscosity reflects the equivalent viscosity of a non-Newtonian fluid moving at the same velocity as its Newtonian fluid counterpart (/33/) and is derived by equating the Darcian velocity with the Herschel-Bulkley velocity, eq.(4.26), i.e., $|u_{\text{HB}}| = |u_{\text{D}}|$. The viscosity becomes a function of the pressure gradient in the gel phase, depicted in fig.4.14.b. The non-Newtonian fluid model is implemented fully implicitly, which turned out to be stable and robust.⁴⁷

Eq.(4.26) facilitates the use of various rheological fluid models. Assuming a fluid behaviour index n of 1 and no yield stress ($\tau_0 = 0$) is equivalent to the constant viscosity case $\mu_{\text{gel}} = K$ (i.e, a Newtonian fluid). With $\tau_0 = 0$ and $n \neq 1$, the fluid exhibits power law fluid behaviour.

Enhanced Cleanup Model. The simulation model is basically an extended version of the load water cleanup model, see section 4.3.2 (p.46). The water and the gas phase represent the original formation fluids. The load water, i.e., the low viscous fracturing fluid invading the formation, exhibits essentially formation water properties and is therefore modelled via the water phase. The fracturing fluid inside the fracture is modelled using a third (gel) phase.

At first, leakoff of the load water is modelled by injecting an appropriate volume of water into the fracture. Subsequently, the water inside the fracture is replaced with the gel phase by updating the corresponding saturations. Within the matrix domain, two-phase flow of gas and water (including the capillary pressure) can be conventionally described with the Brooks-Corey model (appendix D), neglecting the third phase. Inside the fracture domain, the relative permeabilities are assumed equal to the corresponding phase saturations. There are no capillary forces acting in the fracture domain.

⁴⁷An explicit or semi-implicit realisation on iteration level caused oscillations in certain situations. This issue requires further investigations.

4 Simulation of Hydraulically Fractured Wells

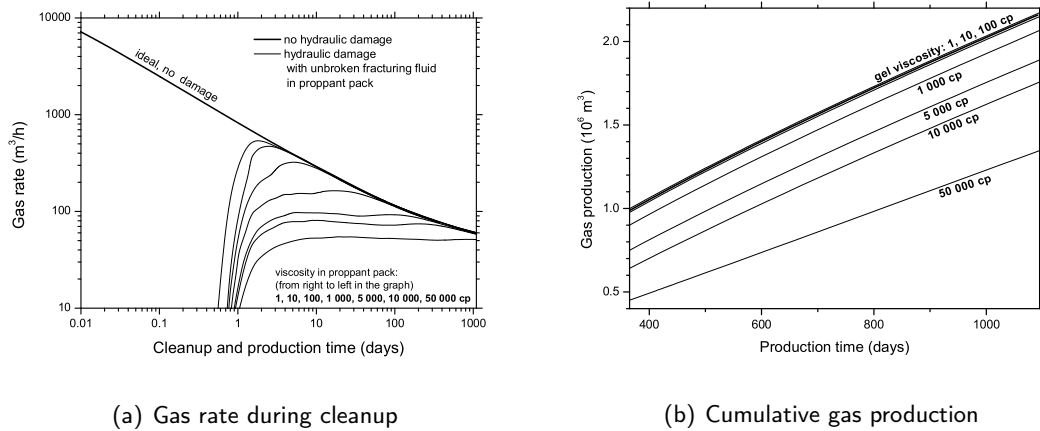


Figure 4.15: Cleanup process with unbroken fracturing fluid in the fracture (without yield stress)

4.4.3 Simulation Results

The basic parameter-set for the simulations is summarised in table 4.4 (p.52). Relative permeabilities and capillary pressures are according to fig.D.1 (p.114).

Constant Viscosity Effects. At first, simulations are conducted assuming a constant viscosity of the fracturing fluid with $n = 1$ and $\tau_0 = 0$ (i.e., Newtonian fluid). In the simulation runs, viscosity of the fracturing fluid is varied from 1 cp to 50000 cp, representing a total unbroken fracturing fluid. Everything else is left unchanged as in the investigation of load water recovery from the previous section. Gas rates and recovery are presented in fig.4.15.a and b. As can be seen, increasing the viscosity dampens the gas rate peak after the gas breakthrough. In the course of the production, the gas rate asymptotically approaches the ideal, undamaged gas rate. Results are in close agreement to that of VONEIFF et al. /141/.⁴⁸ Ultimate recovery is lower if degraded fracturing fluid exhibits viscosities larger than 100 cp (see fig.4.15.b).

The viscosity affects the shape of the invasion zone and the position of gas breakthrough (like the dimensionless fracture conductivity), see fig.4.16.a and b. Highly viscous fracturing fluids inside the fracture manifest in a more pronounced gas breakthrough near the well, hindering the reduction of water saturation near the tips. On the contrary, low viscosities will provoke a more uniform saturation profile around the fracture.

Effect of Yield Stress on Cleanup. The next set of runs are performed, taking into account the yield stress of the gel within the fracture. The yield stress of the gel phase is taken from MAY et al. /33/, since laboratory data is not available. For a guar/zirconate system (22.5 kg/m^3) with no breaker at 120°C , a yield stress τ_0 of 1 Pa is assumed. In the framework of history

⁴⁸Based on that observation, MAY et al. /33/ stated that all polymer from the fracturing fluid is eventually recovered if viscosity is constant. Furthermore, ultimate gas recovery was assumed to approach that of the single-phase undamaged well (even in the case of 30000 cp viscosity). Regarding a typical saturation distribution in the fracture plane after 3 years of production provokes contrary results. If there is still a residual fracturing fluid saturation of 0.5, the relative gas permeability of the gas phase is reduced to 50 %, lowering the effective fracture conductivity in the same percentage but resulting in identical rates.

4 Simulation of Hydraulically Fractured Wells

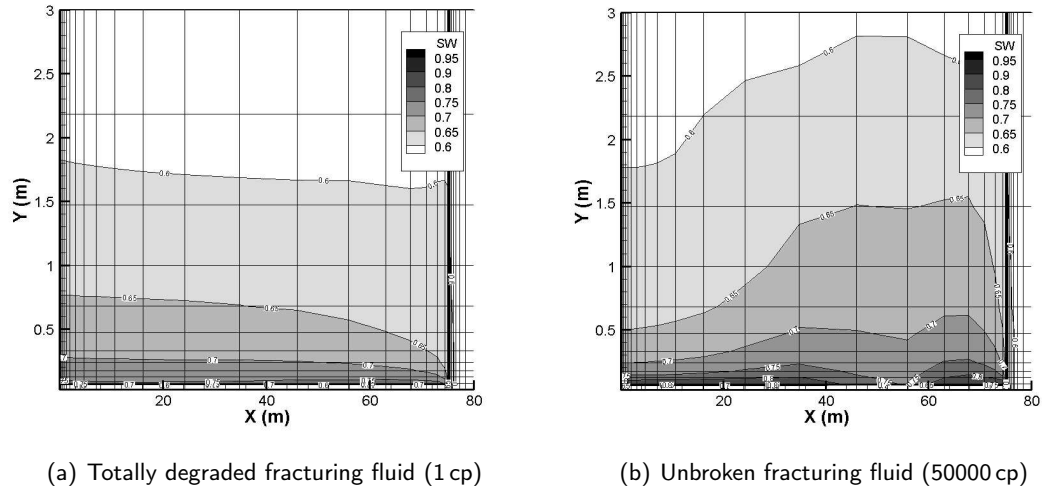


Figure 4.16: Saturation distribution at the end of the cleanup process assuming constant viscosity fracturing fluids (Newtonian-type)

matching, the authors modified the initial yield stress to about 15 Pa to achieve closest match of the field data. Shear thinning is, according to data from the service companies, typically not relevant under the prevailing temperature conditions, $n \approx 1$. The fluid consistency index K is chosen to be 50 cp, equivalent to a completely degraded fluid. The tortuosity constant C is equal 1, no channelling occurs when the fluid yields. Inside the fracture, there is no irreducible gel saturation, i.e., $S_{gel,irr} = 0$.

Results are presented in fig.4.17.a-f. and summarised in table 4.6. The recovery of all three phases are referring to the case $\tau_0 = 0$ Pa. For the initial value of the yield stress, $\tau_0 = 1$ Pa, the gel phase recovery of about 50 % fits quite well to field experiences. The ratio declines with higher yield stress. Load water recovery is in most cases not affected, with significant changes only registering for the largest yield stresses and low conductivities. The same holds for the gas recovery, see also fig.4.17.a and b.

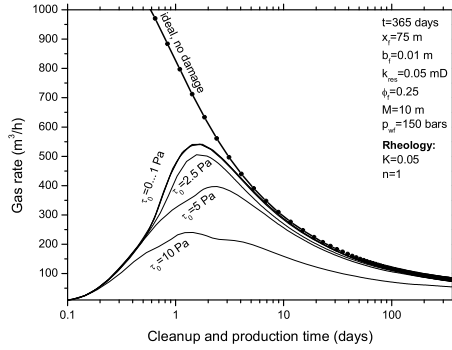
Table 4.6: Effect of yield stress on recovery ratio (first column: $F_{CD} = 10$, second: $F_{CD} = 100$)

Yield stress τ_0 (Pa)	0.5		1		2.5		5		10	
Gas recovery (%)	0.99	1	0.98	1	0.94	0.96	0.9	0.93	0.61	0.93
Load water rec. (%)	0.95	1	0.94	0.99	0.93	0.99	0.88	0.98	0.60	0.97
Gel phase rec. (%)	0.71	0.63	0.57	0.54	0.38	0.40	0.20	0.29	0.06	0.16

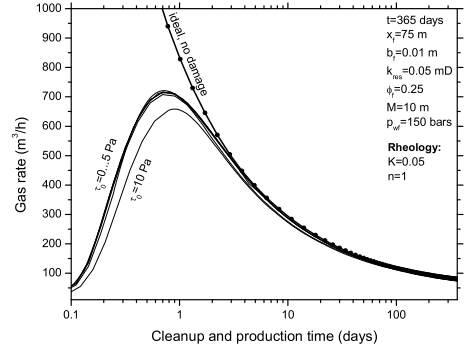
Larger fracture conductivities contribute to a better gel cleanup. According to fig.4.17.c and d., a higher portion of the fracture length with gel is then un-yielded. Furthermore, the gel damage caused by blocking effects is less severe then. As expected, gas breakthrough is not affected by the occurrence of a yield stress. Due to the pressure gradient imposed by the well, the gel phase is un-yielded next the well almost instantaneously after the well was set in production.

This partially coincides with conclusions of MAY et al. /33/ who stated that *any* yielding

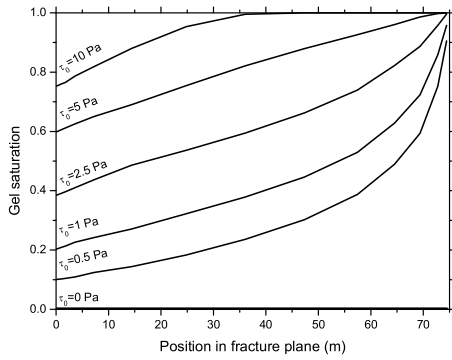
4 Simulation of Hydraulically Fractured Wells



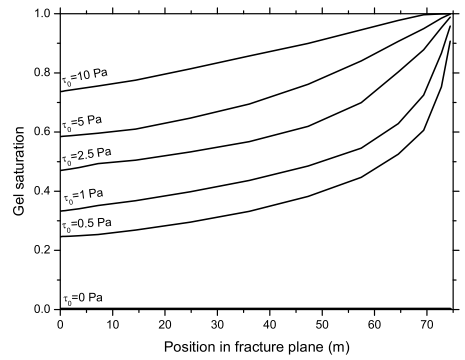
(a) Gas rates for $F_{CD}=10$



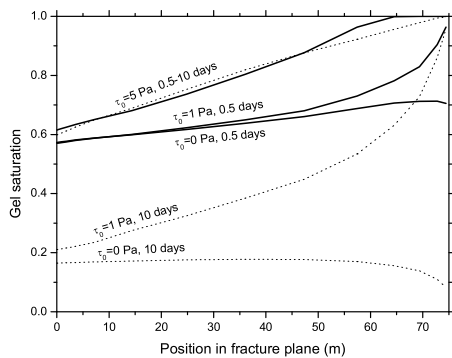
(b) Gas rates for $F_{CD}=100$



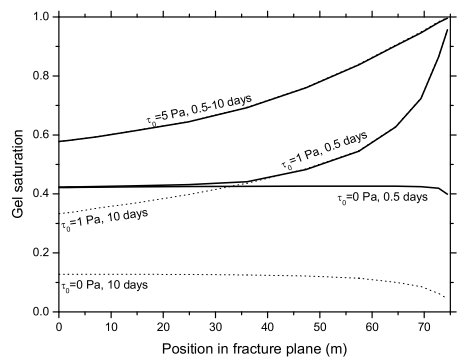
(c) Gel saturation for $F_{CD}=10$ after 1 year



(d) Gel saturation for $F_{CD}=100$ after 1 year



(e) Development of gel saturation for $F_{CD}=10$



(f) Development of gel saturation for $F_{CD}=100$

Figure 4.17: Gas rates (a-b), gel saturation within the fracture after one year of production (c-d) and development of gel saturation within fracture plan (e-f) for various yield stresses and $k_{res} = 0.05$ mD

4 Simulation of Hydraulically Fractured Wells

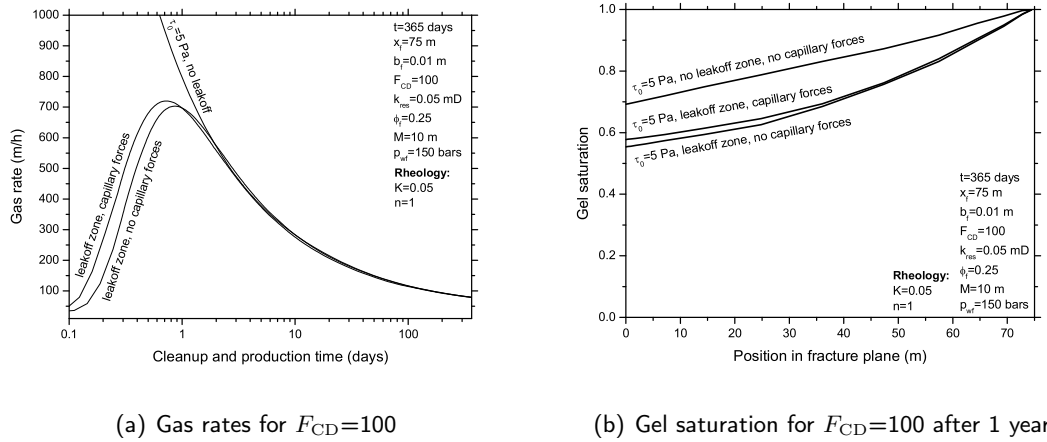


Figure 4.18: Effect of capillary forces and leakoff invasion zone on gel phase cleanup

occurs almost instantaneously. Regarding the temporal development of the gel saturation within the fracture in fig.4.17.e and f., their observation can only be verified in the case of very large yield stresses (i.e., $\tau_0 = 10$ Pa if $F_{CD} = 10$). Otherwise, the saturation distribution varies until its stationary state is reached, typically lasting several days. This is presented in the figure for $t = 10$ days.

The gel saturation distribution within the fracture, fig.4.17.c and d, depends on the yield stress, and on the resulting threshold pressure. However, there is no sharp front, but rather an almost linear distribution from the wellbore to the completely yielded position (i.e., the fracture tip for low yield stresses). This implies a decreasing proppant pack permeability, and possibly even total blockage, towards the fracture tips. Assuming a Newtonian-type fracturing fluid with high viscosity, this phenomenon can not be reproduced. In this case, the saturation is typically uniformly distributed and even decreases near the fracture tips. BALHOFF and MILLER /156/ assumed a clean and a fouled region inside the fracture, divided by a sharp interface, in order to derive their analytical solution. The present results casts some doubts on this idea.

All simulations were conducted considering strong capillary forces prevailing in a 0.05 mD reservoir. The according multi-phase flow functions are shown in fig.D.1. The simulation results indicate that capillary forces do not significantly impact the cleanup of the gel phase within the fracture (see fig.4.18.a and b). This is contrary to the presumptions of MAY et al. /33/ who did not include capillary forces. The gas rate with and without capillary forces approach the rate of the undamaged well (i.e., no free water) during the first two days of cleanup. The saturation distribution for both cases is almost identical after one year of production.

4.5 Discussion

The current chapter presents an extensive review of hydraulic fracture simulation topics. Starting with a simple single-phase model (gas), the complexity of the simulations is successively increased by consideration of two-phase (gas+load water) and three-phase flow (gas+load water+gel). Investigations are conducted with regard to tight-gas conditions but results are not necessarily restricted to those. The simulations are performed for fractured vertical wells utilising structured grids. Although not yet considered, the principle results hold for multiple fractured wells in the same way. Adaptation to appropriate grids, including unstructured grids, needs further work but should be simply achievable.

Non-Darcy flow is important when determining productivity of fractured wells in tight-gas reservoirs. Inertial flow affects the productivity despite the low gas rates, which has been neglected in the past literature. The simulator implementation of the non-Darcy flow coefficients also accounts for permeability changes in fracture and matrix as a consequence of stress sensitivity. Furthermore, new type-curves are presented for non-Darcy flow in fracture and reservoir, permitting the determination of non-Darcy flow related parameters. Multi-phase, non-Darcy flow can be taken into account but was neglected in the current work. Investigations on its impact require further research.

Tight-gas reservoirs are stress sensitive; a variety of correlations quantify the relation of effective stress and reservoir permeability. The reservoir stress dependency impacts the productivity to a much higher degree than the fracture closure. Fracture closure is less important when predicting long term performance of the well. However, for well test analysis it may be of interest to increase the certainty of the results and, hence, that of the fracture parameters under evaluation. The coupled solution of geomechanical and flow equations in tight-gas reservoirs is currently an objective of further research.

Particular attention is given to the investigations of cleanup processes by means of a two-phase cleanup model. The analysis of the loadwater recovery following the stimulation treatment support the thesis that hydraulic damage, solely considered, does not impair productivity. To suffer real reductions of the productivity, permeability in the fracture vicinity needs to be severely impaired. Fractured wells are generally much less sensitive to near wellbore damage than a radial well, due the different flow pattern. The combined effect of mechanical and hydraulic damage is considered by adjusting the capillary pressure within the damage zone. It should be reminded that there is generally great uncertainty, if no experimental data is available concerning the multi-phase flow in the damaged zone.

Two important questions center around yield-stress behaviour in the polymers. Do they exhibit a true yield stress? Is the yield stress responsible for poor cleanup? Therefore, an enhanced three-phase cleanup model is presented for the investigations of the polymer gel cleanup. Yield stress is taken into account by means of the Herschel-Bulkley rheology model. Using literature data for the crosslinked fluid parameters, about 50% of the gel phase can be recovered in the simulations. The gel saturation gradually increases towards the fracture tips, lowering the fracture conductivities there. The residing gel damages proppant pack permeability and porosity or causes fracture face damage, simultaneously reducing the production potential. This coincides with observations in the field where fracture half lengths, conductivities and productivity are lower than anticipated. First investigations suggest that loadwater recovery including capillary forces has little influence on the gel cleanup and vice versa. This issue needs further investigation. Also, experimental data of fracturing fluid rheology is required to obtain more certain results.

5 Simulation of Underbalanced Drilling Operations

As shown in the previous chapter, hydraulic fracturing may cause severe damage to the formation during the treatment. Other techniques to develop a low permeability reservoir are, hence, aimed for obtaining at least marginal economic efficiency. Such a technique is underbalanced drilling (UBD). UBD is not a stimulation technique which creates or enhances existing permeability in marginal quality formation, but rather it maximises the potential of the present reservoir strata (BENNION et al. /164/).

UBD is defined as a drilling operation where the pressure of the circulating drilling fluid is lower than the pore pressure of the target formation of interest. The most widely recognised benefit of underbalanced drilling is the reduction of the formation damage, in terms of minimising the drilling fluid leakoff and fines migration into the formation. This often greatly impairs the productivity of common reservoirs, especially in low permeability reservoirs.

The main targets of the following investigations are (i) the development of an appropriate simulation strategy for UBD processes, and (ii) a detailed investigation on the suitability of UBD for tight-gas formations. Therefore, a multi-phase UBD simulation model is introduced. The model incorporates discrete consideration of the well with proper, time varying boundary conditions, i.e., pressure and saturation within the well. Capillary forces which facilitate counter-current imbibition are also taken into account. This and the framework of the modelling has, to the best knowledge of the author, not been presented in the past literature.

Reservoir permeability, penetration rate, thickness of the formation as well as the underbalanced conditions are subject of a sensitivity analysis. The main emphasis is placed on the derivation of the relation between productivity and the multi-phase flow characteristics of the reservoir rock. The process of counter-current imbibition is analysed. Furthermore, the flexibility of the technical realisation, is illustrated by means of a UBD simulation for a horizontal well utilising unstructured grids.

5.1 Background

The terminology under- and overbalance refers to the relative pressure difference from reservoir to the bottomhole circulating pressure. Conditions can prevail from controlled overbalance (e.g., to control differential sticking) to controlled underbalance (for fractured reservoirs, low pressure or low permeability gas reservoirs).

Advantages of UBD include increasing penetration (drilling) rates and stimulation of gas production due to the differential pressure between the formation and the wellbore. Real-time formation evaluation allows for production testing and evaluation of production versus geology. Thus, productive reservoir zones and formation properties can be already determined during the drilling, provided that there is proper flow monitoring at the surface. A discussion of this subject can be found in KARDOLUS and VAN KRUIJSKIJK /165/, VAN KRUIJSDIJK and COX /166/ and LARSEN and NILSEN /167/.

5 Simulation of Underbalanced Drilling Operations

UBD is important for preventing strong formation damage resulting from the drilling. With less damage, wells clean up faster and produce at higher rates. However, formation damage can not be completely excluded in water wet formations when using a water based mud system, due to the capillary forces prevailing there (see also section 4.3). As soon as the fluid comes in contact with the rock, it rapidly imbibes along the sandface into the matrix. This is due to adverse capillary pressure forces, as discussed by BENNION et al. /164/.¹

Eventually, a cone-type invasion zone will be formed. The extent of that zone depends, e.g., on the exposure time of the fluid to the sandface as well as on fluid, reservoir and drilling parameters. The severity of damage associated with the imbibition effect depends on the gas relative permeability function near the residual water saturation. Furthermore, the productivity can be drastically curtailed in case of (i) additional interactions between the invading fluid and the matrix (such as clay swelling) or (ii) permeability alteration within the near wellbore zone (such as dilatancy effects).

Two main questions arise in context of UBD-simulation: (i) whether UBD impacts the longtime performance of the well, e.g., by minimising formation damage, and (ii) how much gas is produced during the drilling process? The first question is mainly related to the economics of the project. The second question is important for technological concerns, e.g., to provide continuous underbalanced conditions by controlling the mud system. Furthermore, the surface equipment for the drilling needs to be dimensioned properly.

In the literature, there are very few papers dealing with numerical or analytical prediction of inflow during UBD and the subsequent production period. A semi-analytical model to compute the inflow during drilling was introduced in /165/. Analytical methods and spreadsheet applications for inflow predictions during drilling, based on a pseudo-stationary approach, were presented in /167/. Restrictively, it has to be noted that neither of both studies incorporated multi-phase flow and, therefore, capillary effects.

Recently, XIONG and SHAN /168/ compared OBD and UBD for a broad range of permeabilities. The authors used a commercial numerical simulator with Cartesian geometry and a local refinement for the horizontal well. Filtrate invasion, mud cake and permanent formation damage were taken into account. The impact on the productivity was evaluated by means of net present value. It was concluded that reservoir permeability and initial water saturation are key factors for a successful UBD operation. Moreover, capillary pressure and relative permeability were determined to play an important role in the UBD productivity improvement, although the authors solely considered a single case with imbibition using a simplified model. However, with regard to typical tight-gas conditions, they stated that UBD may not be a good choice for low permeability reservoirs with high initial water saturations.

DING et al. presented a model for overbalanced horizontal drilling simulation with investigation of the subsequent natural cleanup for oil based mud /169/ (without imbibition) and water based mud /170/. They considered the kinetics of the mud filtrate invasion, filter cake deposition and erosion, as well as permeability damage using both numerical and experimental techniques. The authors utilised a two-phase simulation model with a cylindrical grid to discretise the reservoir and the well.² However, their approach should be adapted to handle permeability reductions due to the invaded fluid (e.g., with an exponential distribution) and to consider filter cake in the current simulator.

¹ There is no filter cake formation for efficient fluid loss control during UBD.

² Limitations should be expected concerning predictions of the long time productivity due to the strong symmetry assumption.

5 Simulation of Underbalanced Drilling Operations

MTCHEDLISHVILI et al. /171/ simulated the gas production during UBD of a highly deviated well in the tight-gas German Rotliegendes formation, considering various conditions to determine the most effective configuration. They investigated the impact of the countercurrent imbibition on the long time productivity, where simulations were conducted using a commercial multi-phase, three-dimensional Black-Oil reservoir simulator. The authors facilitated a special support-tool to precisely consider all available geological and drilling data with respect to well trace and rate of penetration in the reservoir simulation model.

5.2 Simulation Methodology

Setting the appropriate boundary conditions is the crucial factor for UBD simulation. The pressure in the well is controlled and monitored during the drilling process in the field. Furthermore, the well is considered to be entirely filled with the drilling fluid. To get a proper depiction of the drilling process, both the known drilling pressure and the saturation conditions needs to be applied in the numerical reservoir model.

Using conventional, non-discrete well models, it is practically not feasible to realise the conditions prevailing during UBD by common well constraints. The lack of a "constant saturation" well control mode³ in commercial simulators is a main reason for the variety of simplifications assumed so far in previous studies.

XIONG and SHAN /168/ considered two steps to investigate the impact of UBD on well productivity. The first step consisted of an injection of water into a stationary well to account for the imbibition during drilling. This is in many points mistaken, since the actual drilling process is not characterised by an *a priori* known flow rate across the well boundary.⁴ Additionally, this rate is not constant. The second step simulated the gas production. The drilling process with the advancing penetration rate and increasing gas influx was entirely neglected by the authors.

An external coupling was introduced in /171/ to transform the UBD conditions into a commercial reservoir simulator. The well was discretised using both radial and 3D unstructured grids with a cylindrical well refinement. The well grid blocks were connected with a fully water saturated domain to provide a constant water supply according to the drilling success (similar to a connected, separated pipe parallel to the well). According to the penetration rate, the connections were stepwise opened to imitate the drilling progress. This process was controlled by an external interface module.⁵ The methodology enabled the simulation of *spontaneous*, countercurrent imbibition during UBD, although by means of a "weak" coupling. Nonetheless, many numerical problems, such as poor convergence, were encountered when using 3D unstructured grids.

Contrary to conventional reservoir simulators, the current code enables the easy and robust application of constant pressure as well as the constant saturation boundary conditions since the well is discretely considered and treated as "porous" media. Both parameters can be predefined for each specified well grid block. Treatment of boundary condition and well modelling issues are explained in more detail in section 3.2.

³There, a zero saturation gradient, i.e., $\partial S_w / \partial r = 0$ is assumed between the well and the well block (AZIZ and SETTARI /7/).

⁴In the framework of history matching the measured fluid loss can be applied for an injection of an appropriate water volume.

⁵Updating corresponding grid block properties and performing restarts after each segment had been penetrated during a time step.

5 Simulation of Underbalanced Drilling Operations

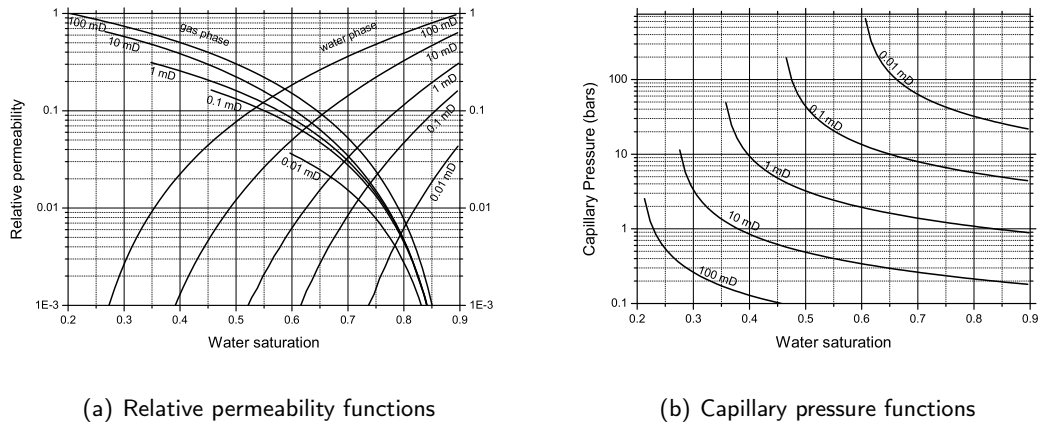


Figure 5.1: Multi-phase flow functions for UBD simulation runs

The well is represented by a series of grid blocks (i.e., well segments). During the UBD-operation, the well segments are successively opened from entry to the exit point of the corresponding reservoir interval. The length of the segments is usually oriented to the geological layering but should not be too coarse. The pressure in the segments is equal to the UBD pressure. Pressure variations within the well segments, e.g., due to the hydrostatic pressure gradient, can also be taken into account.

5.3 Simulation Model Setup

To perform a sensitivity study on UBD, a simulation model needs to be setup using the new UBD simulation methodology. A 2D $r-z$ grid system is built for the vertical well with a radius of 0.1 m. The grid blocks grow logarithmically with growing distance from the wellbore. Solely transient flow is considered since it is the main flowing period in tight-gas formations. The vertical length of each segment is 5 m. Formation is homogeneous and isotropic with respect to permeability.

The two-phase flow conditions may result due to the imbibition process during drilling. The resulting multi-phase flow is captured by means of relative permeabilities and capillary pressure functions based on a Brooks-Corey model (appendix D). The endpoint permeabilities are adapted from North German Rotliegendes sandstones for low permeabilities (less than 1 mD) and chosen according to realistic conditions for higher values. The functions are depicted in fig.5.1. PVT properties are set according to typical conditions in tight-gas reservoirs (see subsection 4.2.1).

Two phases represent the relevant fluids: water (mud & formation water) and dry gas in the formation. To initialise the model, the following assumptions are made: (i) the existing formation water phase is at residual saturation (there is no free water in the reservoir), and (ii) the drilling fluid is water based (this implies, that the infiltrated fluid has identical properties like the connate water within the reservoir). The residual saturations are based on a correlation of the ITE Clausthal (PUSCH et al. /172, p.172/).

5 Simulation of Underbalanced Drilling Operations

Validation of the UBD Simulation Model. At first, the numerical model is validated by comparison with analytical solutions. The principal course of the drilling and production process can be traced in fig.5.2. After the drilling period, the well is arbitrarily shut for 40 hours. To suppress the imbibition of water from the well into the formation during the shut-in, the water is completely removed at the beginning of the shut-in. Subsequently, the well is set in production with the corresponding bottom hole flowing pressure.

The analytical solutions neglect the water imbibition during the drilling process. Hence, they represent a undamaged scenario and give approximations of the gas inflow and production rates under single-phase conditions. In fig.5.2, the numerical model is compared with analytical solutions. It shows close agreement to the developed superposed constant pressure solution, where depth steps (according to the penetration rate) are taken into account. Deviations (<10%) arise when comparing with Larsen's quasi-stationary analytical solution (/167/). Additionally, fig.5.2 contains the results of a UBD process, where imbibition is regarded. Then, gas rates during drilling and subsequent production are lower, but still higher when compared to an overbalanced drilled well.

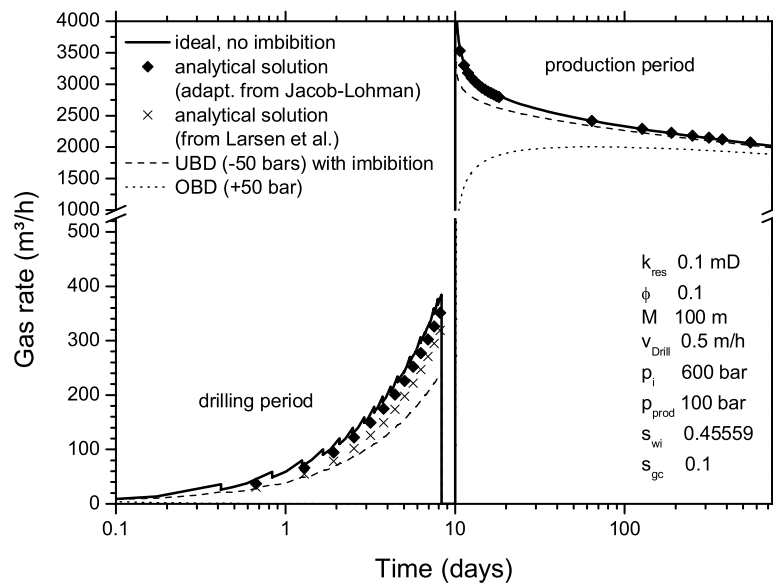


Figure 5.2: Drilling process with subsequent production: comparison of numerical results with analytical solutions

5.4 Influence of UBD and Reservoir Parameters on the Productivity of the Well

To evaluate the impact of UBD on the well productivity after the drilling, a sensitivity analysis is conducted. Although most of the effects are obvious *a priori*, quantification requires the application of the simulation tool, capturing the physics behind UBD. The parameters of the analysis are summarised in table 5.1. The basic set of parameters is marked bold therein.

Table 5.1: Range of reservoir parameters for sensitivity study

Permeability (mD)	0.01-100 (0.1)
Porosity	0.1,0.2 (0.1)
Reservoir thickness (m)	20-400 (100)
Penetration rate (m/h)	0.1-2.5 (0.5)
Initial field pressure (bars)	300,600 (600)
UBD pressure (bars)	270-580 (550)
Production time (years)	2
Production pressure (bars)	100,300

Impact of Reservoir Permeability. Reservoir permeabilities are considered ranging from good conditions (100 mD) to ultra tight conditions (0.01 mD). Other parameters are set to default values according to table 5.1.

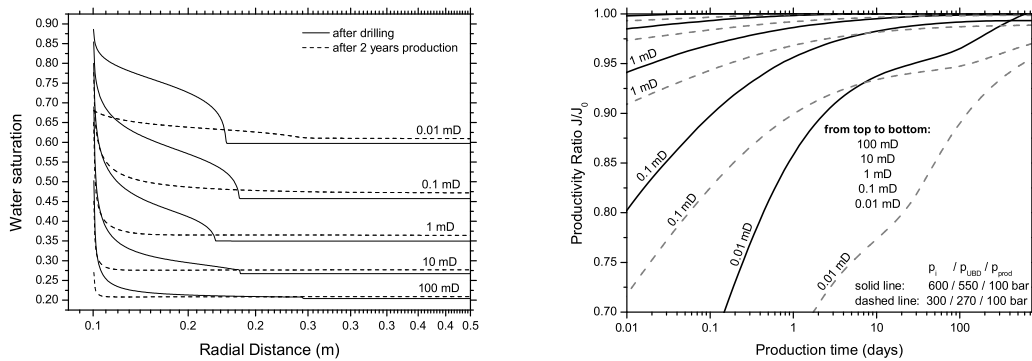
The water saturation conditions at the end of the drilling process are marked with the solid line in fig.5.3.a.⁶ As expected, lower permeability tends to result in higher water imbibition. During the subsequent shut-in, the imbibition process transports the water deeper into the formation while simultaneously flattening the saturation profile next to the well (not depicted). The process depends on the magnitude of the capillary forces prevailing in the vicinity of the well.

In the course of the post-drilling production period, the water is again transported out of the matrix. However, not all of the water can be removed due to the adverse mobility ratio of gas/water and the capillary forces. Saturation distributions at the end of the production period are shown by the dashed line in fig.5.3.a. Water trapping occur for permeabilities lower than 1 mD, which may lower the production potential of the well.

To discuss its impact on the well, productivity of the damaged case is compared against the undamaged ideal case in fig.5.3.b (i.e, if no fluid enters the formation during drilling). The productivity ratio is evaluated for two different scenarios. In the first case the field pressure is 600 bars with 100 bars bottom hole pressure. The second case assumes an initial field pressure

⁶The steep slope is partly caused by the capillary end effect (discussed by HUANG and HONARPOUR /173/) which establishes a water saturation profile, with its maximum possible value ($1 - S_{gc}$) immediately at the sandface. The simultaneous flow of both phases is associated with the condition that the capillary pressure decreases to the value of capillary pressure within the well with the zero capillary pressure, or at least, to the lowest possible value (AZIZ and SETTARI /7, p.184/). This is especially the case of capillary forces dominated imbibition flow. The end effect commonly appears in drainage processes rather than imbibition processes. During UBD, the gas drainage occurs from the beginning, while water imbibition is usually accomplished before its end. The extent of that zone depends on the capillary forces and the ratio of gas and water flow rates. Here, the zone is only observable on a millimetre (max. centimeter) scale in the numerical experiments. As shown in fig.5.3.a, the code can properly resolve this phenomenon.

5 Simulation of Underbalanced Drilling Operations



(a) Saturation distribution after drilling and 2 years (b) Productivity compared against undamaged well production

Figure 5.3: Effect of reservoir permeability (0.01-100 mD) on gas rate and saturation conditions

of 300 bars (with 270 bars UBD), again with bottom hole pressure of 100 bars. As expected, the damage degree is higher for the smaller drawdown and lower permeabilities.

Impact of Reservoir Thickness. Reservoir thickness is varied in the range 20-400 m. Producing bottom hole pressure amounts to 300 bars.

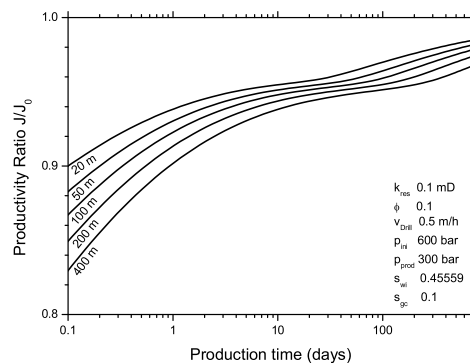


Figure 5.4: Effect of reservoir thickness on gas rate

Results in fig.5.4 confirm the proportionality of exposure time and damage degree. In the case of larger drilling intervals, more water can imbibe into the formation. However, significance of the effect is rather small.

Impact of Underbalanced Conditions. UBD pressure is varied from extreme underbalanced (300 bars) to slight UBD-conditions (near the balanced state).

The gas rates during drilling are depicted in fig.5.5.a. As expected, the inflow increases with lower UBD pressures since gas pressure gradient is higher. Accompanying this, less water can

5 Simulation of Underbalanced Drilling Operations

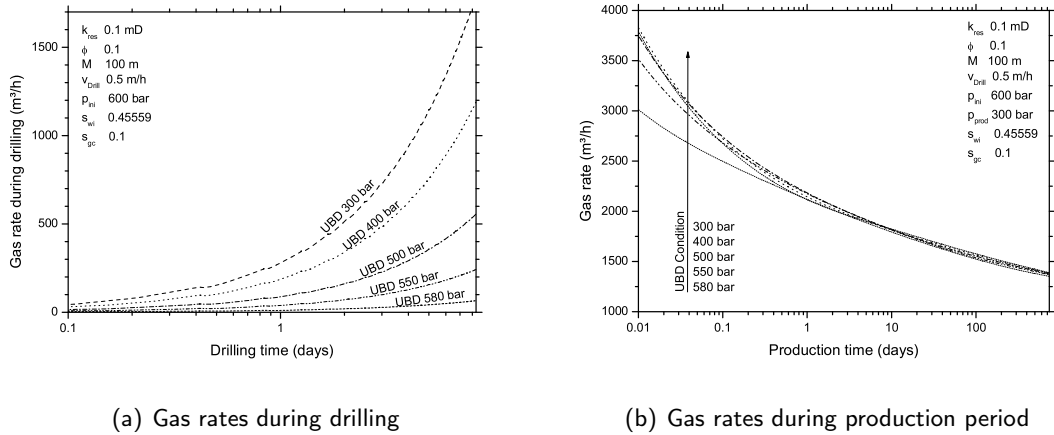


Figure 5.5: Effect of UBD conditions on gas rate during drilling and production

imbibe into the formation. Consequently, gas rate impairment during the production period is lower, shown in fig.5.5.b. The stimulating effect of the UBD pressure, however, diminishes during the first days of the production.

Impact of Drilling Velocity. UBD operations can significantly improve the penetration rate compared to overbalanced drilling. Additionally, the shorter the exposure time, the less damage ought to be expected. To illustrate the phenomenon, simulations are conducted with penetration rates $v_{D_{rill}} = 0.1...2.5$ m/h.

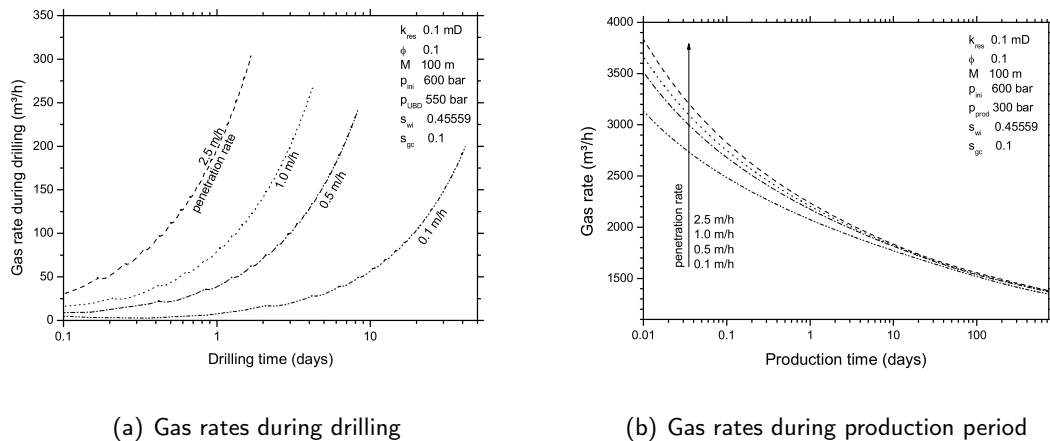


Figure 5.6: Effect of penetration rate on gas rate and saturation conditions during drilling and production

As presented in fig.5.6.a, higher penetration rates will increase the gas rates during the drilling (since pressure gradients are higher). Additionally, productivity is less impaired during the subsequent production period, see fig.5.6.b. In case of very small penetration rates (0.1 m/h), a permanent formation damage should be expected.

5.5 Investigations on the Spontaneous Imbibition during UBD

Tight-gas formations will be particularly affected by water imbibition despite the UBD condition. Although gas flows into the well during drilling, water (i.e., water based components of the mud) imbibes into the formation. This countercurrent flow of water will initiate during UBD provided, that the corresponding pressure conditions exist.

As soon as the drilling bit comes in contact with the formation, the imposed gas pressure gradient across the sandface causes an influx of gas into the well. Successively, while the pressure transient dissipates deeper into the formation, the pressure gradient across the sandface flattens and the pressure profile approaches pseudo-steady state conditions in the vicinity of the well.

The capillary equilibrium, prevailing in the formation between the phases, is severely disturbed if the drilling mud is suddenly exposed to the matrix. The flow of water is driven by the water phase pressure gradient in a radial direction:

$$\frac{\partial p_w}{\partial r} = \frac{\partial}{\partial r}(p_g - p_{cap}(S_w)) = \frac{\partial p_g}{\partial r} - \frac{dp_{cap}}{dS_w} \frac{\partial S_w}{\partial r} . \quad (5.1)$$

Near the residual water saturation, the derivative of the capillary pressure on the right hand side of eq.(5.1) will exceed the gas pressure gradient. As long as that condition prevails, water flows into the formation. However, the gradient dp_{cap}/dS_w vastly declines with increasing water saturations (see fig.5.1.b), lowering the driving force for the water influx.

Fig.5.7 presents the temporal development of the conditions prevailing at the sandface for a tight (0.1 mD) and a high permeability reservoir (100 mD) during UBD. The initial field pressure is 600 bars with 300 bars and 550 bars UBD conditions. In the tight formation (0.01 mD), the slight UBD condition can not prevent the water imbibition. However, equilibrium of pressures and saturations is established rather quickly. Although water is subsequently transported deeper into the formation, the equilibrium state prevents any further water influx across the sandface. Assuming a UBD condition of 300 bars, far less water enters the formation. Since capillary pressure at residual water saturation needs to take a finite value, the 300 bars pressure difference can prevent water imbibition at first. This is, however, a numerical issue.⁷

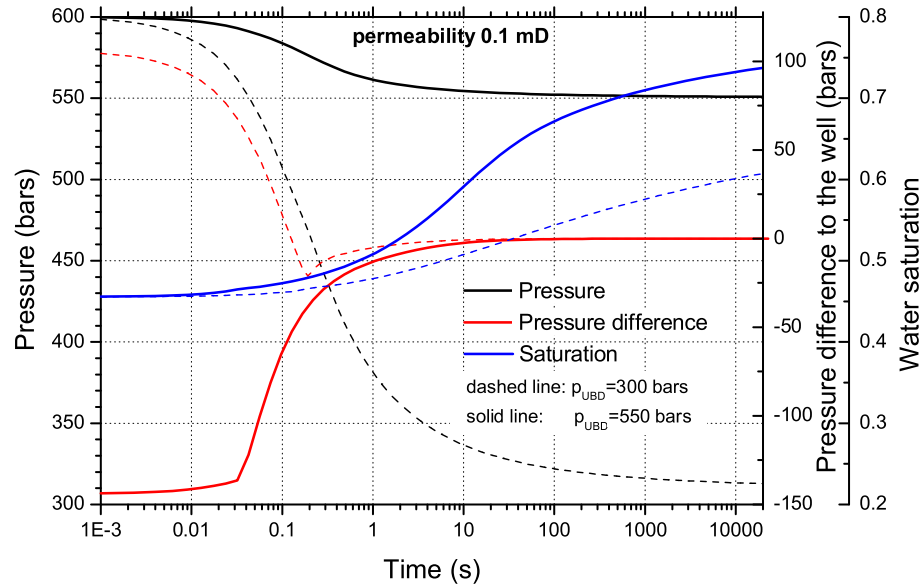
The high permeability reservoir, fig.5.7.b, shows considerably lower capillary forces. In the case of 300 bars UBD pressure, the conditions prevent *de facto* the water imbibition. On the contrary, with a 550 bars UBD condition, just a very small amount of water enters the formation.

5.6 UBD in Horizontal Wells

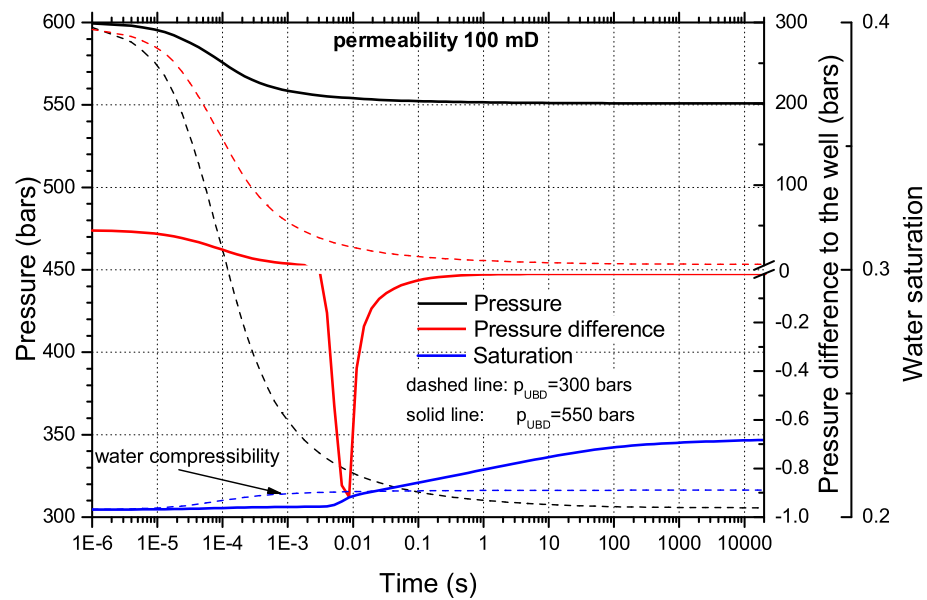
The UBD model can be applied to more complex geometry. For illustration, the underbalanced drilling process of a horizontal well is simulated with one year production. The square drainage area of the reservoir is 400 m x 400 m with a net thickness of 60 m. The horizontal well is centrally aligned with a perforated length of 100 m. Parameters are summarised in table 5.1. Unstructured grids are utilised to discretise the horizontal well, where the well is refined with cylindrical grid blocks. The cross section of the reservoir is similar to the hybrid hexagonal-cylindrical well grid shown in fig.3.4.b, but uses rectangular bulk grids instead. Along the well track, the stream tube approach is considered. At the end of the drilling, saturation conditions along the well track are as shown in fig.5.8.a. Gas production during drilling and production are presented in fig.5.8.b.

⁷It should be noted that water imbibition initiates immediately (i.e., when capillary pressure gradient is infinite).

5 Simulation of Underbalanced Drilling Operations



(a) Reservoir permeability 0.1 mD



(b) Reservoir permeability 100 mD

Figure 5.7: Temporal development of the pressure, pressure gradient and water saturation at the sandface

5 Simulation of Underbalanced Drilling Operations

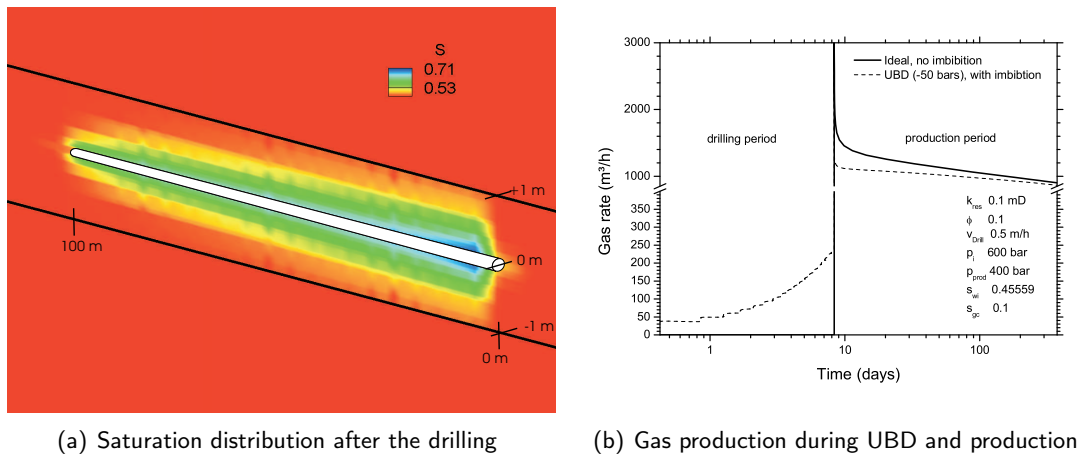


Figure 5.8: Simulation of UBD of a 100 m horizontal well in a 0.1 mD reservoir

5.7 Discussion

A new UBD simulation methodology was presented in the current chapter. The numerical model applies to arbitrary geometries and provides an accurate depiction of the physical processes behind UBD. Special emphasis is placed on the realisation of "actual" UBD boundary conditions. The level of details can be easily extended, e.g., to regard permanent formation damage or more complex rheology of the drilling fluid. The reliability is demonstrated by comparison with analytical solutions for single-phase problems, where good agreement is achieved.

The sensitivity analysis points out that the degree of water encroachment is the key factor for a successful UBD operation. Water encroachment is caused by the countercurrent imbibition as a consequence of the capillary forces. It is frequently accompanied by phase trapping which has not been investigated in previous studies. Phase trapping can severely reduce the productivity of a well. In principle, every water-wet formation exposed to a water based drilling fluid will be affected. Water imbibition depends on the capillary forces prevailing in the formation. Therefore, hydraulic damage is far more pronounced in tight-gas formations.

In the framework of this work, only hydraulic damage is considered as a consequence of the imbibition process. Permanent permeability reductions or hysteresis effects can further curtail the gas flow. Non-equilibrium effects⁸ between the phases are not captured by the classical multi-phase flow model. For validation of the current model, experimental data and theoretical models of the countercurrent imbibition should be reconsidered.⁹

⁸Strong saturation gradients may not be well captured by the classical theory.

⁹A mathematical model for spontaneous capillary imbibition has been presented by ROSE /174/; experimental investigations were reported, e.g., by LI et al. /175/.

6 Summary

The present thesis focusses on two main issues: (i) the development of a multi-phase simulation tool for the characteristics of tight-gas reservoirs, and (ii) the investigation of advanced stimulation techniques by means of the tool. The latter mainly implies the analysis of certain damaging mechanisms, as well as the derivation of general modelling guidelines for fractured wells and underbalanced drilling.

A special simulation tool is developed, realised in a Fortran-MATLAB coupling. The numerical model is based on the control-volume method with finite differences. Therefore, the integrated form of the multi-phase flow equations is derived for three immiscible phases (gas, water and gel). The implemented flow equation accounts for inertial non-Darcy effects, non-Newtonian fluid rheology and stress dependency of permeability via a simplified approach.

The discretisation framework is fully unstructured, using the connection list approach and the common two-point flow stencil. Its versatility is demonstrated by simulating on radial, Cartesian and unstructured Voronoi grids, and by coupling wellbore and reservoir flow within one unified code. Toolboxes are developed for typical tasks, e.g., providing unstructured Voronoi grids for fractured vertical wells as well as structured BENNETT-type fracture grids. The simulation tool facilitates the inclusion of third party gridding postprocessors in the future.

The Voronoi grid should be seen as an extended option of the simulator. Voronoi grids are "fit for purpose grids", which can be constructed according to the resulting flow pattern. On a full-field scale, they are well suited, e.g., for the simulation of multiple fractured horizontal wells since localised grid refinement provides flow details without impacting the model in other connected regions. The simulation tool utilises a natural ordering scheme which is probably not the most efficient one. Additionally, higher order methods for Voronoi grids are *de facto* not available. Both issues are areas for future research.

Wells and boundary conditions can be handled very flexible in the code. Contrary to conventional treatment in simulators, wells are discretely included in the simulator. This facilitates: (i) proper representation of boundary conditions, e.g., flow rates, constant pressure, constant saturation, (ii) simple treatment in the numerical model, e.g., no extra well model with supplementary residual equations, and (iii) the consideration of crossflow and multiple perforation flow. A special passive/active technique permits, besides the common active/passive flags, the definition of a constant pressure and, optionally, a constant saturation for every grid block. This is mainly intended for those grid blocks representing boundaries and wells.

The numerical solution is obtained fully implicitly using Newton's linearisation technique, with a numerical Jacobian matrix calculation. Due to the complex physical system considered here and the aim of flexibility, the numerical derivation of Jacobian matrix drastically simplifies the simulator development, while maintaining the convergence behaviour of Newton's method. Non-Darcy flow is linearised semi-implicitly with relaxation of the non-Darcy control parameter. Contrary to the conventional fully implicit treatment, the present approach facilitates the consideration of extremely "turbulent" flow with control parameters close to zero. The system of linear equations is solved using both direct and iterative solvers. The code is validated with analytical and numerical solutions from commercial simulators for the entire application

6 Summary

spectrum in close agreement.

Hydraulic fracturing as stimulation techniques is an essential part of the investigations. Special models are developed for the simulation of such wells, incorporating specific processes in tight-gas reservoirs. Inertial non-Darcy flow and stress dependency of reservoir permeability are shown to affect the accuracy of simulation models, despite low gas rates. Considering a realistic scenario, with non-Darcy flow and permeability (stress) dependent non-Darcy flow coefficients, stress dependency of reservoir permeability and fracture closure, a total reduction of 40% is possible in a 10 year production period under realistic conditions.

New type-curves are presented for non-Darcy flow in fracture and reservoir, allowing for the determination of non-Darcy flow related parameters. To take account of non-Darcy flow in the reservoir, a new dimensionless parameter is introduced. The inertial non-Darcy flow in the fracture mainly affects the early flow and, hence, well test analyses. Contrary to this, non-Darcy flow in the reservoir acts on the late time flow, impacting mainly on production forecasts.

The stress sensitivity of tight-gas rocks is crucial when simulating such reservoirs. The stress dependency of the reservoir permeability impacts the productivity to a much higher degree than the fracture closure. Fracture closure is less important when predicting long term performance of the well. However, for well test analysis it may be of interest to increase the certainty of the results and, hence, that of the fracture parameters under evaluation.

A two-phase model is presented for the simulation of cleanup processes in terms of load water recovery. The fracturing fluid is treated as the water phase. The load water, causing hydraulic damage, hardly curtails productivity. The damage depends on (i) the extent of the invasion zone, (ii) the water saturation in this zone and (iii) the relative permeability of gas at this water saturation. Under such conditions, phase trapping is not likely. To get considerable reductions in productivity, permeability in the fracture vicinity needs to be severely impaired. Due to the flow pattern, fractured wells are generally less sensitive against near wellbore damage than radial wells. Furthermore, the effect of reduced conductivities inside the fracture diminishes quickly.

An enhanced three-phase cleanup model is presented for the investigations of the polymer gel cleanup, incorporating a yield power law rheology (the Herschel-Bulkley model). Assuming literature data for the value of the yield stress, about 50% of the polymer gel phase can be recovered during the cleanup. The residing gel damages fracture conductivity and causes fracture face damage, reducing the production potential. The yield stress model captures saturation conditions in the fracture with increasing values towards the tips. This coincides with observations in the field where fracture half lengths, conductivities and productivity are lower than anticipated. The combined occurrence of loadwater recovery including capillary forces and the gel cleanup, are investigated for the first time. First results indicate that both processes are only weakly coupled.

A new simulation methodology is presented to investigate underbalanced drilling. The model is applied for a vertical and a horizontal well, depicting the physical processes behind UBD and providing "actual" UBD boundary conditions. These conditions and multi-phase flow with capillary forces are considered for the first time in the literature. A sensitivity analysis points out that the degree of water encroachment is the key factor for a successful UBD operation. Countercurrent imbibition, causing water encroachment is also analysed. Hydraulic damage turns out to be far more pronounced in tight-gas formations.

Bibliography

- /1/ Pasternak M. Exploration und Produktion von Erdöl und Erdgas in Deutschland 2002. *Erdöl Erdgas Kohle*, (7/8):260–270, Jul./Aug. 2003. presented at the DGMK-Spring meeting 28-29 April 2003 held in Celle, Germany.
- /2/ Liermann N.; Jentsch M. Tight-Gas-Reservoirs - Erdgas für die Zukunft. *Erdöl Erdgas Kohle*, (7/8):270–273, Jul./Aug. 2003. presented at the DGMK-Spring meeting 28-29 April 2003 held in Celle, Germany.
- /3/ Economides M.J.; Nolte K.G., editor. *Reservoir Stimulation*. John Wiley & Sons Ltd - Chichester New York Brisbane Toronto Singapore, 3. edition, 2000. ISBN 0-471-49192-6.
- /4/ Fracture Technologies Ltd. URL=<http://www.wellwhiz.com>.
- /5/ Email communication with Mike Goldwater (WellWhiz developer, Auric Hydrates Ltd.), 24.07.2003.
- /6/ Oral communication with Tommy Miller (ECLIPSE Office Product Manager, Schlumberger GeoQuest).
- /7/ Aziz K.; Settari A. *Petroleum Reservoir Simulation*. Elsevier Science Publisher Ltd., 1979. ISBN 0-85334-787-5. 4.reprint (1990).
- /8/ Aziz K.; Durlofsky L. Fundamentals of Reservoir Simulation: Notes on Reservoir Simulation. Lectures Notes P EN 223, Stanford University, Petroleum Engineering Department, 2001-2002.
- /9/ Bear J. *Dynamics of Fluids in Porous Media*. Dover Publications, New York, 1988. ISBN 0-486-65675-6.
- /10/ Lake L.W. *Enhanced Oil Recovery*. Prentice Hall, Englewood Cliffs, New Jersey, 1989. ISBN 0-13-281601-6.
- /11/ Häfner F.; Sames D.; Voigt H.-D. *Wärme- und Stofftransport*. Springer-Verlag, Berlin Heidelberg New York, 1992. ISBN 3-540-54665-0.
- /12/ Heinrich B. *Finite Difference Methods on Irregular Networks*. Number 33 in Mathematical Research. Akademie Verlag, Berlin, 1987.
- /13/ Nghiem L. An Integral Approach for Discretizing the Reservoir Flow Equations. *SPE Reservoir Engineering*, (SPE-Paper 12121):685–690, May 1988.
- /14/ Forsyth P.A. A Control Volume, Finite-Element Method for Local Mesh Refinement in Thermal Reservoir Simulation. (SPE-Paper 18415), 1990. presented at the 10. SPE Symposium on Reservoir Simulation held in Houston, Texas.

Bibliography

- /15/ Fung L.S.-K.; Hiebert A.D; Nghiem L. Reservoir Simulation With A Control-Volume Finite-Element Method. (SPE-Paper 21224), 1991. presented at the 11. SPE Symposium on Reservoir Simulation held in Anaheim, California.
- /16/ Fung L.S.-K.; Buchanan W.L.; Sharma R. Hybrid-CVFE Method for Flexible Grid Reservoir Simulation. *SPE Reservoir Engineering*, (SPE-Paper 25266):387–398, Aug. 1994.
- /17/ Pedrosa Jr.O.A.; Aziz K. Use of a Hybrid Grid in Reservoir Simulation. *SPE Reservoir Engineering*, (SPE-Paper 13507):611–621, Nov. 1986.
- /18/ Verma S.; Aziz K. A Control Volume Scheme for Flexible Grids in Reservoir Simulation. (SPE-Paper 37999), 1997. presented at the Reservoir Simulation Symposium held in Dallas, Texas.
- /19/ Palagi C. *Generation and Application of Voronoi Grid to Model Flow in Heterogeneous Reservoirs*. PhD thesis, Department of Petroleum Engineering, Stanford University, Stanford, California, 1992.
- /20/ Heinemann Z.; Brand C.; Munka M.; Chen Y.M. Modeling Reservoir Geometry with Irregular Grids. (SPE-Paper 18412), 1989. presented at the 1989 SPE Reservoir Simulation Symposium in Houston, Texas.
- /21/ Sonier F.; Eymard R. Mathematical and Numerical Properties of Control-Volume Finite-Element Scheme for Reservoir Simulation. (SPE-Paper 25267), 1993. presented at the 12th Symposium on Reservoir Simulation held in New Orleans, Louisiana.
- /22/ Rozon B.J. A Generalized Finite Volume Discretization Method for Reservoir Simulation. (SPE-Paper 18414), 1989. presented at the Reservoir Simulation Symposium held in Houston, Texas.
- /23/ Nekrassov A. *Development of a Reservoir Simulation Tool with the Local Equilibrium Approach to Composite Water-Hydrocarbon Systems for Application to the Multi-Phase Flow both in Petroleum Reservoirs and in Aquifers Taking into Account the Hydrodynamic Dispersion*. PhD thesis, Fakultät für Geowissenschaften, Geotechnik und Bergbau der TU Bergakademie Freiberg, Freiberg, Germany, 2002.
- /24/ Gunasekera D.; Cox J.; Lindsey P. The Generation and Application of K-Orthogonal Grid Systems. (SPE-Paper 37998), 1997. presented at the 14th SPE Symposium on Reservoir Simulation held in Dallas, Texas.
- /25/ Thomas J.W. *Numerical Partial Differential Equations: Finite Difference Methods*, volume 22 of *Texts in Applied Mathematics*. Springer-Verlag, New York Heidelberg Berlin, 1999. ISBN 0-387-98346-5.
- /26/ Langtangen H.P. *Computational Partial Differential Equations: Numerical Methods and Diffpack Programming*, volume 2 of *Lecture Notes in Computational Science and Engineering*. Springer-Verlag, Berlin Heidelberg New York, 1999. ISBN 3-540-65274-4.
- /27/ Autorenkollektiv. *Geohydrodynamische Erkundung von Erdöl-, Erdgas- und Grundwasserlagerstätten*, volume 1 of *Wissenschaftlich-Technischer Informationsdienst WTI*. Zentrales Geologisches Institut Berlin, 1985. Jahrgang 26.

Bibliography

- /28/ Katz D.L.; Lee R.L. *Natural Gas Engineering: Production and Storage*. McGraw-Hill Publishing Company, 1990. ISBN 0-07-033352-1.
- /29/ Forchheimer P. Wasserbewegung durch Boden. *ZVDI*, 45:1781 foll., 1901.
- /30/ Geertsma J. Estimating the Coefficient of Inertial Resistance in Fluid Flow Through Porous Media. *Society of Petroleum Engineers Journal (SPEJ)*, (SPE-Paper 4706): 445–450, Oct. 1974.
- /31/ Firoozabadi A.; Katz D.L. An Analysis of High-Velocity Gas Flow Through Porous Media. *Journal of Petroleum Technology*, 31(SPE-Paper 6827):211–216, Feb. 1979.
- /32/ Valko P.; Economides M.J. Performance of Longitudinally Fractured Horizontal Wells. *Society of Petroleum Engineers Journal*, (Mar. 1996):11–19, 1996.
- /33/ May E.A.; Britt L.K.; Nolte K.G. The Effect of Yield Stress on Fracture Fluid Cleanup. (SPE-Paper 38619), 1997. presented at the SPE Annual Technical Conference and Exhibition held in San Antonio, Texas.
- /34/ Barenblatt G.I.; Entov V.M.; Ryzhik V.M. *Theory of Fluid Flows through Natural Rocks*. Kluwer Academic Publishers, Dordrecht, 1990. ISBN 0792301676.
- /35/ Barenblatt G.I.; Patzek T.W.; Silin D.B. The Mathematical Model of Non-Equilibrium Effects in Water-Oil Displacement. (SPE-Paper 75169), 2002. presented at the SPE/DOE Thirteenth Improved Oil Recovery Symposium held in Tulsa, Oklahoma.
- /36/ Dake L.P. *Fundamentals of Reservoir Engineering*. Development in Petroleum Science 8. ELSEVIER Science B.V., 1. edition, 1998. ISBN 0-444041830-X. 17. impression.
- /37/ Chierici G.L. *Principles of Petroleum Reservoir Engineering*, volume 1. Springer-Verlag Berlin Heidelberg New York, 1994. ISBN 3-540-56037-8.
- /38/ Helmig R. *Multiple Flow and Transport Processes in the Subsurface: A Contribution to the Modeling of Hydrosystems*. Springer, 1997. ISBN 3-540-62703-0.
- /39/ The MathWorks Inc. *MATLAB 6.5: The Language of Technical Computing*, 2002. Part: Using MATLAB, Version 6.
- /40/ Faires J.D.; Burden R.L. *Numerische Methoden: Näherungsverfahren und ihre praktische Anwendung*. Spektrum Akademischer Verlag, Heidelberg Berlin Oxford, 1994. ISBN 3-86025-138-4.
- /41/ Schwetlick H.; Kretzschmar H. *Numerische Verfahren für Naturwissenschaftler und Ingenieure*. Mathematik für Ingenieure. Fachbuchverlag GmbH Leipzig, 1991. ISBN 3-343-00580-0.
- /42/ Press W.H.; Teukolsky S.A.; Vetterling W.T.; Flannery B.P. *Numerical recipes in Fortran: the art of scientific computing*. Cambridge University Press, 2. edition, 1992. ISBN 0-521-43064-X.
- /43/ Au A.D.K.; Vinsome K. Techniques For Fully Implicit Reservoir Simulation. (SPE-Paper 9302), 1980. presented at the 55th Annual Fall Technical Conference and Exhibition of the SPE of AIME held in Dallas, Texas.

Bibliography

- /44/ Lim K.T.; Schiozer D.J.; Aziz K. A New Approach for Residual and Jacobian Array Construction in Reservoir Simulators. *SPE Computer Applications*, (SPE-Paper 28248): 93 foll., 1995. presented at the 1994 SPE Petroleum Computer Conference held Dallas, Texas.
- /45/ Cao H. *Development of Techniques for General Purpose Simulators*. PhD thesis, Department of Petroleum Engineering, Stanford University, Stanford, California, 2002.
- /46/ Beckner B.L.; Hutfilz J.M.; Ray M.B.; Tomich J.F. EM^{power}: New Reservoir Simulation System. (SPE-Paper 68116), 2001. presented at the SPE Middle East Oil Show held in Bahrain.
- /47/ Grabowski J.W.; Vinesome P.K.; Behie A.; Rubin B. A Fully Implicit General Purpose Finite-Difference Thermal Model for In-Situ Combustion and Steam. (SPE-Paper 8396), 1979.
- /48/ Sammon P.H.; Rubin B. Practical Control of Timestep Selection in Thermal Simulation. *SPE Reservoir Engineering*, (SPE-Paper 12268):163 foll., March 1986.
- /49/ Saad Y.; Schultz M.H. GMRES: A generalized minimal residual algorithm for solving nonsymmetric linear systems. *SIAM J. Sci. Comput.*, (7):856–869, 1986.
- /50/ Behie A.; Forsyth P.A. Practical Considerations for Incomplete Factorization Methods in Reservoir Simulation. (SPE-Paper 12263), 1983. presented at the 7. SPE Symposium on Reservoir Simulation held in San Francisco, California.
- /51/ D’Azevedo E.; Forsyth P.A.; Tang W.-P. An Automatic Ordering Method for Incomplete Factorization Iterative Solvers. (SPE-Paper 21226), 1991. presented at the Eleventh SPE Symposium on Reservoir Simulation held in Anaheim, California.
- /52/ Stüben K.; Clees T. *SAMG User’s Manual Release 21c*. Fraunhofer Institute SCAI, Schloss Birlinghoven D-53754 St. Augustin, Germany, Aug. 2003.
- /53/ Schlumberger GeoQuest. *Eclipse 100 Technical Description 2003a*, 2003.
- /54/ Li D.; Engler T.W. Modeling and Simulation of Non-Darcy Flow in Porous Media. (SPE-Paper 75216), 2002. presented at the SPE/DOE Improved Oil Recovery Symposium held in Tulsa, Oklahoma, 13-17 April 2002.
- /55/ Schlumberger GeoQuest. *Eclipse 100 Reference Manual 2003a*, 2003.
- /56/ van Poolen H.K.; Breitenbach E.A.; Thurnau D.H. Treatment of Individual Wells and Grids in Reservoir Modeling. *SPEJ*, pages 341–346, Dec. 1968. also in *Trans. AIME*, volume 243.
- /57/ Peaceman D.W. Interpretation of Well-Block Pressures in Numerical Reservoir Simulation With Nonsquare Gridblocks and Anisotropic Permeability. *SPEJ*, (SPE-Paper 10528):531–543, June 1983.
- /58/ Deimbacher F.X.; Heinemann Z.E. Time-Dependent Incorporation of Locally Irregular Grids in Large Reservoir Simulation Models. (SPE-Paper 25260), 1993. presented at the SPE Symposium on Reservoir Simulation held in New Orleans, Louisiana.

Bibliography

- /59/ Heinemann Z.E. Interactive Generation of Irregular Simulation Grids and Its Practical Application. (SPE-Paper 27998), 1994. presented at the University of Tulsa Centennial Petroleum Engineering Symposium held in Tulsa, Oklahoma.
- /60/ Deimbacher F.X.; Komlosi F.; Heinemann Z.E. Fundamental Concepts and Potential Applications of the Windowing Technique in Reservoir Simulation. (SPE-Paper 29851), 1995. presented at the SPE Middle East Oil Show held in Bahrain.
- /61/ Holmes J.A.; Barkve T.; Lund O. Application of a Multisegment Well Model to Simulate Flow in Advanced Wells. (SPE-Paper 50646), 1998. presented at the SPE European Petroleum Conference held in The Hague, The Netherlands.
- /62/ Bohl W. *Technische Strömungslehre*. Vogel Fachbuch: Kamprath Reihe. 11. edition, 1998. ISBN 3-8023-1740-8.
- /63/ Heinemann Z.E.; Brand C.W. Gridding Techniques in Reservoir Simulation. pages 339–426, 1988. Proc. First International Forum on Reservoir Simulation held in Alpbach, Austria.
- /64/ Palagi C.; Aziz K. Use of Voronoi Grid in Reservoir Simulation. (SPE-Paper 22889), 1991. presented at the 66th Annual Technical Conference and Exhibition of the Society of Petroleum Engineers held in Dallas, Texas.
- /65/ Palagi C.; Aziz K. The Modeling of Vertical and Horizontal Wells With Voronoi Grid. (SPE-Paper 24072), 1982. presented at the Western Regional Meeting held in Bakersfield, California.
- /66/ HOT ENGINEERING. *SURE-User Guide*, 2002.
- /67/ Kocberber S. An Automatic, Unstructured Control Volume Generation System für Geologically Complex Reservoirs. (SPE-Paper 38001), 1997. presented at the 14th SPE Symposium on Reservoir Simulation held in Dallas, Texas.
- /68/ Shewchuk R.J. *Triangle: Engineering a 2D Quality Mesh Generator and Delaunay Triangulator*. School of Computer Science, Carnegie Mellon University, Pittsburgh, Pennsylvania 15213, 1996. Public Domain Software, URL=<http://www.cs.cmu.edu/~quake/triangle.html>.
- /69/ Gunasekera D.; Childs P.; Herring J. A Multi-Point Flux Discretization Scheme for General Polyhedral Grids. (SPE-Paper 48855), 1998. presented at the SPE 6th International Oil&Gas Conference and Exhibition held Beijing, China.
- /70/ Appleyard J.R.; Cheshire I.M. The Cascade Method for Accelerated Convergence in Implicit Simulators. (SPE-Paper 12804), 1982. presented at the European Petroleum Conference held in London, U.K.
- /71/ Naccache P.F. A Fully-Implicit Thermal Reservoir Simulator. (SPE-Paper 37985), 1997.
- /72/ Gable C. et al. *LaGriT: Los Alamos Grid Toolbox*. Los Alamos National Laboratory, Los Alamos. URL=<http://www.t12.lanl.gov/home/lagrit/index.html>.

Bibliography

- /73/ Cherry T.A.; Gable C.W.; Trease H. *Numerical Grid Generation in Computational Fluid Dynamics and Related Fields*, chapter 3-Dimensional Wells and Tunnels for Finite Element Grids. Mississippi State Univ. Press, Engineering Research Center, 1996.
- /74/ Gidley J.L. *Recent Advances in Hydraulic Fracturing*, volume 12 of *SPE Monograph Series*. Society of Petroleum Engineers, 1989. ISBN 1-55563-020-0.
- /75/ Häfner et al. Simulation des Produktionsverhaltens gefracter Bohrungen in geringpermeablen Gaslagerstätten (Simulation of Production Behaviour of Hydraulically Fractured Wells in Tight-Gas Reservoirs). Intermediate report, DGMK Research Project 593-9/1, 2001. unpublished.
- /76/ McGuire W.J.; Sikora V.T. The Effect of Vertical Fractures on Well Productivity. *Journal of Petroleum Technology*, 12(SPE-Paper 1618-G):72–74, Oct. 1960.
- /77/ Prats M. Effect of Vertical Fractures on Reservoir Behavior-Incompressible Fluid Case. *Society of Petroleum Engineers Journal*, 1(SPE-Paper 1575-G):105–118, June 1961.
- /78/ Russel D.G.; Truitt N.E. Transient Pressure Behavior in Vertically Fractured Reservoirs. *Journal of Petroleum Technology*, 16(SPE-Paper 967):1159–1170, Oct. 1964.
- /79/ Dowdle W.L.; Hyde P.V. Well Test Analysis of Hydraulically Fractured Gas Wells. (SPE-Paper 6437), 1977. presented at the Deep Drilling and Production Symposium of the SPE of AIME held in Amarillo, Texas.
- /80/ Bastian P.A.; Holditch S.A.; Sherman J.B. Analysis of a Hydraulically Fractured, Low-Permeability Gas Reservoir Using Numerical Simulation. (SPE-Paper 21511), 1991. presented at the SPE Gas Technology Symposium in Houston, Texas.
- /81/ Holditch S.A. Factors Affecting Water Blocking and Gas Flow from Hydraulically Fractured Wells. *Journal of Petroleum Technology*, (SPE-Paper 7561):1515–1524, Dec. 1979.
- /82/ Soliman M.Y.; Hunt J.L. Effect of Fracturing Fluid and Its Cleanup on Well Performance. (SPE-Paper 14514), 1985.
- /83/ Ehrl E.; Schueler S.K. Simulation of a Tight Gas Reservoir with Horizontal Multifractured Wells. (SPE-Paper 65108), 2000. presented at the SPE European Conference held in Paris, France.
- /84/ Friedel T.; Nekrassov A.; Behr A.; Mtschedlishvili G.; Häfner F. Representation of Fractured Well to Numerical Modeling Postfracturing-Production from Tight Reservoirs. 2002. presented at the European Conference on the Mathematics of Oil Recovery, ECMOR 8 held in Freiberg, Germany.
- /85/ Banerjee R.; Gunasekera D.; Fletcher K.J.C. Simulation of Hydraulically Fractured Horizontal and Vertical Wells to Well Testing Accuracy Using Unstructured Grids. *Proc. ECMOR VII*, (M-21), 2000.
- /86/ Behr A.; Mtshedlishvili G.; Friedel T.; Häfner F. Initialization of Reservoir Model with Hydraulically Fractured Well for Simulation of Post-Fracture Performance. (SPE-Paper

Bibliography

- 82298), 2003. presented at the European Formation Damage Conference held in The Hague, Netherlands.
- /87/ Settari A. Simulation of Hydraulic Fracturing Processes. *Society of Petroleum Engineers Journal*, (SPE-Paper 7693):487–500, Dec. 1980.
- /88/ Nghiem L.X. Modeling Infinite-Conductivity Vertical Fractures With Source and Sink Terms. *Society of Petroleum Engineers Journal*, (SPE-Paper 10507):633–644, Aug. 1983.
- /89/ Nghiem L.X.; Forsyth Jr. P.A.; Behie A. A Fully Implicit Hydraulic Fracture Model. *Journal of Petroleum Technology*, (SPE-Paper 10506):1191–1198, July 1984.
- /90/ Settari A.; Puchyr P.J.; Bachman R.C. Partially Decoupled Modeling of Hydraulic Fracturing Processes. (SPE-Paper 16031), 1987.
- /91/ Schlumberger GeoQuest. *Eclipse Office User Guide 2003a*, 2003.
- /92/ Bennett C.O.; Reynolds A.C.; Raghavan R.; Elbel J.L. Performance of Finite-Conductivity, Vertically Fractured Wells in Single-Layer Reservoirs. (SPE-Paper 11029), 1986.
- /93/ Millheim K.K.; Cichowicz L. Testing and Analyzing Low-Permeability Fractured Gas Wells. *Journal of Petroleum Technology*, (SPE-Paper 1768):193 foll., Feb. 1968.
- /94/ Wattenbarger R.A.; Ramey Jr. H.J. Well Test Interpretation of Vertically Fractured Gas Wells. *Journal of Petroleum Technology*, (SPE-Paper 2155):625 foll., May 1969.
- /95/ Holditch S.A.; Morse R.A. The Effects of Non-Darcy Flow on the Behavior of Hydraulically Fractured Gas Wells. *Journal of Petroleum Technology*, (SPE-Paper 5586):1169 foll., Oct. 1976.
- /96/ Cooke Jr. C.E. Conductivity of Fracture Proppants in Multiple Layers. *Journal of Petroleum Technology*, 25(SPE-Paper 4117):1101–1107, Sep. 1973.
- /97/ Guppy K.H.; Cinco-Ley H.; Ramey Jr. H.J.; Sameniogo-V. F. Non-Darcy Flow in Wells with Finite-Conductivity Vertical Fractures. *Society of Petroleum Engineers Journal (SPEJ)*, (SPE-Paper 8281):681 foll., Oct. 1982.
- /98/ Guppy K.H.; Cinco-Ley H.; Ramey Jr. H.J. Pressure Buildup Analysis of Fractured Wells Producing at High Flow Rates. *Journal of Petroleum Technology*, (SPE-Paper 10187): 2656 foll., Nov. 1982.
- /99/ Guppy K.H.; Cinco-Ley H.; Ramey Jr. H.J. Effect of Non-Darcy Flow on the Constant Pressure Production of Fractured Wells. *Society of Petroleum Engineers Journal*, (June 1981):390–400, 1981.
- /100/ Umuayponwivat S.; Ozkan E.; Pearson C.M.; Vincent M. Effect of Non-Darcy Flow on the Interpretation of Transient Pressure Responses of Hydraulically Fractured Wells. (SPE-Paper 63176), 2000. presented at the SPE Annual Technical Conference and Exhibition held in Dallas, Texas.

Bibliography

- /101/ Vincent M.C.; Pearson C.M.; Kullman J. Non-Darcy and Multiphase Flow in Propped Fractures: Case Studies Illustrate the Dramatic Effect on Well Productivity. (SPE-Paper 54630), 1999. presented at the 1999 SPE Western Regional Meeting, Anchorage, Alaska.
- /102/ Settari A.; Bale A.; Bachman R.C.; Floisand V. General Correlation for the Effect of Non-Darcy Flow on Productivity of Fractured Wells. (SPE-Paper 75715), 2002. presented at the SPE Gas Technology Symposium held in Calgary, Alberta.
- /103/ Jin L.; Penny G.S. A Study on Two Phase, Non-Darcy Gas Flow Through Proppant Packs. (SPE-Paper 49248), 1998. presented at the SPE Annual Technical Conference and Exhibition held in New Orleans, Louisiana.
- /104/ Fourar M.; Lenormand R. Inertial Effects in Two-Phase Flow through Fractures. *Oil & Gas Science and Technology - Rev. IFP*, 55(3):259–268, 2000.
- /105/ Roberts B.E.; van Engen H.; van Kruysdijk C.P.J.W. Productivity of Multiply Fractured Horizontal Wells in Tight Gas Reservoirs. (SPE-Paper 23113), 1991. presented at the Offshore Europe Conference held in Aberdeen, U.K.
- /106/ Gil J.A.; Ozkan E.; Raghavan R. Fractured-Well-Test Design and Analysis in the Presence of Non-Darcy Flow. (SPE-Paper 71573), 2001. presented at the SPE Annual Technical Conference and Exhibition held in New Orleans, Louisiana.
- /107/ Alvarez C.H.; Holditch S.A.; McVay D.A. Effect of Non-Darcy Flow on Pressure Transient Analysis of Hydraulically Fractured Gas Wells. (SPE-Paper 77468), 2002. presented at the SPE Annual Technical Conference and Exhibition held in San Antonio, Texas.
- /108/ Belhaj H.A.; Agha K.R.; Butt S.D.; Islam M.R. Simulation of Non-Darcy Flow in Porous Media Including Viscous, Inertial and Frictional Effects. (SPE-Paper 84879), 2003. presented at the SPE International Improved Oil Recovery Conference in Asia Pasific held in Kuala Lumpur, Malaysia.
- /109/ Martins J.P.; Milton-Taylor D.; Leung H.K. The Effect of Non-Darcy Flow in Propped Hydraulic Fractures. (SPE-Paper 20709), 1990. presented at the 65th Annual Technical Exhibition of the Society of Petroleum Engineers held in New Orleans, Louisiana.
- /110/ Horne R.N. *Modern Well Test Analysis: A Computer-Aided Approach*. Petroway, Inc., 926 Bautista Court, Palo Alto, CA. 94303, 5. edition, 1995. ISBN 0-9626992-1-7.
- /111/ Gidley J.L. A Method for Correcting Dimensionless Fracture Conductivity for Non-Darcy Flow Effects. *SPE Production Engineering*, 6/4(SPE-Paper 20710):391–394, 1991. presented at the SPE Annual Technical Conference and Exhibition held in New Orleans, Louisiana.
- /112/ Li D.; Engler T.W. Literature Review on Correlations of the Non-Darcy Coefficient. (SPE-Paper 70015), 2001. presented at the SPE Permian Basin Oil and Gas Recovery Conference held in Midland, Texas.
- /113/ Byrnes A.P.; Castle W. Comparison of Core Petrophysical Properties Between Low-Permeability Sandstone Reservoirs: Eastern U.S. Medina Group and Western U.S.

Bibliography

- Mesaverde Group and Frontier Formation. (SPE-Paper 60304), 2000. presented at the SPE Rocky Mountain Regional/Low Permeability Reservoirs Symposium and Exhibition held in Denver, Colorado.
- /114/ STIMLAB-Consortium. URL=<http://www.corelab.com/stimlab/default.asp>.
- /115/ Wong S.W. Effect of Liquid Saturation on Turbulence Factors for Gas-Liquid Systems. *Journal of Canadian Petroleum Technology*, (Oct.-Dec. 1970):274 foll., 1970.
- /116/ Penny G.S.; Jin L. The Development of Laboratory Correlations Showing the Impact of Multiphase Flow, Fluid, and Proppant Selection Upon Gas Well Productivity. (SPE-Paper 30494), 1995. presented at the SPE Technical Conference and Exhibition held in Dallas, Texas.
- /117/ Fatt I.; Davis D.H. Reduction in Permeability with Overburden Pressure. *Journal of the American Institute of Mechanical Engineers, Petroleum Transactions*, 195:329 foll., 1952.
- /118/ Dobrynin V.M. Effect of Overburden Pressure on Some Properties Of Sandstones. *Society of Petroleum Engineers Journal*, (SPE-Paper 461):360–366, Dec. 1962.
- /119/ Tiab D.; Donaldson E.C. *Petrophysics: Theory and Practice of Measuring Reservoir Rock and Fluid Transport Properties*. Gulf Publishing Company, 1. edition, 1996. ISBN 0-88415-634-6.
- /120/ Vairogs J. Effect of Rock Stress on Gas Production From Low-Permeability Reservoirs. *Journal of Petroleum Technology*, (SPE-Paper 3001):1161–1167, Sep. 1971.
- /121/ Friedel T.; Behr A.; Voigt H.-D.; Mtchedlishvili G.; Häfner F. Simulation des Produktionsverhaltens gefracter Bohrungen in geringpermeablen Gaslagerstätten (Simulation of Production Behaviour of Hydraulically Fractured Wells in Tight-Gas Reservoirs). *Erdöl Erdgas Kohle*, (7/8):274–278, Jul./Aug. 2003. presented at the DGMK-Spring meeting 22-23. April 2002 held in Celle, Germany.
- /122/ Settari A.; Sullivan R.B.; Bachman R.C. The Modeling of the Effect of Water Blockage and Geomechanics in Waterfracs. (SPE-Paper 77600), 2002. presented at the SPE Annual Technical Conference and Exhibition held in San Antonio, Texas.
- /123/ Davies J.P.; Holditch S.A. Stress Dependent Permeability in Low Permeability Formation, East Texas Gas Reservoirs: Travis Peak. (SPE-Paper 39917), 1998. presented at the SPE Rocky Mountain Regional/Low- Permeability Reservoirs Symposium and Exhibition held in Denver, Colorado.
- /124/ Lorenz J.C. Stress-Sensitive Reservoirs. *Journal of Petroleum Technology*, (SPE-Paper 50977):61 foll., Jan. 1999.
- /125/ Voigt H.D. Berechnung der Erdgasvorräte nach der Druckabfallmethode bei deformierbaren Porenraum. *Zeitschrift für angewandte Geologie*, 25:15–20, 1979.
- /126/ Häfner et al. Simulation des Produktionsverhaltens gefracter Bohrungen in geringpermeablen Gaslagerstätten (Simulation of Production Behaviour of Hydraulically Fractured

Bibliography

- Wells in Tight-Gas Reservoirs). Final report, DGMK Research Project 593-9/1, 2002. in print.
- /127/ Zeng Z.; Grigg R.; Ganda S. Experimental Study of Overburden and Stress Influence on Non-Darcy Gas Flow in Dakota Sandstone. (SPE-Paper 84069), 2003. presented at the SPE Annual Technical Conference and Exhibition held in Denver, Colorado.
- /128/ Bennion D.B.; Thomas F.B.; Ma T. Formation Damage Processes Reducing Productivity of Low Permeability Gas Reservoirs. (SPE-Paper 60325), 2000. presented at the SPE Rocky Mountain Regional/Low Permeability Reservoirs Symposium and Exhibition held in Denver, Colorado.
- /129/ Penny G.S.; Soliman M.Y.; Conway M.W.; Briscoe J.E. Enhanced Load Water-Recovery Technique Improves Stimulation Results. (SPE-Paper 12149), 1983. presented at the SPE Annual Technical Conference and Exhibition held in San Francisco, California.
- /130/ Tannich J.D. Liquid Removal from Hydraulically Fractured Gas Wells. *Journal of Petroleum Technology*, (SPE-Paper 5113):1309–1317, Nov. 1975.
- /131/ Sherman J.B.; Holditch S.A. Effect of Injected Fracture Fluids and Operating Procedures on Ultimate Gas Recovery. (SPE-Paper 21496), 1991. presented at the SPE Gas Technology Symposium held in Houston, Texas.
- /132/ Montgomery K.T.; Holditch S.A.; Berthelot J.M. Effect of Fracture Fluid Invasion on Cleanup Behavior and Pressure Buildup Analysis. (SPE-Paper 20643), 1990. presented at the SPE Annual Technical Conference and Exhibition held in New Orleans, Louisiana.
- /133/ Iqbal G.M.; Civan F. Simulation of Skin Effects and Liquid Cleanup in Hydraulically Fractured Wells. (SPE-Paper 25482), 1991.
- /134/ Friedel T.; Mtshedlishvili G.; Behr A.; Voigt H.D.; Häfner F. Numerical Analysis of Cleanup Processes in German Tight-Gas Formations with Fractured Wells. *OIL GAS European Magazine*, (3), 2004.
- /135/ Friedel T.; Behr A.; Mtchedlishvili G.; Voigt H.-D.; Bannach A.; Hauer R.; Häfner F. Simulation des Produktionsverhaltens mehrfach gefracter Horizontalbohrungen in Tight-Gas Reservoirs (Simulation of Production Behaviour of Multiple Fractured Horizontal Wells in Tight-Gas Reservoirs). 2003. presented at the DGMK-Spring meeting 28-29 April 2003 held in Celle, Germany.
- /136/ Behr A.; Mtchedlishvili G. Leakoff Modeling of Fluid Injected in Gas Reservoir at Fracture Stimulation. 2003. presented at the Underground Injection Science and Technology Conference held in Berkeley, California.
- /137/ Howard G.C.; Fast C.R. *Hydraulic Fracturing*, volume 2. Society of Petroleum Engineers, Dallas, 1970. SPE Monograph Series.
- /138/ Settari A. A New General Model in Hydraulic Fracturing of Fluid Loss. *Society of Petroleum Engineers Journal*, (SPE-Paper 11625):491 foll., Aug. 1985.

Bibliography

- /139/ Mayerhofer M.J.; Economides M.J.; Nolte K.G. An Experimental and Fundamental Interpretation of Fracturing Filter-Cake Fluid Loss. (SPE-Paper 22873), 1991. presented at the 66th SPE Annual Technical Conference and Exhibition held in Dallas, Texas.
- /140/ Hagoort J.; Weatherill B.D.; Settari A. Modeling the Propagation of Waterflood-Induced Hydraulic Fractures. *Society of Petroleum Engineers Journal*, (SPE-Paper 7412):293 foll., Aug. 1980.
- /141/ Voneiff G.W.; Robinson B.M.; Holditch S.A. The Effect of Unbroken Fracture Fluid on Gas Well Performance. (SPE-Paper 26664), 1994.
- /142/ Schlumberger. Oilfield Glossary. URL=<http://www.glossary.oilfield.slb.com>.
- /143/ Willberg D.M.; Card R.J.; Britt L.K.; Samuel M.; England K.W.; Cawiezel K.E.; Krus H. Determination of the Effect of Formation Water on Fracture Fluid Cleanup Through Field Testing in the East Texas Cotton Valley. (SPE-Paper 38620), 1997. presented at the SPE Annual Technical Conference and Exhibition held in San Antonio, Texas.
- /144/ Oral communication with Michael Köhler (Preussag Energie Lingen), 16.07.2003.
- /145/ Reitenbach V.; Alkan H.; Pusch G.; Zemke J. Der Einfluss von Rissflächenendeffekten auf die Produktivität von Erdgasbohrungen (Influence of Fracture-Capillary End Effects on the Productivity of Gas Wells). 2001. presented at the DGMK-Spring meeting 26-27 April 2001 held in Celle, Germany.
- /146/ van Poolen H.K. Do Fracture Fluids Damage Productivity? *Oil and Gas Journal*, (May 1957):120–124, 1957.
- /147/ Cinco-Ley H.; Samaniego V.F. Effect of Wellbore Storage and Damage on the Transient Pressure Behavior of Vertically Fractured Wells. (SPE-Paper 6752), Oct. 1977. presented at the 52nd Annual Fall Technical Conference and Exhibition of the SPE held in Denver, Colorado.
- /148/ Willberg D.M.; Steinsberger N.; Hoover R.; Card R.J.; Queen J. Optimization of Fracture Cleanup Using Flowback Analysis. (SPE-Paper 39920), 1998. presented at the Rocky Mountain Regional/Low-Permeability Reservoirs Symposium and Exhibition held in Dallas, Texas.
- /149/ Tjon Joe Pin R.M.; DeVine C.S. Modeling Formation Damage Based Upon Residual Polymeric Fragment Size Distribution. (SPE-Paper 39209), 1997. presented at the SPE Eastern Regional Meeting held in Lexington, Kentucky.
- /150/ Pope D.; Britt L.; Constien V.; Anderson A.; Leung L. Field Study of Guar Removal from Hydraulic Fractures. (SPE-Paper 31094), 1996. presented at the SPE International Symposium on Formation Damage Control held in Lavayette, Louisiana.
- /151/ Valkø P.; Economides M.J. *Hydraulic Fracture Mechanics*. John Wiley & Sons Ltd - Chichester New York Brisbane Toronto Singapore, 1. edition, 1995. ISBN 0-471-95664-3. 2.reprint.

Bibliography

- /152/ Rae P.; di Lullo G. Fracturing Fluids and Breaker Systems - A Review of the State-of-the-Art. (SPE-Paper 37359), 1996. presented at the SPE Eastern Regional Meeting held in Columbus, Ohio.
- /153/ Cooke Jr. C.E. Effect of Fracturing Fluids on Fracture Conductivity. *Journal of Petroleum Technology*, 27(SPE-Paper 5114):1273–1282, Oct. 1975.
- /154/ Almond S.W.; Bland W.E. The Effect of Break Mechanism on Gelling Agent Residue and Flow Impairment in 20/40 Mesh Sand. (SPE-Paper 12485), 1984. presented at the Formation Damage Control Symposium held in Bakersfield, California.
- /155/ Shah S.N.; Lord D.L.; Tan H.C. Recent Advances in the Fluid Mechanics and Rheology of Fracturing Fluids. (SPE-Paper 22391), 1992. presented at the SPE International Meeting on Petroleum Engineering held in Beijing, China.
- /156/ Balhoff M.; Miller M.J. Modeling Fracture Fluid Cleanup in Hydraulic Fractured. (SPE-Paper 77596), 2002. presented at the SPE Annual Technical Conference and Exhibition held in San Antonio, Texas.
- /157/ Al-Fariss T.; Pinder K.L. Flow of a Shear-Thinning Liquid With Yield Stress Through Porous Media. (SPE-Paper 13840), 1985.
- /158/ Walters H.G.; Morgan R.G.; Harris P.C. Kinetic Rheology of Hydraulic Fracturing Fluids. (SPE-Paper 71660), 2002. presented at the SPE Annual Technical Conference and Exhibition held in New Orleans, Louisiana.
- /159/ McDonald A.E. Approximate Solutions for Flow on non-Newtonian Power Law Fluids through Porous Media. (SPE-Paper 7690), 1979. presented at the 1979 SPE of AIME Fifth Symposium on Reservoir Simulation held in Denver, Colorado.
- /160/ Ikoku C.U.; Ramey H.J.Jr. Numerical Solution of the Nonlinear Non-Newtonian Partial Differential Equation. (SPE-Paper 7661), 1978.
- /161/ Murtha J.A.; Ertekin T. Numerical Simulation of Power-Law Fluid Flow in a Vertically Fractured Reservoir. (SPE-Paper 12011), 1983. presented at the 58th Annual Technical Conference and Exhibition held in San Francisco, California.
- /162/ Azouz I.; Shirazi S.A.; Pilehvari A.; Azar J.J. Numerical Simulation of Laminar Flow of Newtonian and Non-Newtonian Fluids in Conduits of Arbitrary Cross-Section. (SPE-Paper 24406), 1992.
- /163/ Ikoku C.U.; Ramey H.J.Jr. Transient Flow of Non-Newtonian Power-Law Fluids in Porous Media. *Society of Petroleum Engineers Journal*, (SPE-Paper 7139):164–174, June 1979. presented at 48th. Annual California Regional Meeting held in San Francisco, California.
- /164/ Bennion D.B.; Thomas F.B.; Bietz R.F.; Bennion D.W. Underbalanced Drilling: Praises and Perils. (SPE-Paper 52889), 1996. presented at the SPE Permian Basin Oil and Gas Recovery Conference held in Midland, Texas.
- /165/ Kardolus C.B.; van Kruijsdijk C.P.J.W. Formation Testing While Underbalanced Drilling. (SPE-Paper 38754), 1997. presented at the SPE Annual Technical Conference held in San Antonio, Texas.

Bibliography

- /166/ van Kruijsdijk C.P.J.W.; Cox R.J.W. Testing While Underbalanced Drilling: Horizontal Well Permeability Profiles. (SPE-Paper 54717), 1999. presented at the SPE European Formation Damage Conference held in The Hague, The Netherlands.
- /167/ Larsen L.; Nilsen F. Inflow Predictions and Testing While Underbalanced Drilling. (SPE-Paper 56684), 1999. presented at the SPE Annual Technical Conference held in Houston, Texas.
- /168/ Xiong H.; Shan D. Reservoir Criteria for Selecting Underbalanced Drilling Candidates. (SPE-Paper 81621), 2003. presented at the IADC/SPE Underbalanced Technology Conference and Exhibition held in Houston, Texas.
- /169/ Ding Y.; Longeron D.; Renard G.; Audibert A. Modelling of Near-Wellbore Damage Removal by Natural Cleanup in Horizontal Open Hole Completed Wells. (SPE-Paper 68951), 2001. presented at the SPE European Formation Damage Conference held in The Hague, The Netherlands.
- /170/ Ding Y.; Longeron D.; Renard G.; Audibert A. Modelling of Both Near-Wellbore Damage and Natural Cleanup of Horizontal Wells Drilled With a Water-Based Mud. (SPE-Paper 73733), 2002. presented at the SPE International Symposium and Exhibition on Formation Damage Control held in Lafayette, Louisiana.
- /171/ Mtchedlishvili G.; Voigt H.D.; Friedel T. Simulation of the Gas Inflow during the UBD Conditions and the Investigation of the Long-Time Production Performance. Internal report, Freiberg University of Mining and Technology, Department of Drilling Engineering, 2003. unpublished.
- /172/ Häfner et al. Simulation des Produktionsverhaltens gefracter Bohrungen in geringpermeablen Gaslagerstätten (Simulation of Production Behaviour of Hydraulically Fractured Wells in Tight-Gas Reservoirs). Final report, DGMK Research Project 593-9/2, 2003. unpublished.
- /173/ Huang D.D.; Honarpour M.M. Capillary End Effects in Coreflood Calculations. (SCA-Paper 9634), 1996. presented at the International Symposium of the Society of Core Analysis held in Montpellier, France.
- /174/ Rose W. Modeling forced versus spontaneous capillary imbibition processes commonly occurring in porous sediments. *Journal of Petroleum Science and Engineering*, (30): 155–166, 2001.
- /175/ Li K.; Chow K.; Horne R.N. Effect of initial water saturation on spontaneous water imbibition. (SPE-Paper 76727), 2002. presented at the SPE Western Regional/AAPG Pacific Section Joint Meeting held in Anchorage, Alaska.
- /176/ Gringarten A.C.; Ramey H.G.; Raghavan R. Unsteady-State Pressure Distributions Created by a Well With a Single Infinite-Conductivity Vertical Fracture. *Society of Petroleum Engineers Journal*, (SPE-Paper 4014):347–360, Aug. 1974.
- /177/ Cinco-Ley H.; Samaniego-V.F.; Dominguez N.A. Transient Pressure Behavior for a Well With a Finite-Conductivity Vertical Fracture. *Society of Petroleum Engineers Journal*, (SPE-Paper 6014):253–264, Aug. 1978.

Bibliography

- /178/ Ward J.S.; Morrow N.R. Capillary Pressure and Gas Relative Permeabilities of Low-Permeability Sandstone. *SPEFE*, (SPE-Paper 13882):345 foll., 1987.
- /179/ Häfner et al. Simulation des Produktionsverhaltens gefracter Bohrungen in geringpermeablen Gaslagerstätten (Simulation of Production Behaviour of Hydraulically Fractured Wells in Tight-Gas Reservoirs). Intermediate report, DGMK Research Project 593-9/2, 2003. unpublished.

TABLE OF APPENDIX

Table of Appendix

A	Validation of the Simulation Model	96
B	Algorithms for Determination of Fractured Well Grids	104
C	Non-Darcy Flow Type-Curves	105
C.1	Non-Darcy Flow Type-Curves for Fractured Wells with Constant Pressure Production	105
C.2	Non-Darcy Flow Type-Curves for Fractured Wells with Constant Rate Production	109
C.3	Type-Curves for Damaged Fractured Wells with Constant Pressure Production .	111
D	Multi-Phase Flow Functions in Tight-Gas Reservoirs	113

A Validation of the Simulation Model

Test-Case 1: Verification of Single-Phase Flow Model with Hydraulically Fractured Well

Structured fracture grids, based on the investigations of BENNETT et al. (see appendix B), are used for the verification of the single-phase model with real gas. Both finite and infinite conductivity fractures are considered. The numerical solution is *de facto* identical to the corresponding dimensionless analytical solution of GRINGARTEN et al. /176/ (IC-fractures) and CINCO-LEY et al. /177/ (FC-fractures) as shown in the type-curves, fig.(a).

The unstructured Voronoi fracture grids, fig.3.4.e. (page 26), are verified by comparison against the analytical solution for infinite conductivity fractures and a commercial simulator based on unstructured fracture grids (BANERJEE et al. /85/) considering a slightly compressible fluid in type-curve fig.(b). The dimensionless fracture conductivity is 2400 with a wellbore radius of 0.1 m and a reservoir permeability of 10 mD. The reservoir is rectangular and bounded (unit slope in the derivative plot). In contrast, the analytical solution takes only the infinite acting period into account.

In general, both the research simulation tool as well as the commercial simulator exhibit good agreement of pressure resp. the derivative of the pressure, even for very small times. Concluding from both cases, the simulator is suitable to model hydraulically fractured vertical wells to well testing accuracy.

Test-Case 2: Verification of Single-Phase Non-Darcy Flow

At first, the non-Darcy flow is verified against the analytical solution for radial flow of a slightly compressible fluid (water). Parameters are summarised in table below.

Well rate (m ³ /s)	1.00E-03
Permeability (mD)	10
Thickness (m)	10
Porosity	0.2
Viscosity (mPa.s)	1
Total compressibility (1/Pa)	5E-10
Density (kg/m ³)	1000
Well radius (m)	0.1
Non-Darcy flow coefficient β_t (1/m)	5.00E+11

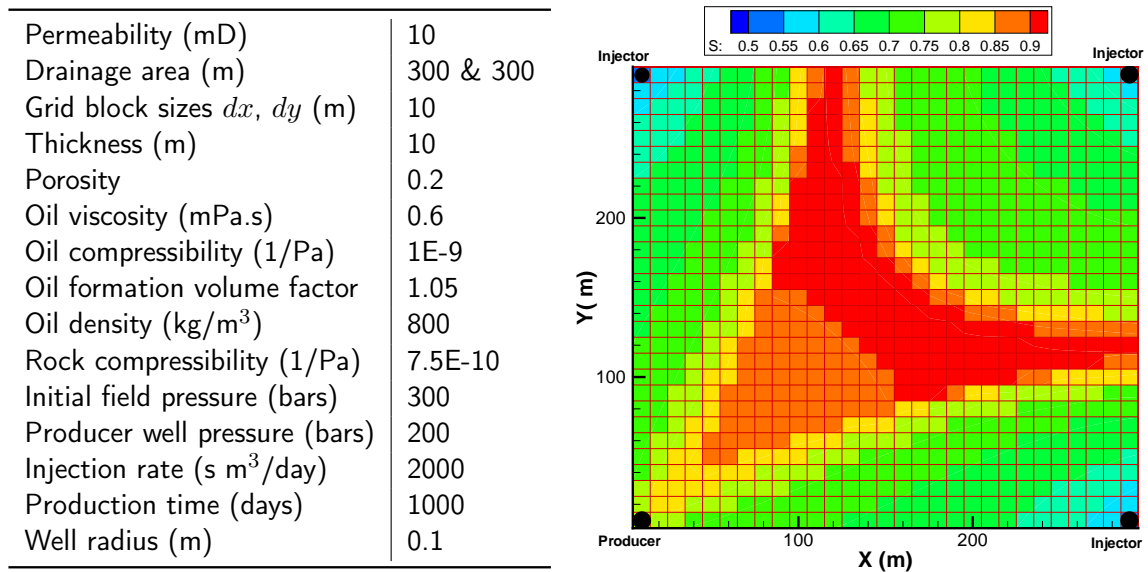
Results are shown in fig.(c). The uppermost curve is valid for sole Darcy-flow during infinite acting period. Analytical constant-rate solution and simulator results are *de facto* identical. The lower curve present the simulator results including non-Darcy flow. There, the transient flow is accurately honoured. In contrast, the analytical solution for non-Darcy flow assumes stationary flow. Once (at least almost) stationary conditions are met during late times, there is a good agreement to the simulator results.

A Validation of the Simulation Model

Fig.(d) presents the verification of the fractured well non-Darcy flow. BENNETT-type of structured fracture grids are utilised (appendix B). Simulator results are compared against the type-curves of GUPPY et al. /99/ for non-Darcy flow with constant pressure boundary conditions in dimensionless form. Both curves consider transient flow; real gas was assumed for the generation if the type-curves. Again, the graphs exhibit very close agreement.

Test-Case 3: Verification of Two-Phase Flow Model

The two-phase model of a common five-spot pattern is validated against the results of a commercial simulator. Model parameters are summarised in the table below. The gas PVT properties are according to a composition listed in subsec.4.2.1. The two-phase flow functions are derived by means of a Brookes-Corey model (fig.5.1.b). Discretisation with location of



the oil producer and the gas injectors is shown in figure above on the right side. Initially, the reservoir is water filled, the gas is at residual saturation (0.1). Oil and gas production rates of both codes in fig.(e) are identical, also the time of gas breakthrough. The saturation distribution between producer and injectors at the end of the production coincide for both simulators, also the temporal development of the grid block saturation of the producer, both shown in fig.(f).

Test-Case 4: Verification of Three-Phase Flow Model with Structured Fracture Grids

The three-phase model is validated by means of a commercial simulator. A fractured vertical well is initially filled with a gel phase of constant viscosity. The fracture is surrounded by a water saturated zone (approx.0.5 m) with critical gas saturation (0.1). The rest of the reservoir is gas filled with water at residual saturation (0.5). During cleanup, the well produces with constant bottom hole pressure. Input properties are listed in the table below.

A Validation of the Simulation Model

Permeability (mD)	0.05
Thickness (m)	10
Porosity	0.1
Fracture half length (m)	250
Dimensionless fracture conductivity	10
Gel viscosity (mPa.s)	1.0
Gel compressibility (1/Pa)	5.5E-10
Gel formation volume factor	1.05
Gel density (kg/m ³)	800
Water viscosity (mPa.s)	0.25
Water compressibility (1/Pa)	5.5E-10
Water formation volume factor	1.05
Water density (kg/m ³)	1000
Rock compressibility (1/Pa)	7.5E-10
Initial field pressure (bars)	600
Producer well pressure (bars)	150

BENNETT-type of structured fracture grids are again utilised (appendix B). Multiphase flow functions in the formation are based on a Brookes-Corey model, with endpoint permeabilities 0.12 (gas) and 0.11 (water). Capillary pressure at residual water saturation is 330 bars. Within the fracture, the relative permeability equals the corresponding phase saturation. Additionally, there is no capillary pressure.

Results are shown in the figures below. The left hand side, fig.(g), presents the temporal development of phase saturations in the well block. The rates are shown in the figure aside, fig.(h). Both rates and saturation are in good agreement with the results of the commercial simulator.

Test-Case 5: Verification of Non-Newtonian Fluid Flow Model

The implementation of non-Newtonian fluids is verified by means of the analytical solution of IKOKU and RAMEY /163/ for transient radial flow of non-Newtonian power law fluid. In /160/, the authors corrected their solution using a numerical solution of the corresponding partial differential solution, which is the base for the following comparison. The power law model accounts for pseudo-plastic fluid behaviour **without** a yield stress.

The dimensionless pressure, p_{DNN} , is defined:

$$p_{DNN} = \frac{p - p_i}{\left(\frac{Q}{2\pi h}\right)^n \frac{\mu_{eff} t_w^{1-n}}{k_{res}}} , \quad (A.1)$$

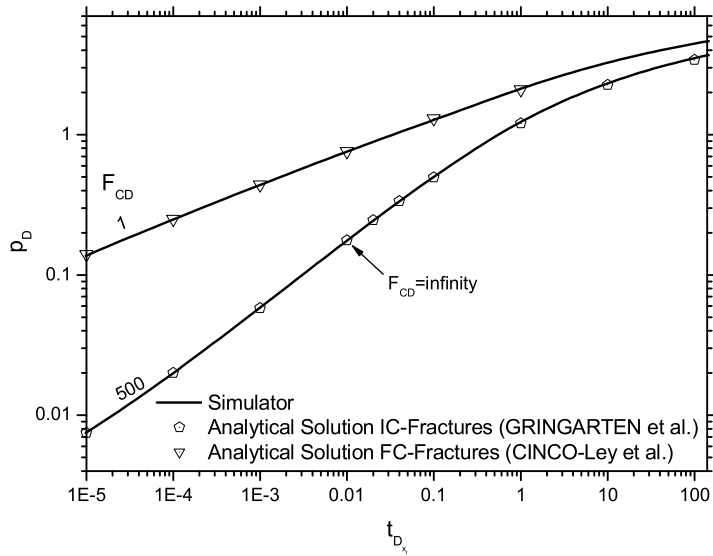
and the dimensionless time:

$$t_{DNN} = \frac{t}{Gr_w^{3-n}} \quad \text{with} \quad G = \frac{n\phi c_t \mu_{eff}}{k_{res}} \left(\frac{2\pi h}{Q}\right)^{1-n} . \quad (A.2)$$

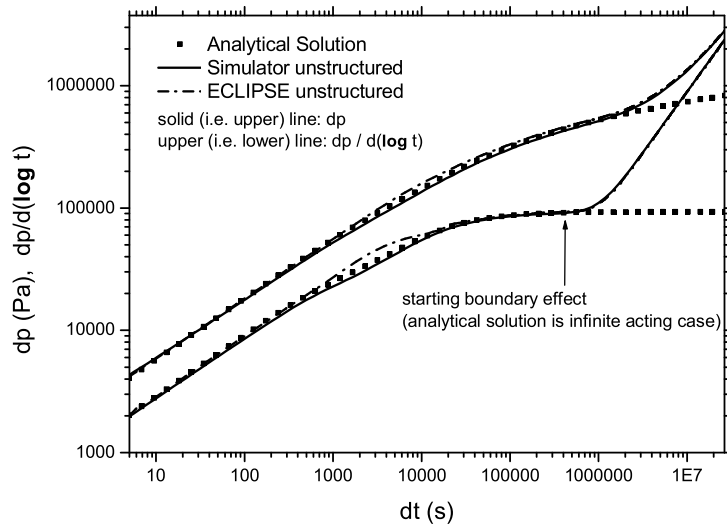
The effective viscosity is calculated with eq.4.27.

Results, shown in the fig.(i), exhibit good agreement to the results of IKOKU and RAMEY. Verification of non-Newtonian fluid with yield stress is impossible so far since analytical solutions or appropriate fluid models in commercial simulators are not available.

A Validation of the Simulation Model

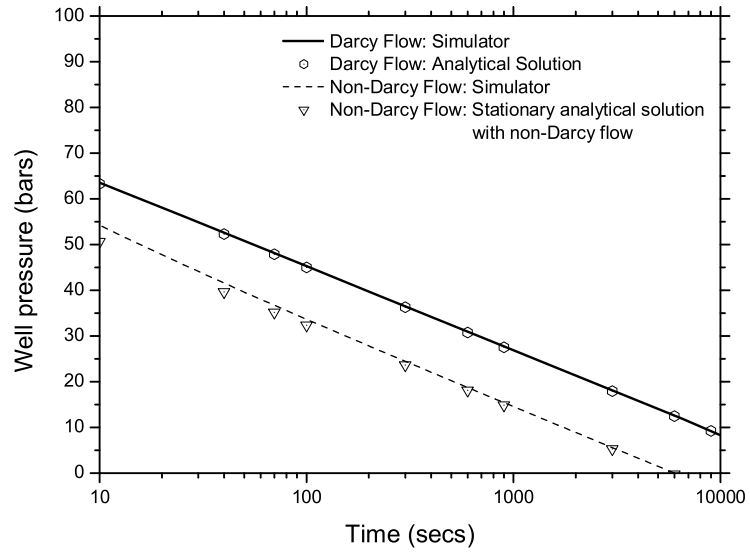


(a) Structured grids: comparison for constant rate production of infinite and finite conductivity fracture with dimensionless analytical solutions from GRINGARTEN et al. and CINCO-LEY et al.

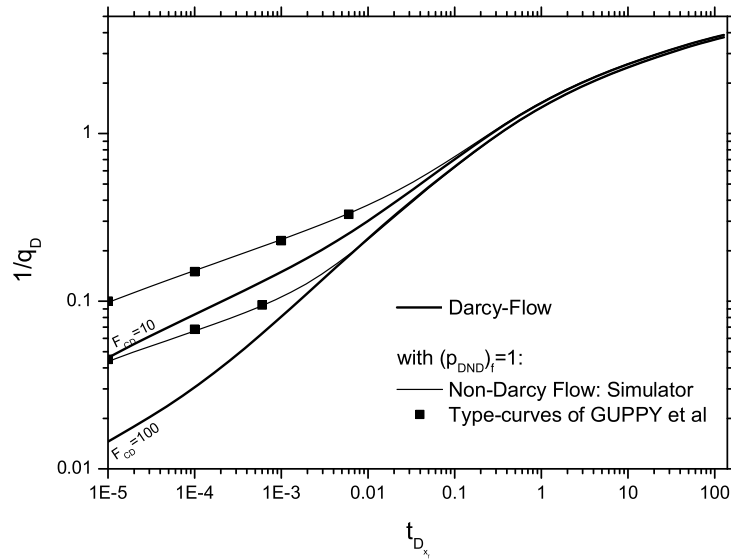


(b) Unstructured fracture grids: comparison of constant rate production from an infinite conductivity fracture against a commercial simulator (ECLIPSE) and the analytical solution of GRINGARTEN et al.

A Validation of the Simulation Model

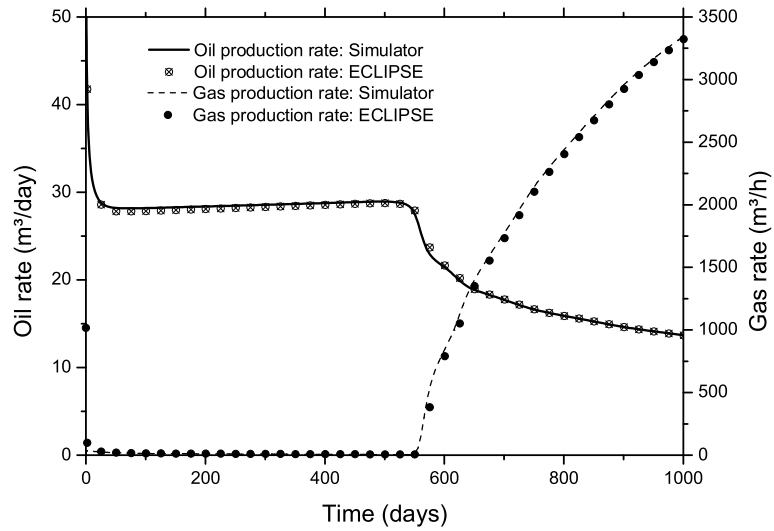


(c) Verification of non-Darcy and Darcy flow at a radial well with analytical solution and stationary, turbulent skin factor for constant rate production

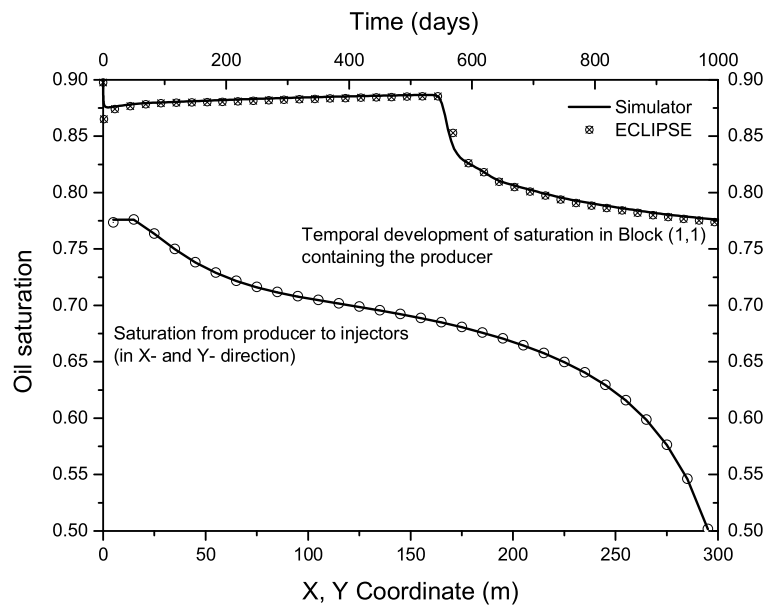


(d) Verification of non-Darcy flow in fractured vertical wells with GUPPY's type-curves for constant pressure production

A Validation of the Simulation Model

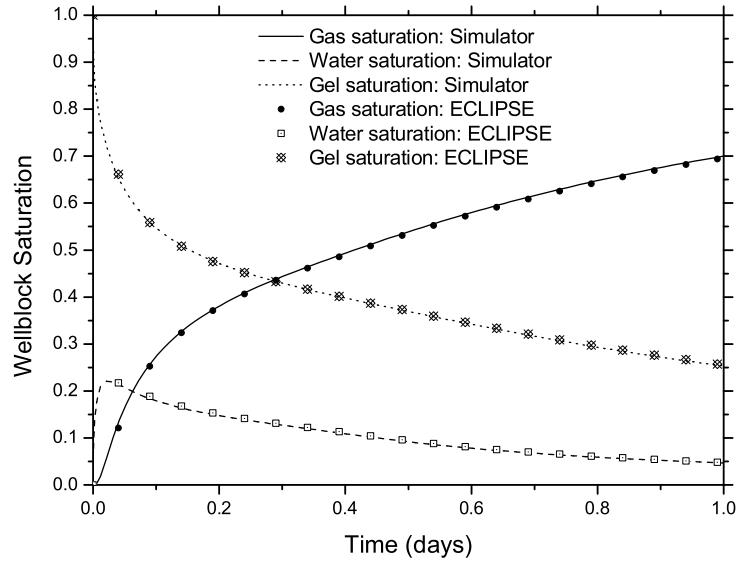


(e) Water and gas production compared against ECLIPSE results

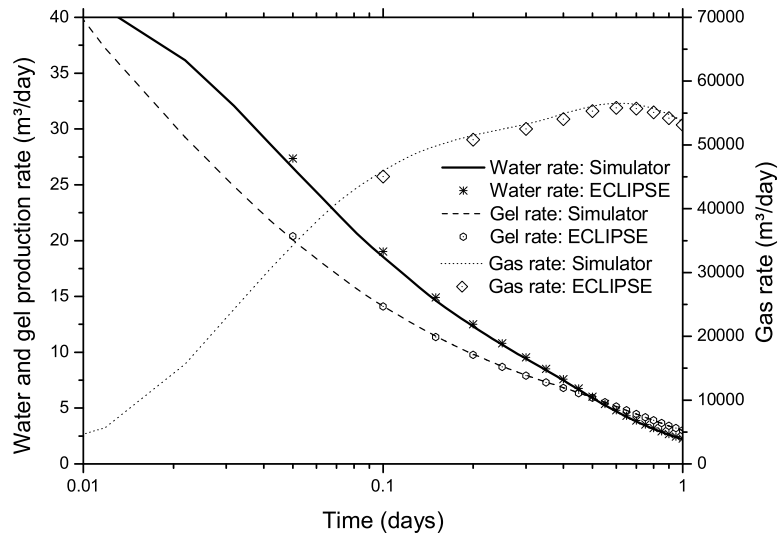


(f) Temporal development of saturation in producer grid block and cross-section from producer to injector

A Validation of the Simulation Model

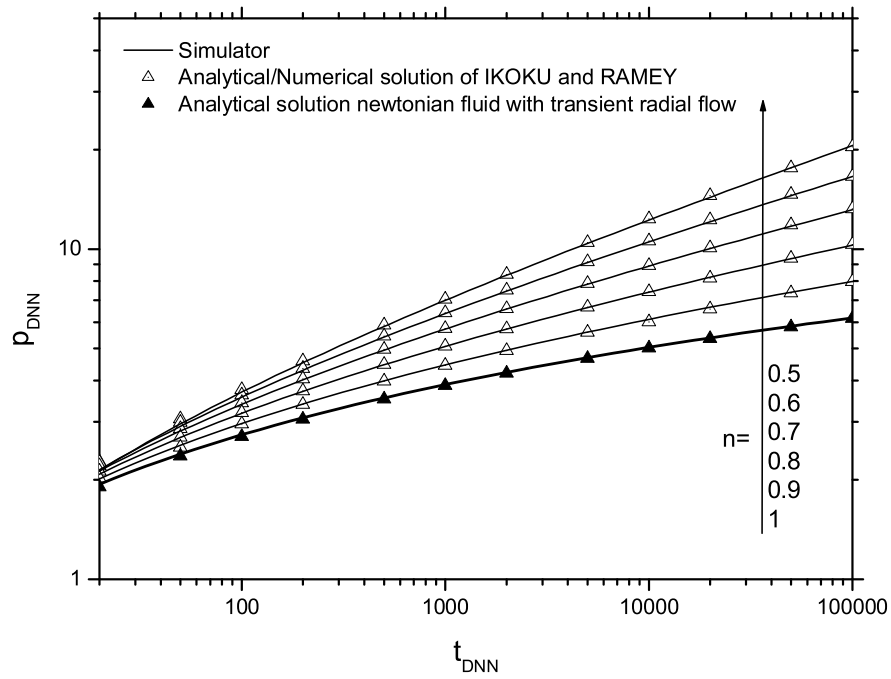


(g) Temporal development of saturation in well block compared against ECLIPSE results



(h) Production rates compared against ECLIPSE results

A Validation of the Simulation Model



(i) Verification of non-Newtonian (power law) fluid model with analytical solutions from IKOKU and RAMEY

B Algorithms for Determination of Fractured Well Grids

The following algorithms were presented by BENNETT et al. /92/.

For all grid blocks

$$\Delta x_{i+1}/2 \leq 2\Delta x_{i-1}, \quad i = 2 \dots (Nx - 1)$$

$$\Delta y_{j+1}/2 \leq 2\Delta y_{j-1}, \quad j = 2 \dots (Ny - 1).$$

Near the fracture ($x/L_x \leq 1.5, y/L_y \leq 1$)

$$\Delta x/L_x \leq 1 \cdot 10^{-2} \text{ at the well for } F_{CD} \geq 100$$

$$\Delta x/L_x \leq 1 \cdot 10^{-3} \text{ at the well for } F_{CD} < 100$$

$$\Delta x/L_x \leq 1.5 \cdot 10^{-2} \text{ at the fracture tip}$$

$$\max(\Delta x/L_x) \leq 0.15$$

$$b_f/L_x = 2\Delta y_1/L_x \leq 2 \cdot 10^{-3}$$

$$\Delta y_1 = \Delta y_2 = \Delta y_3 = \Delta y_4$$

$$\max(\Delta y/L_x) \leq 0.20$$

Away from the fracture ($x/L_x > 1.5, y/L_y > 1$)

$$\max(\Delta x/L_x) \leq 0.17$$

$$\max(\Delta y/L_x) \leq 0.17$$

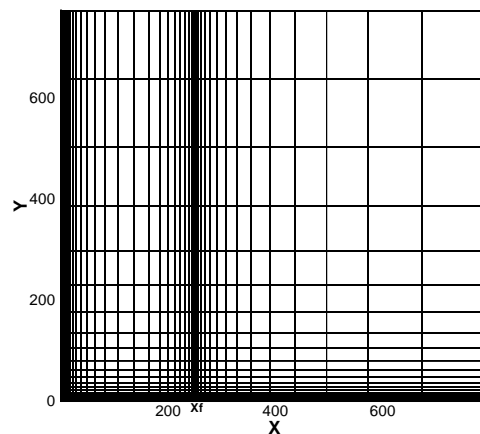
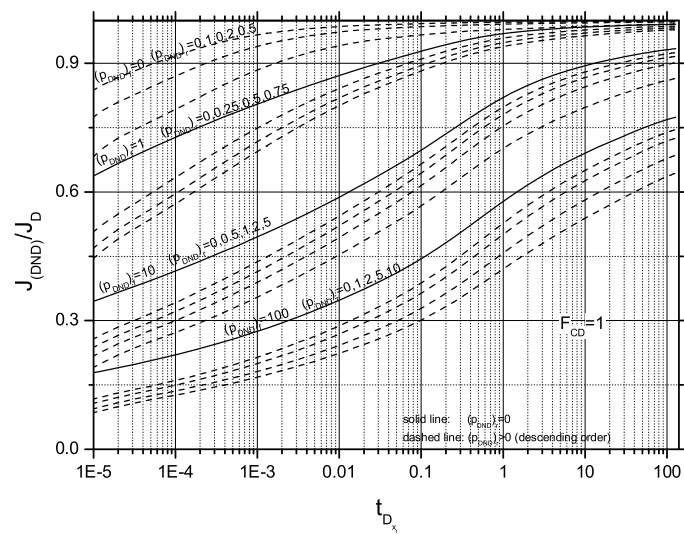
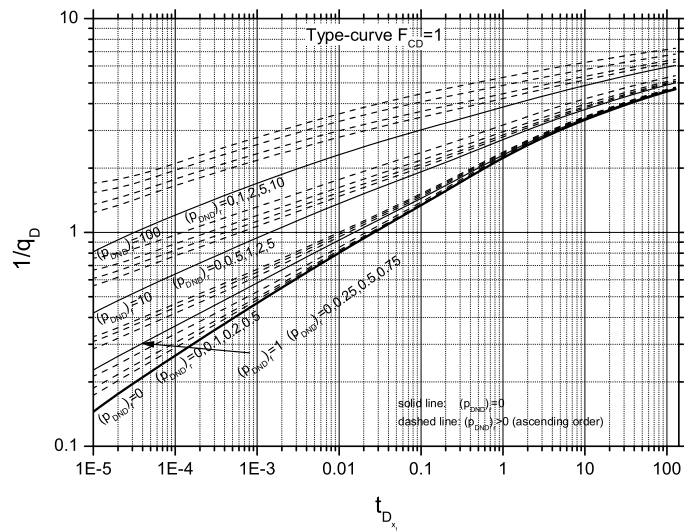


Figure B.1: Example of fracture grid (with quarter symmetry)

C Non-Darcy Flow Type-Curves

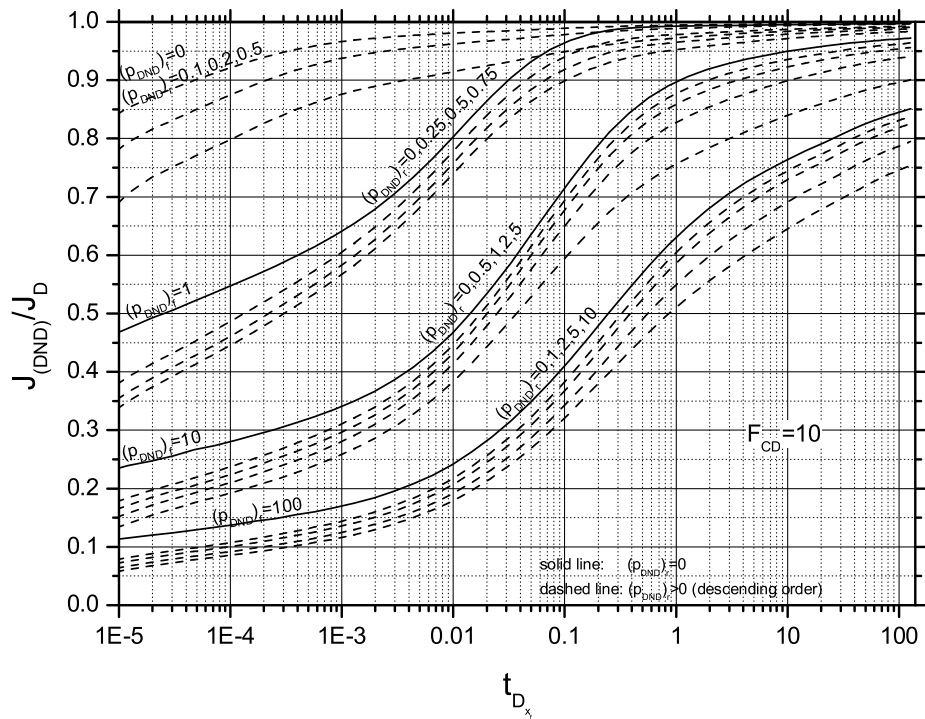
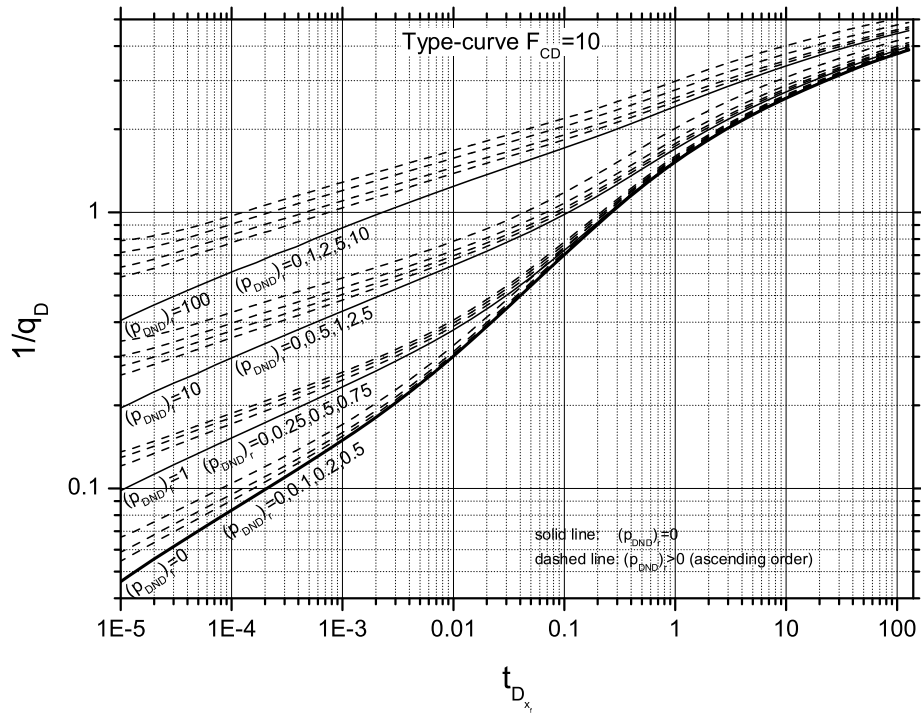
C.1 Non-Darcy Flow Type-Curves for Fractured Wells with Constant Pressure Production

$$F_{CD}=1$$



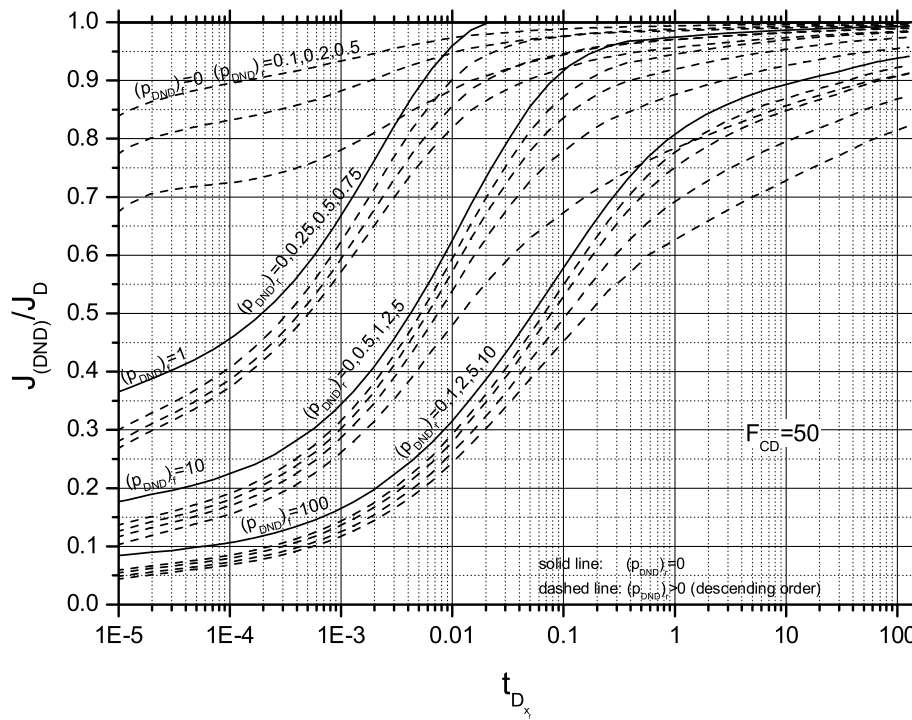
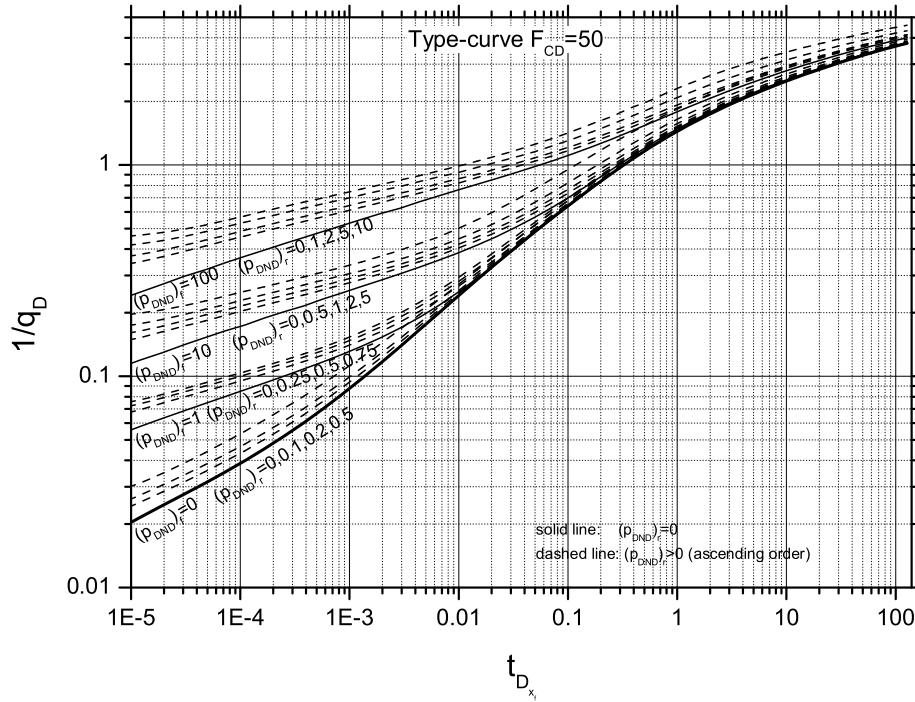
C Non-Darcy Flow Type-Curves

$F_{CD}=10$



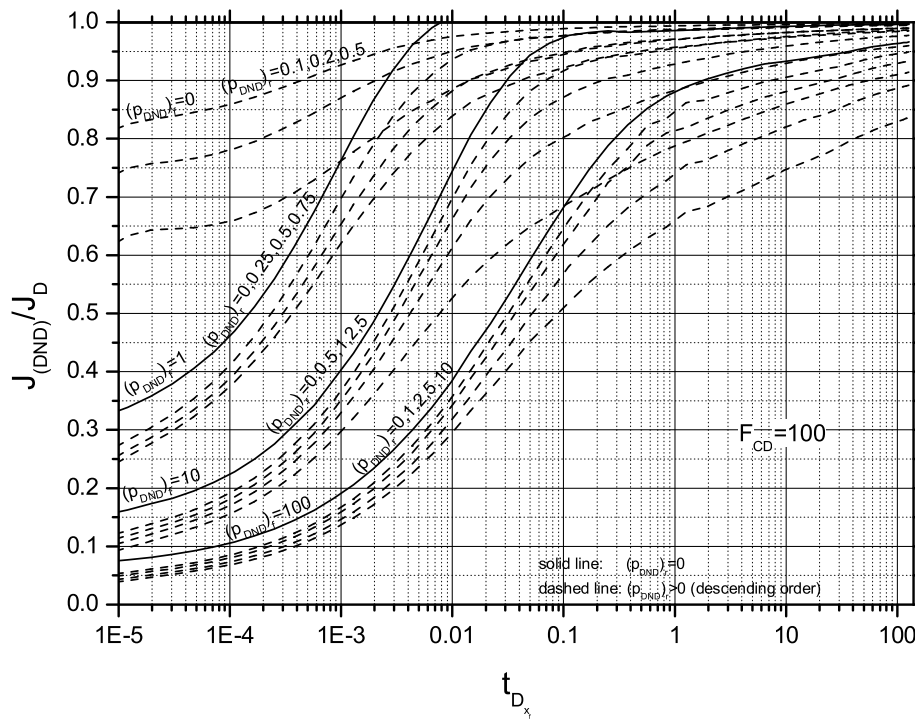
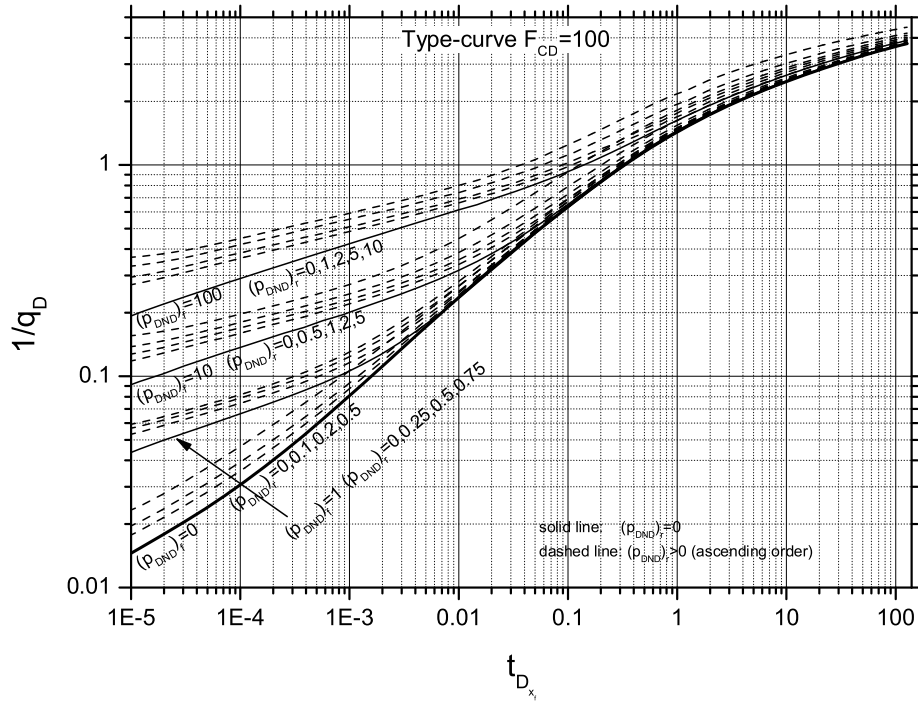
C Non-Darcy Flow Type-Curves

$F_{CD}=50$



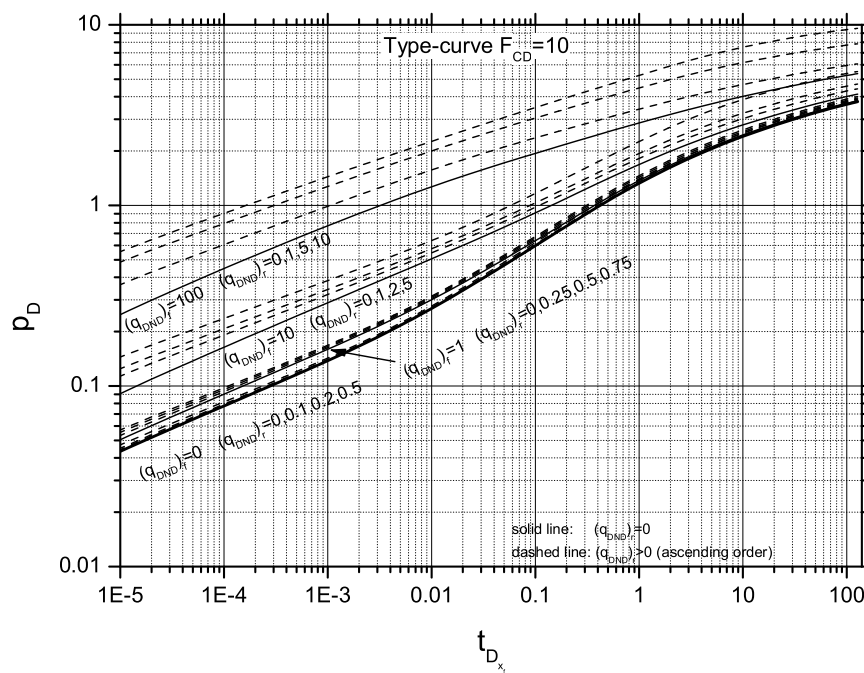
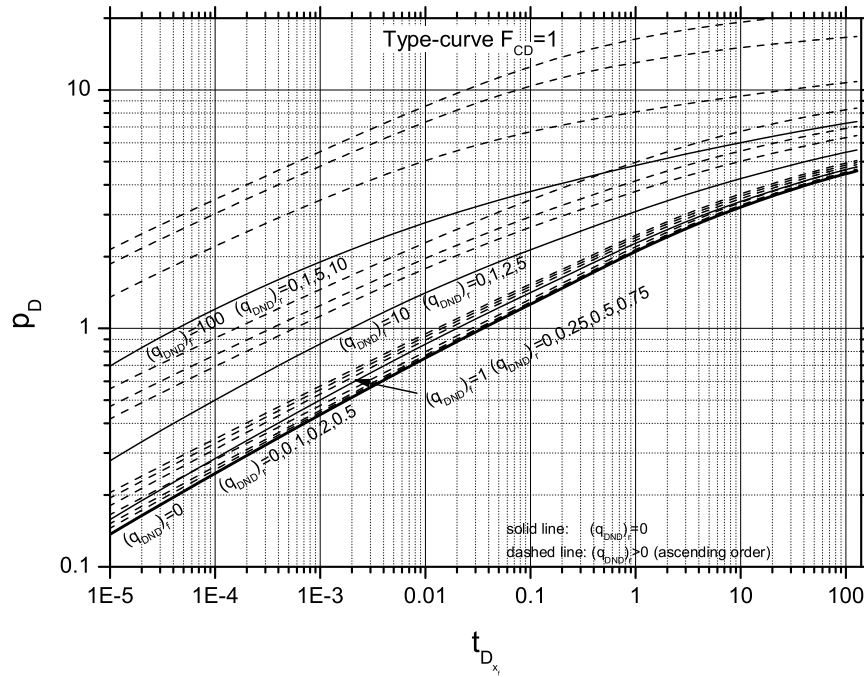
C Non-Darcy Flow Type-Curves

$F_{CD}=100$



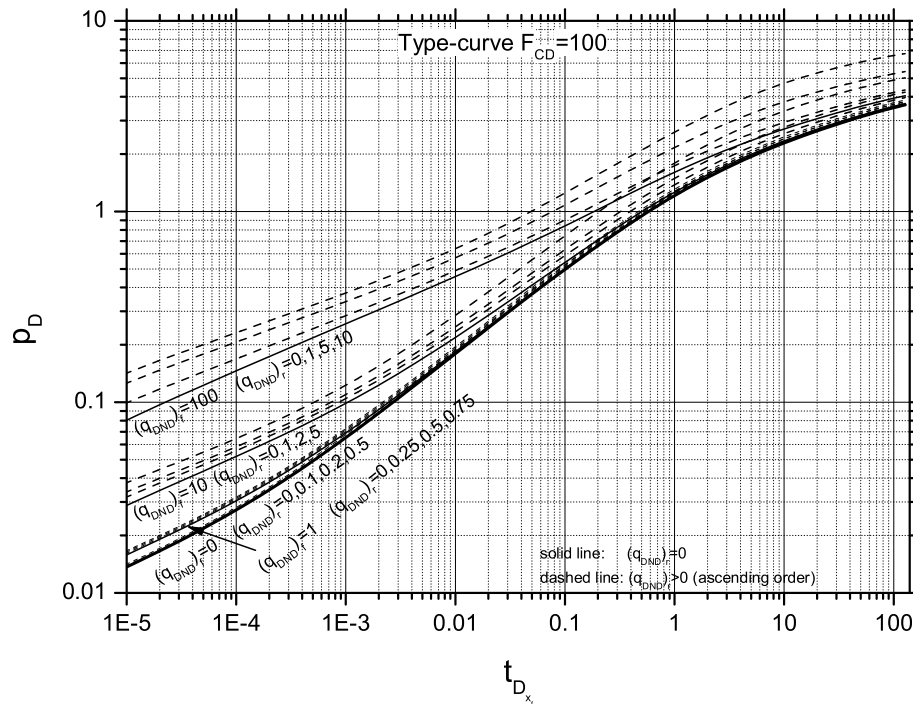
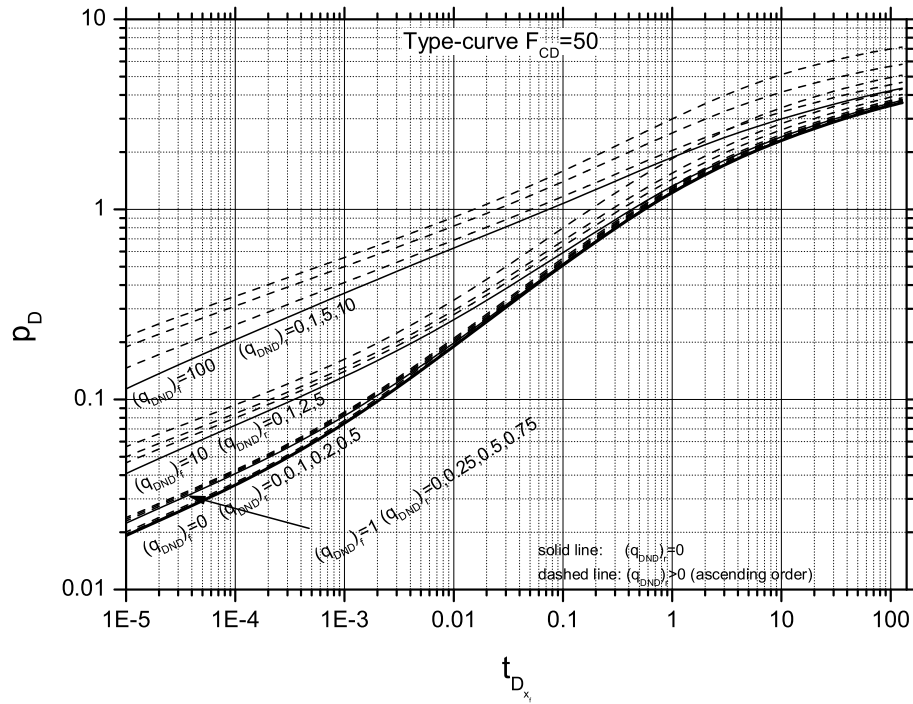
C.2 Non-Darcy Flow Type-Curves for Fractured Wells with Constant Rate Production

$F_{CD}=1$ and 10



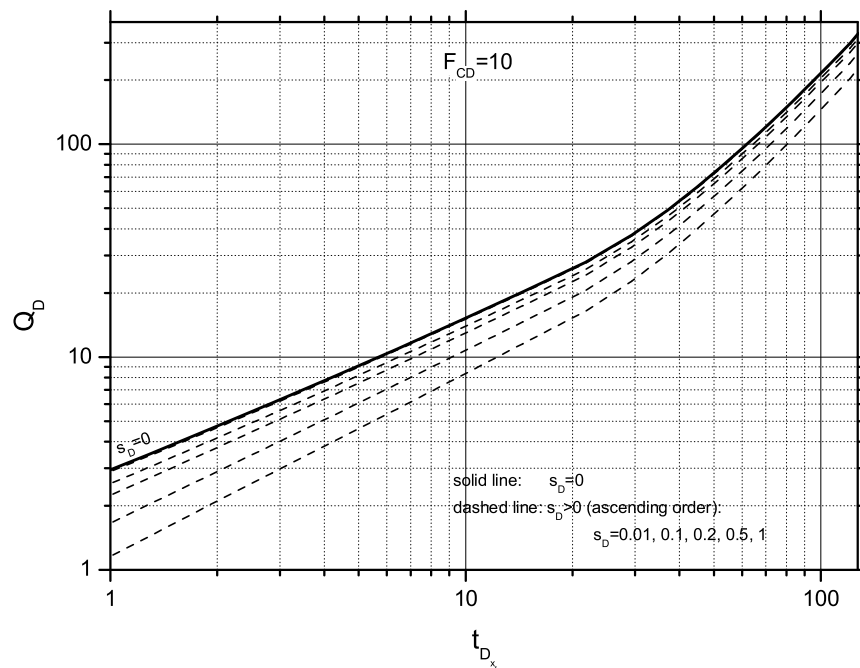
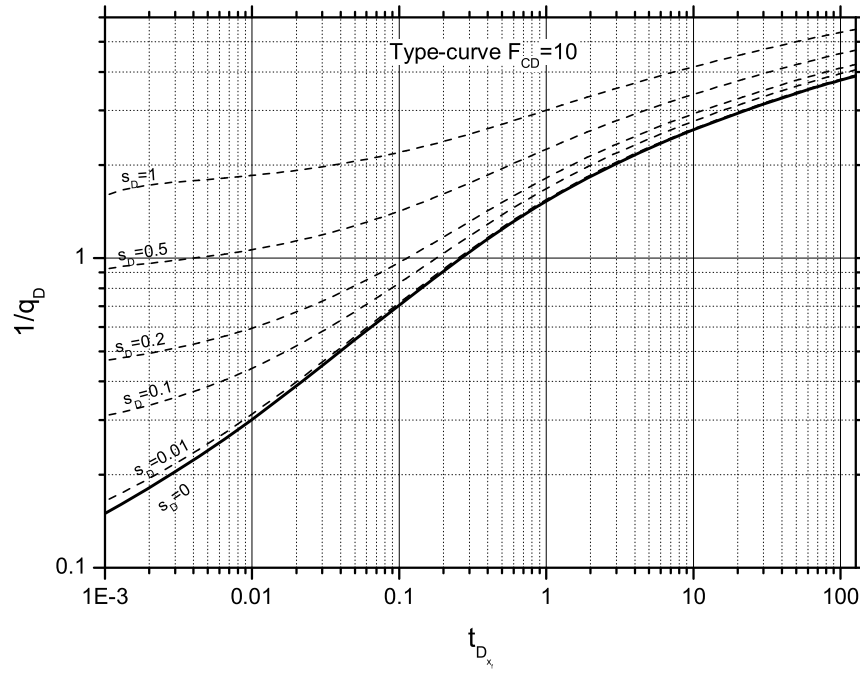
C Non-Darcy Flow Type-Curves

$F_{CD}=50$ and 100



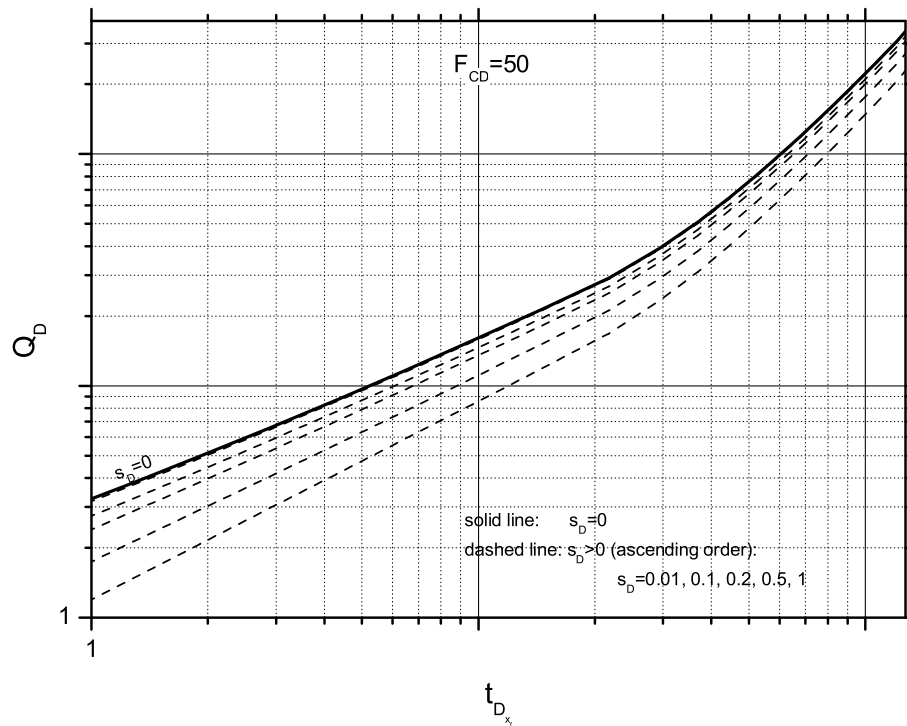
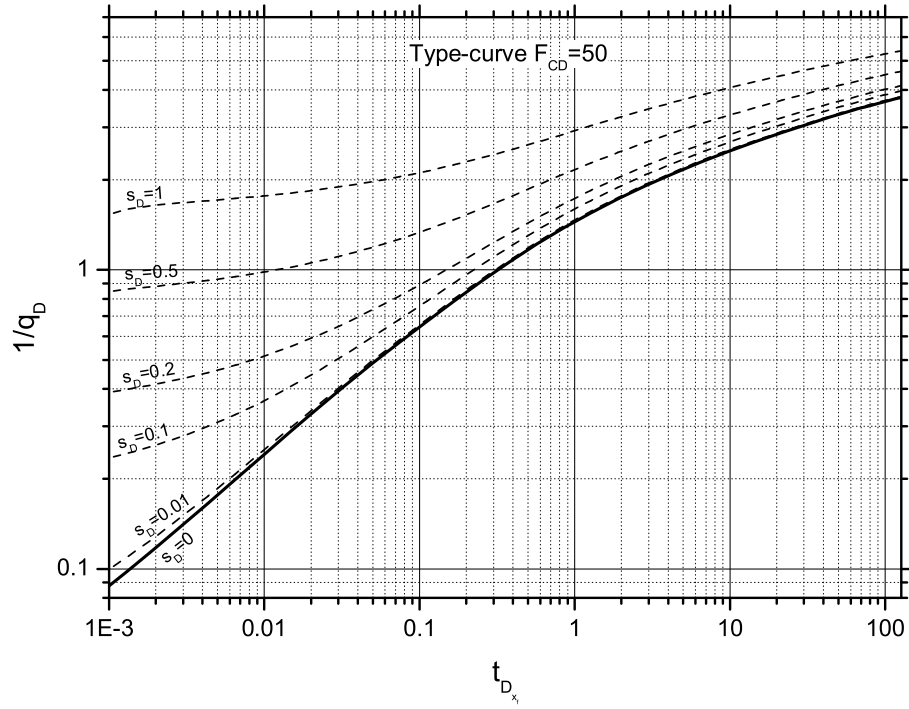
C.3 Type-Curves for Damaged Fractured Wells with Constant Pressure Production

$$F_{CD}=10$$



C Non-Darcy Flow Type-Curves

$F_{CD}=50$



D Multi-Phase Flow Functions in Tight-Gas Reservoirs

The algorithms to calculate relative permeability and capillary pressure are based on the Brookes-Corey correlation and were presented by the ITE (in /126/). For the calculation of relative permeability and capillary pressure, a dimensionless water saturation S_{wd} is introduced:

$$S_{wd} = \frac{S_w - S_{wi}}{1 - S_{gc} - S_{wi}} . \quad (D.1)$$

The relative permeability of the gas and water phase $k_{r,g}(S_w)$, $k_{r,w}(S_w)$ are calculated using the BROOKS-COREY correlation assuming a material parameter λ (HUANG and HONARPOUR /1996/):

$$k_{r,g}(S_w) = k_{r,g}(S_{wi}) * (1 - S_{wd})^2 * \left(1 - S_{wd}^{\frac{2}{\lambda}+1}\right) , \quad (D.2)$$

$$k_{r,w}(S_w) = k_{r,w}(S_{gc}) * S_{wd}^{\frac{2}{\lambda}+3} . \quad (D.3)$$

Due to the missing experimental data regarding the endpoint permeabilities from North German tight-gas reservoirs, existing correlations from tight North American Mesaverde sandstones were adapted (WARD and MORROW /178/):

$$k_{r,g}(S_{wi}) = \left(1 - \frac{S_{wi}}{0.7}\right)^{1.5} * (1 - S_{wi}^2) , \quad (D.4)$$

$$k_{r,w}(S_{gc}) = k_a^{0.4224} * \left(\frac{1 - S_{gc} - S_{wi}}{1 - S_{wi}}\right)^4 . \quad (D.5)$$

Capillary pressure can be calculated by means of $p_{cap} = p_d * S_{wd}^{-\lambda}$, where the displacement pressure p_d as material parameter correlates with the absolute permeability of the Rotliegendes sandstones following the ITE (/179/):

$$p_d = 0.886k_a^{-0.693} . \quad (D.6)$$

D Multi-Phase Flow Functions in Tight-Gas Reservoirs

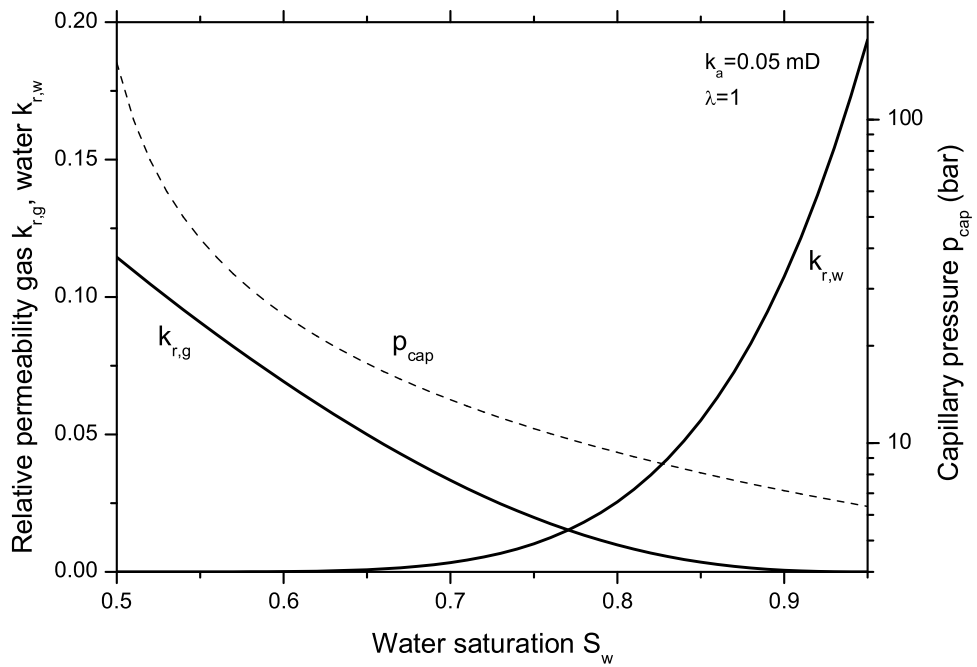


Figure D.1: Multiphase flow functions based on Brooks-Corey correlations ($k_{res} = 0.05$ mD)